ADVANCES IN ROBOT-ASSISTED GAIT REHABILITATION WITH SELF-SELECTED SPEED

by

Babak Hejrati

A dissertation submitted to the faculty of
The University of Utah
in partial fulfillment of the requirements for the degree of

Doctor of Philosophy

Department of Mechanical Engineering

The University of Utah

August 2016

The University of Utah Graduate School

STATEMENT OF DISSERTATION APPROVAL

The dissertation of **Babak Hejrati**

has been approved by the following supervisory committee members:

Jake J. Abbott	, Chair	**3/30/2016** Date Approved
John M. Hollerbach	, Member	**3/30/2016** Date Approved
Andrew S. Merryweather	, Member	**3/30/2016** Date Approved
K. Kenneth Foreman	, Member	**3/30/2016** Date Approved
Kam K. Leang	, Member	**3/30/2016** Date Approved

and by **Tim Ameel** , Chair/Dean of

the Department/College/School of **Mechanical Engineering**

and by David B. Kieda, Dean of The Graduate School.

ABSTRACT

This dissertation explores robotic technologies to generate gait at self-selected speed for application in gait rehabilitation. We present two major research thrusts to improve the current gait rehabilitation for patients with walking impairments. The first thrust includes two studies. The first study aims at demonstrating the potentials of an advanced robotic locomotion interface called the Treadport for gait rehabilitation of spinal cord injury patients. The outcome of this study implies that standard treadmills may impose some constraints on the patients motions that can be overcome on the Treadport. The second study focuses on creating a realistic walking experience on the Treadport. A new controller is proposed for the Treadport based on the major factors influencing walking experience on a locomotion interface. When combined with the users volition, the controller enables the user to naturally self-select their walking speeds as they would when walking over ground.

The second thrust includes three studies. The first study presents the design and fabrication of an Underactuated WEarable Arm swing Rehabilitator called the UWEAR that aims at integrating arm swing in gait rehabilitation. The UWEAR is designed to be used with a body-weight-support treadmill. It is backdrivable, capable of assisting the users arm swing in the sagittal plane, and it has unhindered kinematics in the remaining degrees of freedom. The experimental results show the UWEAR's ability to induce arm swing in its users under various conditions. The second study presents a comprehensive look at the effects of a variety of walking conditions on arm-swing patterns during walking. The results describe the effects of surface slope, walking speed, and physical characteristics on arm-swing patterns in healthy individuals. Finally, the third study proposes a novel method for generating proper arm-swing trajectories in real-time using only measurements of the angular velocity of a person's thighs, to be used during gait rehabilitation. The proposed method generates smooth trajectories that have high correlations with the actual measured arm trajectories of the healthy individuals. The method is verified on gait data sets gathered from patients with Parkinson disease, and even their pathological thigh trajectories result in proper arm-swing trajectories.

CONTENTS

LIST OF FIGURES

LIST OF TABLES

CHAPTER 1

INTRODUCTION

Walking impairments are caused by various conditions such as spinal cord injury (SCI), stroke, and Parkinson diseases in which affected patients lose some degree of their mobility. For example, reported in the year 2014, there were 276,000 people suffering from SCI in the United States with 12,500 new cases each year [1]. Patients with walking impairments often consider gait rehabilitation for improving their gait function; however, rehabilitative exercises usually suffer from two major shortcomings. First, they fail to depict realistic walking experiences for patients during rehabilitation. Thus, these patients often reach a plateau in their walking recovery that makes returning to everyday life difficult. Second, they de-emphasize the role of upper limbs in inducing lower-limb muscle activities. It is found that the inclusion of upper-limb movements in gait rehabilitation can result in a faster walking recovery. This dissertation is comprised of two major parts that address the mentioned shortcomings by using robotic technologies to generate gait at self-selected speed for application in gait rehabilitation rehabilitation.

1.1 The Treadport locomotion interface

Body-weight-supported treadmills (BWSTs) are advantageous for gait rehabilitation due to adequate mobility, partial weight support, control of the experimental environment, and the use of monitoring equipment [2, 3, 4]. BWSTs have been shown to improve gait parameters, effort (speed and distance), balance, and psychological attitudes [5, 6]. However, as mentioned earlier, patients often reach a plateau in their walking recovery such that they do not make any further progress by continuing their exercise on traditional BWSTs. In Chapter 2, we test the hypothesis that plateauing in SCI patients is partly due to an inability of standard rehabilitation treadmills to depict a realistic walking experience. We compare the gait performance of four SCI patients walking on an advanced locomotion interface called the Treadport and on a traditional rehabilitation treadmill. We use kinematic parameters such as hip and knee ranges of motion, spatiotemporal parameters (i.e., normalized walking speed, cadence, and stride), and walking symmetry to make a quantitative comparison. The results of this study indicate that walking on the Treadport led to improvements

in hip and knee ranges of motion, walking speed, and walking symmetry of the patients relative to walking on a traditional treadmill. The outcome of this study implies that standard treadmills mays impose some constraints on a patients' motion that can be overcome on the Treadport.

Treadmill-style locomotion interfaces are the most common types of devices for simulating overground walking in virtual environments for different applications such as skill rehabilitation and gait rehabilitation [7, 8, 5]. Chapter 3 discusses an improved control system for the Treadport that includes a belt controller and a kinesthetic force feedback to enhance the realism of walking on the Treadport. Although the speed of rehabilitation treadmills has traditionally been set by manual control, the trend is for self-selected speed adaptation by measurement of position or some other forms of user intent. This enables the belt speed to be instantaneously set by a user, leading to a more natural locomotion experience. The task for the treadmill belt controller is to realize an accurate and stable belt motion, whether the user is walking or running, going forward or backward, or starting or stopping. To create a realistic walking experience for a user, three important factors have to be considered. First, the belt has to respond properly to the user's motion and re-center them such that the belt's motion does not appear too slow or too fast for the user. Second, walking on an accelerating platform can disturb the user's balance. This issue has to be resolved either by preventing the belt from accelerating/decelerating or by applying a compensating kinesthetic force feedback to the user's body. Third, the user should be able to achieve any self-selected walking speed and comfortably and stably maintain the speed as long as they wish. Through a comprehensive and systematic subject-study, it is shown in Chapter 3 how the designed control system contributes to an improved perception of realistic walking on the Treadport.

1.2 Arm swing for gait rehabilitation

SCI patients undergoing rehabilitation often do not properly swing their arms when they walk, and they must be assisted. It has long been known that leg movements and arm swing are neurally coupled in healthy individuals. Arm swing also contributes to proper balance and gait [9, 10, 11] and metabolic efficiency of walking [12]. All the mentioned benefits of arm swing have motivated researchers to consider patients' whole-body response during gait rehabilitation rather than merely focusing on patients' leg movements [13]. It has been shown that arm movements can actually instigate leg movements through the neural coupling, which is the first clear demonstration of such a cause and effect relationship. This neurological coupling reinforces clinical observations that upper-limb movement improves lower-limb motor patterns. A recent study found that arm swing was absent in 60% of treadmill-based rehabilitation of SCI patients [14]. Tester et al. [14] postulates that the role of arms in traditional rehabilitation, including rigid parallel bars or therapist-controlled

poles, may actually inhibit proper arm-swing motor learning due to the bars/poles being used for partial weight support by the patient, leading to incorrect muscle firing patterns. Chapter 4 presents the design and fabrication of an Underactuated WEarable Arm-swing Rehabilitator (UWEAR) to induce arm swing during gait rehabilitation. The UWEAR is designed to be used along with BWSTs. It is backdrivable, capable of assisting the user's arm swing in the sagittal plane, and has unhindered kinematics in the remaining unactuated degrees of freedom. Various experiments are performed to verify the ability of the UWEAR in inducing arm swing under different conditions.

Although the integration of arm swing in gait rehabilitation has been attempted by previous studies [15, 16, 17], a fundamental question still needs to be answered: What are the correct and normal arm-swing trajectories that should be utilized for gait rehabilitation and assessment during various conditions? Most studies, which propose models for describing arm swing during walking, have been motivated to answer the question of whether arm swing is passive or active [18, 12, 19, 20, 21, 22]. Since further investigation is still required to determine the extent to which arm swing is passive, most current models may not rely on valid assumptions for describing arm swing during locomotion. In addition, typical models currently used have been derived using small samples of human subjects performing a limited number of experimental conditions, and they require the measurement of arms' and joints' mechanical properties, which are not straightforward to obtain. The purpose of Chapter 5 is to provide tools for enabling the integration of arm swing in gait rehabilitation by quantifying normal arm-swing trajectories. To address the limitations of previous studies, this study quantitatively investigates the effect of variations in both walking condition and an individual's physical characteristics on arm-swing patterns during walking.

There exist several rehabilitation devices that include upper limbs' movements during gait rehabilitation. In one study, SCI patients walked on a treadmill with their arms being manually assisted by a therapist with poles [9]. In other research [23], sliding handrails were used for stroke patients who were able to achieve arm swing at a faster speed only by using the handrails. Other studies [24, 25] have used a recumbent stepper machine to show that the active upper-limb movements increase neuromuscular activation of the lower limbs during seated recumbent stepping. More recently, robotic rehabilitation devices that include arm-swing assistance during gait rehabilitation have been proposed [16, 17]. The robotic devices can be more beneficial than other rehabilitation devices for inclusion of arm swing in gait rehabilitation of patients with walking impairment since these robotic devices can provide assistance when needed, and increase the user's engagement in gait rehabilitation. The key open problem for the use of such robotic devices, which induce arm swing for gait rehabilitation without physically connecting upper and lower limbs together, is how to generate arm-swing trajectories in real-time while adapting to the user's own self-selected walking

speed. Chapter 6 proposes a novel method to address the mentioned open problem. The fundamental conjecture is that the user's thighs' angular-velocity data, measured by an IMU or motion-capture system, are sufficient to generate arm-swing trajectories in real-time. These generated trajectories can be applied to the patients by means of robotic devices such as the UWEAR.

Finally, some recommendations for future work are provided in Chapter 7 based on the lessons learned from conducting these two major research works.

CHAPTER 2

INVESTIGATION OF THE TREADPORT FOR GAIT REHABILITATION OF SPINAL CORD INJURY

The following chapter is aimed at testing the hypothesis that plateauing in patients with spinal cord injury may be partly due to an inability of standard rehabilitation treadmills to depict realistic walking.

2.1 Abstract

The goal of this study is to compare the effect of training by the University of Utah's Treadport versus a conventional treadmill on gait improvement of spinal-cord-injury (SCI) patients. Four incomplete SCI subjects who had reached a rehabilitation plateau were selected to have training first on the treadmill and then the Treadport. Spatiotemporal and gait parameters were utilized to make a comparison between the two training conditions. Overall, the results demonstrated statically significant improvements in most of the spatiotemporal as well as some of the gait parameters during training with the Treadport relative to the traditional treadmill.

2.2 Introduction

In recent years there has been a trend in locomotion training of spinal cord injury (SCI) where body-weight-supported treadmills are utilized for treating gait impairments [27] and are considered as the gold standard in gait rehabilitation [28]. The advantages of using a treadmill for neurorehabilitation include adequate mobility of the patient despite the small area occupied by the treadmill, partial weight support, "optimal" control of the experimental environment, and simple use of monitoring equipment [4].

Since the ultimate goal of rehabilitation is to prepare patients for overground walking, a substantial amount of research has been done to compare treadmill walking versus overground walking. Alton et al. [29] found no significant differences in joint kinematics and temporal parameters between treadmill and overground walking. In addition to kinematics, Murray et al. [30] used electromyography (EMG) signals and heart rate to show the similarity of the two conditions. Using kinematic and EMG gait patterns at different walking speed, Nymark et al. [31] also concluded that there are minimal differences between the conditions. Riley et al. [32] showed that the major difference lies in the ground reaction forces, where maximum ground reaction forces were significantly smaller for the treadmill walking. Lee and Hidler [4] stated that, from a therapeutic perspective, the overall kinematic and muscle activation patterns seem to be similar enough to justify use of treadmills for training stroke and SCI patients.

As the result of similarity between overground and treadmill walking, body-weight-supported treadmill training (BWSTT) is a widely accepted method for rehabilitation of SCI and post-stroke patients. Dietz et al. [33] implemented partial weight support on a moving treadmill and observed a significant increase in the amplitude of EMG signals of the patients' disabled legs with complete paraplegia. Dobkin et al. [34] obtained a locomotor-like EMG activity in the subjects without supraspinal descending influence when optimal sensory inputs were applied to them during rehabilitation with a treadmill. Furthermore, Dietz and Harkeman [7] highlighted the effectiveness of providing appropriate sensory cues for SCI patients during BWSTT.

Wernig et al. [6] reported overall improvements in balance, walking speed, and covered distance of their SCI subjects after training on a commercial motor-driven treadmill (Laufband) with a variable speed control and a supporting harness. In addition, robotic systems such as Lokomat [35], [36], LOPES [37], and WalkTrainer [38] have become increasingly common in gait rehabilitation. In summary, strong evidence implies that BWSTT has significant potential to produce physical and psychological improvements in SCI patients [39].

The University of Utah Treadport (Figure. 2.1) is a large tilting-linear-platform locomotion interface that has been designed to provide advanced multisensory and mechanical cues. It is comprised of an active mechanical tether attached to the user through a body harness, a CAVE-like visual display, a motorized winch for partial body-weight support, a passive safety tether, and an active wind tunnel [40, 41, 42]. The six-axis mechanical tether measures body position and orientation for active control of the belt speed and for updating the graphics. Missing in conventional treadmills, the Treadport lets the user select his/her speed by velocity controller proportional to users' displacement rather than manually, which is crucial in simulating real walking condition. This ability to naturally adjust walking speed also results in an improved sense of safety, since the user need not fear the prospect of not being able to keep up with a moving belt; slowing down is as natural on the Treadport as it is in natural walking. In addition, the belt's dimension ($2\,\text{m} \times 1.8\,\text{m}$) provides the user with a large area such that he/she can easily explore the virtual environment without fear of stepping off. Visual cues provided by three displays simulate different environments including, but not limited to, a mountainous terrain and a cityscape. The screens

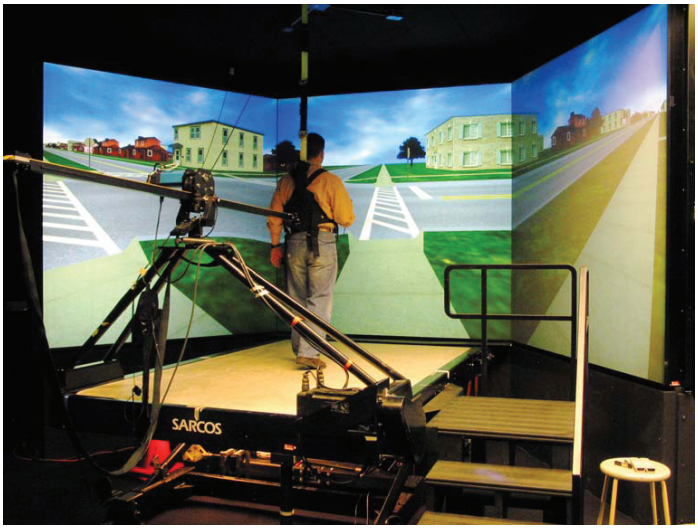

Figure 2.1: Treadport virtual environment comprising a CAVE-like visual display and locomotion interface. This image, shown for clarity, was taken before the addition of the active wind tunnel and Vicon motion capturing system.

are highly diffuse acrylic back-projection screens, and three Hughes-JVC G1000 SXGA projectors create the graphical images.

Although the Treadport is designed for a variety of applications, its key features are particularly suitable for SCI rehabilitation. The objective of this study was to perform an initial investigation of the Treadport as a tool for gait rehabilitation of SCI patients. We hypothesized that using the Treadport instead of a treadmill could lead to better clinical outcomes in terms of spatiotemporal parameters, kinematic parameters, and gait symmetry. Furthermore, that the Treadport would provide an increased sense of safety, comfort, and flexibility for SCI patients, which would in turn enable them to exploit their potential. In addition, exploring the virtual environment requires them to keep their head upright and maintain a proper upper-body posture, which is usually missing in training with traditional treadmills. Repeated measure ANOVA was utilized to compare gait data between the walking conditions for four subjects. The results of this preliminary study indicate that training on the Treadport led to statistically significant improvement in most of the gait parameters of interest compared to a traditional treadmill.

2.3 Methods

2.3.1 Subjects

We selected four subjects (three males and one female) with incomplete SCI as being good candidates for these preliminary studies. The inclusion criteria were that they were currently undergoing rehabilitation at Neuroworx (Sandy, UT) and they were able to ambulate independently over ground, with or without an assistive device. The exclusion criteria included inadequate range of motion, joint contracture affecting functional mobility, poor joint integrity, diminished bone density, and compromised balance. Subjects were medically stable as indicated by physician evaluation. Participants were chosen to represent a range of SCI individuals who may potentially benefit from training on the Treadport. Table 2.1 presents the subjects' information. One of the subjects (Subject 3) sometimes uses canes for assistance, but did not during experiments. Subject 4 usually uses

Table 2.1: Subjects' information

Subject	Gender	Age (years)	Weight (kg)	Height (cm)	Injury type	Rehab Duration (years)
1	female	15	55	165	T-9	1
2	male	24	58	165	L-1	1
3	male	56	76	178	C-4,5	4
4	male	69	87	180	C-5	5

a wheelchair, but he can walk on the Treadport and a treadmill using canes. Each subject was given a consent form approved by the University of Utah Institution Review Board, and for one of the subjects, who was 15 years old, her parents signed a parental permission and authorization document.

2.3.2 Experimental protocol

Two experimental conditions were designed for the study. In the first condition, subjects spent six sessions of twenty minutes training on the treadmill at Neuroworx while a physical therapist was present to directly supervise them. The six sessions were spread out evenly over three weeks. The speed of the treadmill was adjusted for each individual subject based on his/her preference at the onset of each session and kept constant during the session. Partial body weight support was provided for each subject by a hydraulic-pump-actuated winch. At the sixth training session on the treadmill, kinematic and spatiotemporal gait parameters were measured by a VICON (Oxford, UK) motion capturing system. Before starting the second set of experiment, a two month delay was applied to minimize any carryover effect from the treadmill to Treadport.

The second set of experiments was carried out on the Treadport at the University of Utah. Similar to the training sessions on the treadmill, each subject spent six twenty-minute training sessions spread out evenly over three weeks. Subjects walked through a virtual cityscape while a horizontal tether, safety tether, and weight-support tether were attached to them via a rehabilitation-style harness depicted in Figure. 2.2. A safety switch was kept pressed during training by the physician or experimenter to shut off the system as soon as the subject encountered any difficulties. Partial body-weight support was provided by means of a motorized winch hanging from the Treadport's room ceiling. The subject's weight was used to set the initial value for the weight parameter in the Treadport control algorithm. The weight parameter determines the force exerted by the horizontal tether on the subject to simulate inertia force as the belt accelerates. The initial value of the weight parameter for each subject was manually modified slightly during his/her first session to find a proper value according to the subject's comfort. This value was then maintained for all six trials.

In both the treadmill and Treadport experiments, the subjects were instructed to walk as fast as they were comfortable with. In the case of the Treadport, the subjects set their speed as they would during normal walking. In the case of the treadmill, the subjects verbally instructed the physical therapist to adjust the speed of the treadmill.

2.3.3 Data collection

Gait kinematics and spatiotemporal parameters were recorded by the VICON motion capturing system, comprised of six cameras located around a calibrated volume. Cameras had a sampling

(a) (b)

Figure 2.2: (a) Subject 2 on the treadmill at Neuroworx, (b) Subject 4 on the Treadport at the University of Utah

frequency of 200 Hz and high accuracy to detect the position of 9– mm–diameter markers on the subjects' skin as depicted in Figure. 2.2. Motion capturing sessions were independent sessions on different days after accomplishing six sessions of training. Motion capturing started after letting subjects walk for six minutes to reach their steady state on both the treadmill and the Treadport. We captured five trials per subject including at least five gait cycles for each subject.

2.4 Data postprocessing

2.4.1 Joint angles

Kinematic variables are thought to be the best control variables for gait analysis [4]. Since major changes in the joint angles occur in the sagittal plane, we decided to choose the hip and knee joint angles for our study. Due to the visibility constraints imposed by wearing the harness, and also not using any cameras in front of the subjects because of the screens, we did not use the default gait model of the VICON system for motion capturing. On each body segment including torso, femurs, tibia, and foot, we used retro-reflector markers to define them as rigid bodies and then we defined a unit vector in 3D space for each segment. The dot product of two adjacent vectors was taken to evaluate the cosine of joint angles between segments.

2.4.2 Spatiotemporal parameters

Spatiotemporal and timing parameters are of high importance for gait analysis since they reveal more details about the patient's gait and can help us to compare our two walking conditions more comprehensively. The most important events during the gait cycle are heel-strikes and toe-offs, by which all other parameters are defined (Figure. 2.3). Usually, visual inspection of heel and toe markers' trajectories is carried out to detect heel-strikes and toe-offs. However, some researchers have recently proposed new methods to automatically detect these events and evaluate spatiotemporal parameters [43, 44]. To account for subjects' various heights, the three parameters speed, cadence, and stride length were normalized using the procedures in [4] which yields the normalized speed $\widetilde{S}$, cadence $\widetilde{C}$, and stride length $\widetilde{L}_{stride}$:

$$\widetilde{S} = \frac{S}{\sqrt{h \cdot g}} \tag{2.1}$$

$$\widetilde{C} = C\sqrt{\frac{h}{g}} \tag{2.2}$$

$$\widetilde{L}_{stride} = \frac{L_{stride}}{h} \tag{2.3}$$

where h is the subject's height in meters, and g is gravity (9.81 m/s^2).

2.4.3 Symmetry

Symmetry in contralateral joint angles is a characteristic of normal walking. Both legs should repeat almost an identical motion with a phase shift due to the opposite motion of the legs. The cor-

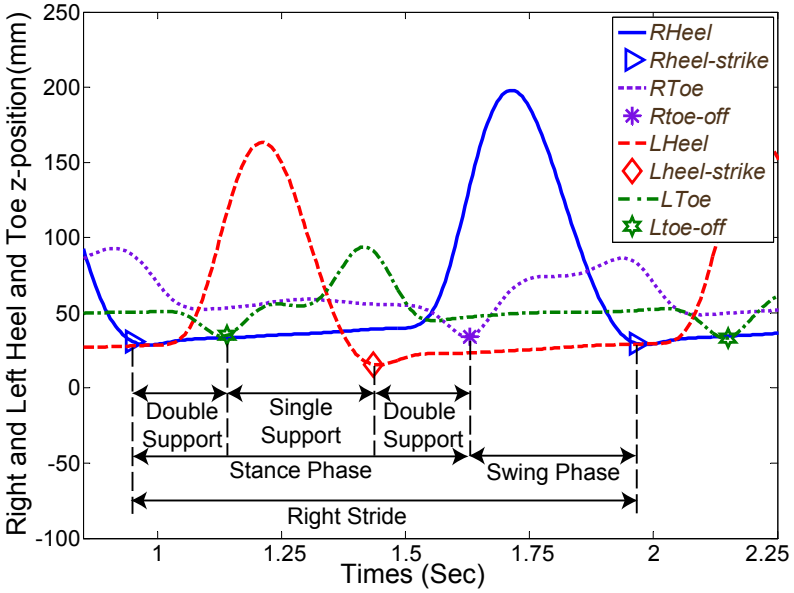

Figure 2.3: Phases in a right stride cycle (Subject 2)

relation coefficient between right and left joint angles was calculated to show the linear dependence between the two signals. First, the signals were synchronized by performing the phase shift before analysis. Figure. 2.4 demonstrates the signals before and after synchronization. The correlation coefficient ρ_{xy} was then calculated from [45].

$$\rho_{xy}(\tau) = \frac{C_{xy}(\tau)}{\sqrt{C_{xx}(0)C_{yy}(0)}} \tag{2.4}$$

where x and y are right and left joint angles, C_{xy} and C_{xx} are cross and auto correlations respectively, and τ is the time delay between two signals (right and left feet's markers).

2.5 Results

To evaluate the effect of training on the Treadport compared to a traditional treadmill, we used kinematic, spatiotemporal, and symmetry parameters. For kinematic parameters, the range of motion (ROM) of hip and knee joint angles are presented in Table 2.2, and Table 2.3 presents the spatiotemporal parameters. In both tables, normal values for human gait have been presented for comparison. Both legs' parameters are illustrated and evaluated separately to account for the asymmetric ambulation of subjects. The Shapiro-Wilk test [46] of normality was performed on the collected data, however ANOVA is robust to this assumption.

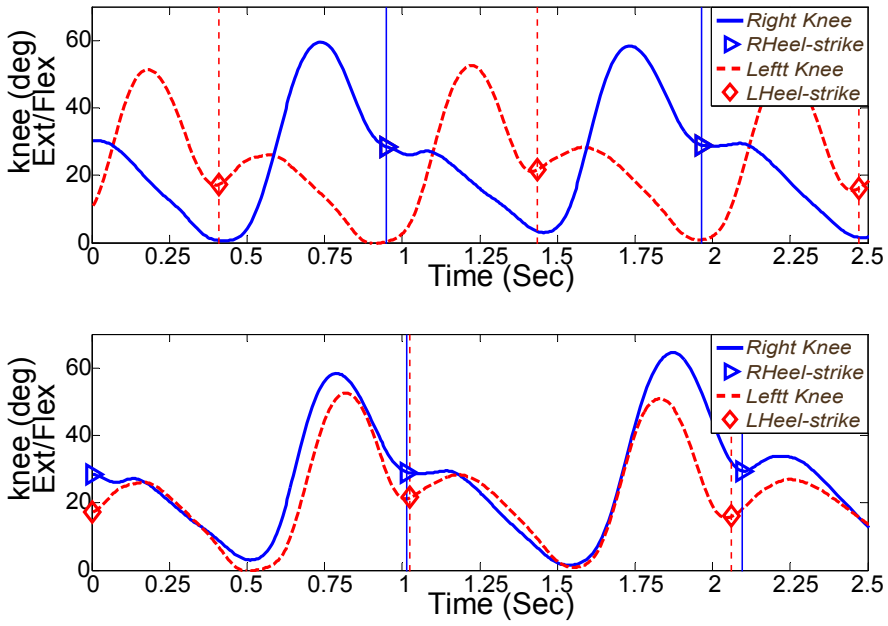

Figure 2.4: Right and left joint angles for Subject 2 (top) before synchronization and (bottom) after synchronization.

Table 2.2: Joint range for hip and knee (degrees) in sagittal plane for treadmill and Treadport walking. Data given as Mean(Standard Deviation). A $+$ symbol indicates a statistically significant ($p < 0.05$) improvement in the Treadport vs. the treadmill. A $-$ symbol indicates a statistically significant decline.

			Treadmill		Treadport	
Subject	Parameter	Ideal values	Left	Right	Left	Right
	Hip	40	28.92(2.25)	22.95(1.42)	30.8(3.5)	$28.87(1.85)^{+}$
1	Knee	65	42.87(1.61)	56.85(0.63)	$48.1(3.1)^{+}$	53.74(2.5)
	Hip	40	22.47(1.67)	25.33(1.62)	27.6(1.33)	25.38(0.85)
2	Knee	65	42.16(2.72)	66.19(3.63)	$50.08(2.42)^{+}$	59.12(2.95)
	Hip	40	28.33(0.47)	28.09(0.01)	$25.85(0.78)^{-}$	$24.27(0.94)^{-}$
3	Knee	65	54.3(0.83)	45.17(0.1)	$59.04(1.04)^{+}$	$51.97(1.57)^{+}$
	Hip	40	19.44(0.57)	17.80(0.2)	21.22(2.48)	17.23(1.32)
4	Knee	65	32.47(1.0)	19.57(1.12)	36.36(2.71)	22.19(2.48)

In Table 2.2 and 2.3, a $(+)$ superscript indicates a statistically significant improvement in the Treadport compared to the treadmill for a given parameter, whereas a $(-)$ denotes a statistically significant decline. For those parameters that do not have any superscripts, no statistically significant changes were observed.

A normal range of motion for the knee joint during walking is within the full range of flexion of $0°$–$65°(70°)$, and a normal range of motion of the hip joint is within $10°$ of extension and $30°$ of flexion [4], [47, 48]. In Table 2.2, a statistically significant change toward the normal range of motion is considered an improvement. Spatiotemporal analysis has an advantage that its techniques are standardized and reasonably reliable. Improvements in spatiotemporal parameters also correlate with improvements in a person's functional ambulation. For the spatiotemporal parameters— normalized stride, normalized cadence, normalized speed, and step length— an increase is considered an improvement [49]. In healthy human walking, the percentage of the gait cycle devoted to the swing phase is approximately 40% and the percentage of stance phase time is 60%; approaching these two values for swing and stance times is desired. The same analogy can be applied to single support and double support time, where approaching 40% and 20%, respectively, is sought [47, 48] (Table 2.3). The correlation coefficient indicates how much the right and left joint signals are similar to each other, where $\rho = 1$ stands for perfect symmetry in walking (Table 2.4).

Since subjects differed in terms of medical conditions and the nature of their injuries, we performed ANOVA within a given subject, rather than across subjects, to quantify any improvement or decline when walking in the Treadport relative to walking on the treadmill. The following summarizes the results of each subject, including their own responses to our questionnaire.

Table 2.3: Spatiotemporal gait parameters for treadmill and Treadport walking. Data given as Mean(Standard Deviation). A $+$ symbol indicates a statistically significant improvement ($p < 0.05$) in the Treadport vs. the treadmill. A $-$ symbol indicates a statistically significant decline.

			Treadmill		Treadport	
Subject	Parameter	Ideal values	Left	Right	Left	Right
1	Normalized Stride Length	0.71–0.73	0.36(0.01)	0.34(0.01)	$0.45(0.02)^{+}$	$0.45(0.02)^{+}$
	Normalized Speed	0.27–0.28	0.11(0.01)	0.10(0.01)	$0.15(0.04)^{+}$	$0.15(0.02)^{+}$
	Normalized Cadence	45–47	38.47(0.73)	35.81(1.89)	40.74(1.66)	$42.27(0.75)^{+}$
	Stance Phase (%)	60	66.57(1.6)	67.81(1.1)	$63.1(1.5)^{+}$	64.8(2.5)
	Swing Phase (%)	40	33.43(1.6)	32.19(0.01)	$36.9(1.5)^{+}$	35.2(2.5)
	Single Support Phase (%)	40	32.27(0.8)	33.03(0.5)	35.5(2.3)	$36.6(1.3)^{+}$
	Double Support Phase (%)	20	34.3(2.18)	34.78(1.45)	$27.6(2.5)^{+}$	$28.87(3.1)^{+}$
2	Normalized Stride Length	0.71–0.73	0.41(0.01)	0.37(0.01)	0.43(0.02)	$0.41(0.024)^{+}$
	Normalized Speed	0.27–0.28	0.15(0.03)	0.14(0.01)	$0.17(0.01)^{+}$	$0.16(0.01)^{+}$
	Normalized Cadence	45–47	46.02(2.10)	44.09(2.66)	48.31(1.53)	45.96(1.89)
	Stance Phase (%)	60	68.2(1.8)	66.8(1.5)	67.7(0.9)	$65.1(0.9)^{+}$
	Swing phase (%)	40	32(1.8)	33.2(1.5)	32.3(0.9)	35.1(0.9)
	Single Support Phase (%)	40	33.1(0.8)	32.3(1.7)	34.9(0.8)	32.2(0.3)
	Double Support Phase (%)	20	34.9(1.8)	34.4(2.5)	$32.8(1.1)^{+}$	32.8(0.8)
3	Normalized Stride Length	0.71–0.73	0.61(0.00)	0.63(0.00)	$0.69(0.01)^{+}$	$0.69(0.01)^{+}$
	Normalized Speed	0.27–0.28	0.17(0.00)	0.17(0.12)	$0.24(0.00)^{+}$	$0.24(0.00)^{+}$
	Normalized Cadence	45–47	33.43(0.61)	34.32(0.06)	$42.74(0.77)^{+}$	$42.19(1.03)^{+}$
	Stance Phase (%)	60	63.9(1.3)	61.2(0.1)	$63.2(0.6)^{+}$	$60.1(0.6)^{+}$
	Swing Phase (%)	40	36.1(1.3)	38.8(0.1)	$37.2(0.6)^{+}$	$39.4(0.6)^{+}$
	Single Support Phase (%)	40	38.1(1.8)	35.5(0.7)	$39.6(0.9)^{+}$	$37.3(0.1)^{+}$
	Double Support Phase (%)	20	25.8(1.31)	25.7(0.7)	$23.4(1.2)^{+}$	$23.3(1.6)^{+}$
4	Normalized Stride Length	0.71–0.73	0.34(0.03)	0.34(0.02)	0.32(0.04)	$0.37(0.01)^{+}$
	Normalized Speed	0.27–0.28	0.03(0.02)	0.03(0.02)	0.04(0.01)	$0.05(0.02)^{+}$
	Normalized Cadence	45–47	13.25(0.29)	13.32(0.15)	$15.92(0.88)^{+}$	$21.2(2.83)^{+}$
	Stance Phase (%)	60	78.6(2.4)	84.7(0.5)	77.6(1.9)	$80.4(0.1)^{+}$
	Swing Phase (%)	40	21.4(2.4)	15.3(0.8)	22.4(1.9)	$19.6(0.1)^{+}$
	Single Support Phase (%)	40	18.2(3.8)	22.3(1.2)	20.1(0.06)	$20.2(0.01)^{-}$
	Double Support Phase (%)	20	60.4(6.2)	62.4(0.9)	57.5(1.9)	$60.3(0.01)^{+}$

Table 2.4: Correlation coefficient ρ_{xy} for treadmill and Treadport walking

	Hip		Knee	
Subject	Treadmill	Treadport	Treadmill	Treadport
1	0.76	0.91	0.89	0.89
2	0.61	0.95	0.82	0.94
3	0.64	0.80	0.97	0.97
4	0.91	0.25	0.85	0.57

Subject 1 was a teenaged female with a T-9 injury. She demonstrated a significant improvement in 10 of 14 spatiotemporal parameters considered, and no significant declines. She demonstrated a large improvement in hip symmetry, and of all of the subjects tested, she demonstrated the most improvement in joint ROM. Subject 1 said "I liked the life-like pictures...but would have liked it if it was a little more like outdoors." and "I liked how wide the Treadport was. It made me less nervous where my feet were because there was more room. I was not worried about falling off if I made a mistake."

Subject 2 was a young man with an L-1 injury. Although results for joint ROM were mixed, he showed a significant improvement in 5 of 14 spatiotemporal parameters. He also, showed a large improvement in both hip and knee symmetry. Subject 2 felt that the Treadport, compared to normal walking, "provides resistance and helps to strengthen leg muscles." He said "Screen projections provide the feeling of direction and movement as opposed to treadmill walking in the same place."

Subject 3 was a middle-aged man with C-4,5 spinal cord injury. Results for joint ROM were mixed. Significant improvements were observed in all of his spatiotemporal parameters. His timing pattern converged to what is considered a normal pattern in the literature. He also developed a more symmetric hip movement. Subject 3 also felt comfortable attempting to jog on the Treadport, which he had never done on a treadmill.

Subject 4 was an elderly man with a C-5 spinal cord injury. He had to use his canes during walking on both the treadmill and Treadport and needed the most amount of weight support compared to other subjects (more than 11 Kg). Due to his condition, analyzing his data is complicated and, to some extent, inconclusive. Although there were significant positive changes in 7 of 14 of his spatiotemporal and timing parameters, his symmetry indices deteriorated dramatically. Subject 4 said "I found it better to use my canes because it is so much wider than the normal treadmill. It is also nice to have scenery on three sides. I can see a real advantage of being able to move sideways, go up and down the hills, even though my ability didn't enable me to do that very well. I could say that it was harder for me because I had to propel it. But, it is more like walking. I think it could be a real advantage for people like me."

2.6 Discussions

In this article, we presented the results of our preliminary study for investigation of the University of Utah Treadport for gait rehabilitation. We hypothesized that training on the Treadport has potential benefits for spinal cord injury, stemming from its virtual outdoor environment, large treadmill size, and self-directed motion. We compared locomotion training on the Treadport to training on a standard rehabilitation treadmill. Four partial-SCI patients were chosen as good candidates for the studies. Kinematic parameters, spatiotemporal parameters, and symmetry indices were utilized as metrics for making a comprehensive comparison. To carry out the gait measurements, a VICON motion capturing system was utilized. An algorithm was proposed for detecting the key gait events during ambulation on the treadmill and the Treadport in the absence of force plates.

The results of this preliminary study indicate that walking in the Treadport has significant benefits relative to walking on a treadmill, across subjects, in terms of the majority of spatiotemporal parameters considered. The study indicates that patients choose to walk faster on the Treadport than on a treadmill, possibly due to an increased sense of safety or due to the motivation provided by the virtual environment. The Treadport also improved gait symmetry in three of four subjects, likely due to the gait being patient driven rather than treadmill driven. The fourth subject, for whom gait symmetry actually declined, was the only subject to use canes during the experiments, indicating that rehabilitation in the Treadport may not be appropriate for certain patients. However, this fourth subject did see a net improvement in spatiotemporal parameters, so results for this subject are somewhat inconclusive. When comparing hip and knee joint range of motion with the treadmill and Treadport, results are mixed, and one system does not appear clearly better than the other. However, as presented in Table 2.2, joint ranges of right and left legs for all the subjects, except for Subject 4, had become more similar by the end of training on the Treadport.

The outcome of this preliminary study would imply that standard treadmills may impose some constrains on a patient's motion that can be overcome on the Treadport. Since the goal of gait rehabilitation is to prepare patients for real-world walking, training should closely simulate real-world conditions. Three major avenues that can be explored by means of the Treadport are the use of different virtual environments to influence and encourage the patients, the application of perturbations to enhance motor learning, and therapy that adapts to the patient's performance in real time.

2.7 Acknowledgments

We would like to thank Dr. Mark Minor for his technical contributions and Kyle Crandall and Erin Parsons for their assistance in data collection. We would also like to thank Dr. Daniel Ferris from the University of Michigan for his helpful suggestions.

CHAPTER 3

KINESTHETIC FORCE FEEDBACK AND BELT CONTROL FOR THE TREADPORT LOCOMOTION INTERFACE

The following chapter is aimed at improving the control system of the Treadport locomotion interface, with results that generalize to any treadmill that utilizes an actuated tether to enable self-selected walking speed.

3.1 Abstract

This paper describes an improved control system for the Treadport immersive locomotion interface, with results that generalize to any treadmill that utilizes an actuated tether to enable self-selected walking speed. A new belt controller is implemented to regulate the user's position; when combined with the user's own volition, this controller also enables the user to naturally self-select their walking speed as they would when walking over ground. A new kinesthetic-force-feedback controller is designed for the tether that applies forces to the user's torso. This new controller is derived based on maintaining the user's sense of balance during belt acceleration, rather than by rendering an inertial force as was done in our prior work. Based on the results of a human-subjects study, the improvements in both controllers significantly contribute to an improved perception of realistic walking on the Treadport. The improved control system uses intuitive dynamic-system and anatomical parameters and requires no *ad hoc* gain tuning. The control system simply requires three measurements to be made for a given user: the user's mass, the user's height, and the height of the tether attachment point on the user's torso.

3.2 Introduction

Treadmills are commonly used in locomotion interfaces to enable users to walk through virtual environments, and are widely used in physical exercise and gait rehabilitation [7, 5, 8]. Although treadmill speed has traditionally been set by manual control, the trend is for self-selected speed adaptation by measurement of user position or some other form of user intent. This provides for the belt speed to be instantaneously set by a user, leading to a more natural locomotion experience. The task for the treadmill controller is to achieve accurate and stable belt motion, whether the user is walking or running, going forward or backward, or starting or stopping.

We have been developing one particular locomotion interface, the Treadport (Fig. 3.1), whose key features include the following: (1) a large belt (1.8×3 meters); (2) a six-axis mechanical tether attached to the back of a user wearing a harness, which is used to measure body position and orientation, to control belt speed, and to apply horizontal kinesthetic force feedback to the user [42]; and (3) a six-degree-of-freedom mechanism-based harness with a telescoping spine to accommodate the complex motion of the user's back without slipping, and with the ability to change the point of force application of the mechanical tether to the user [51]. There is a safety dead-man switch held by the user throughout locomotion on the Treadport, and if the user wants to stop the system for any reason, it can be done by simply releasing the switch. The controller of the Treadport is implemented in dSPACE1103. Other characteristics of the Treadport that are not utilized in the present study include: programmable vertical weight support; a CAVE-like [52] visual display; the

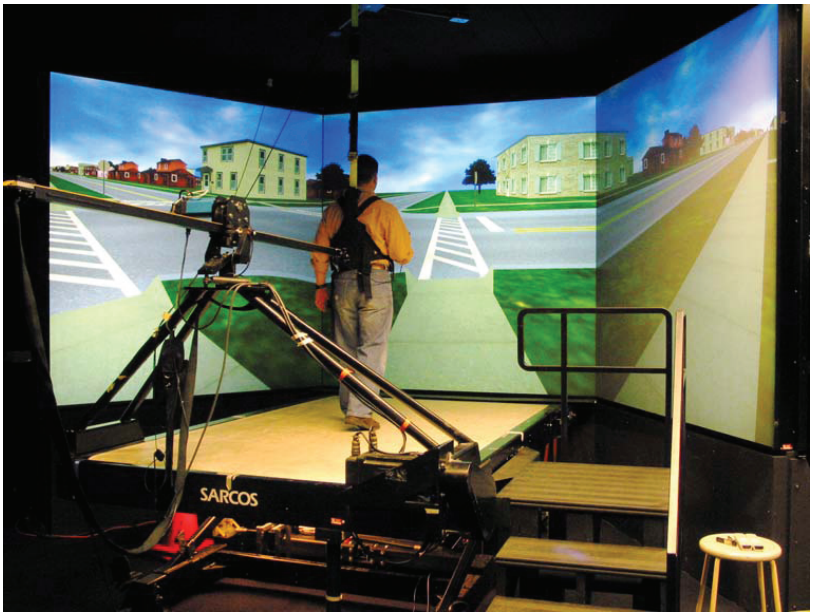

Figure 3.1: Treadport locomotion interface. For clarity, the system is shown before the addition of the wind-display system.

ability to turn in the virtual environment [53]; and a wind display system [54].

A key difference between the Treadport and most other treadmill-style locomotion interfaces is the presence of the mechanical tether, which can generate forces on a user via a harness [55]. The kinematics of the mechanical tether (see Fig. 3.1) include a two-axis rotary joint at the base (sensed with potentiometers, but not actuated), a prismatic joint (sensed with an optical encoder, and actuated with a brushed DC motor), and a three-axis rotary joint at the attachment point with the user's harness (sensed with potentiometers, but not actuated). Without a mechanical tether, it is not possible for treadmill locomotion to be energetically realistic when the user's body remains nearly stationary with respect to the ground, since inertial forces due to body acceleration are missing. Previously, Christensen et al. presented a tether controller that implemented direct inertial force feedback [55]. With recent application of the Treadport to rehabilitation of patients with spinal-cord injury [26], limitations of this controller became apparent due to the fragile walking conditions of these patients. It was felt too difficult to start walking by pulling against the tether, stopping was sometimes unnatural due to the improper recentering controller, and the apparent inertia felt too large.

To address the issues described above, in this paper we present a new kinesthetic-force-feedback controller based on maintaining the user's sense of balance as the belt moves under their feet, regardless of the underlying belt control system. We revisit the Treadport's belt controller by implementing a previously published controller from a non-tether treadmill system and determining

the dynamic properties of that controller that result in the best sense of realism within the Treadport. We also present an adaptive dead-zone algorithm that enables users to stand still on the belt when desired without fear of the belt moving unintentionally. A stability analysis is conducted to ensure the stability of closed-loop system with a user with their own volition in the loop. In human-subject experiments, our new Treadport control system achieves a sense of stable and smooth acceleration and deceleration when moving forward or backward, stopping slowly or quickly, and when standing (and swaying) comfortably without causing involuntary motion of the belt. We demonstrate with statistical significance how users' perception of realistic walking is enhanced by using our new controller: the kinesthetic-force-feedback controller is compared to the previous controller, and the most-preferred dynamic properties of the belt-speed controller are determined in a separate experiment. Although experiments are conducted with the unique Treadport locomotion interface, the results in this paper will generalize to any locomotion device with self-selected speed and a tether capable of applying horizontal forces to the user.

Several methods have been used previously to estimate and generate a user's self-selected walking speed on a treadmill belt. In [55], the desired velocity of the treadmill belt was derived from a proportional-integral (PI) controller. A similar PID approach is taken in [56]. The PI and PID gains were chosen through an *ad hoc* procedure and remained constant for all users. More recently, [57] proposed a second-order dynamic observer to estimate the desired belt velocity. A different approach is taken in [58], in which a rigid bar with a force sensor is attached to the user, and user force against the bar is used to generate belt speed through an admittance controller. Gait parameters such as ground reaction forces [59, 60, 61] and foot-swing velocity [16] can be used to update the treadmill speed.

The major challenge for treadmill-style locomotion interfaces for simulating overground walking is dealing with the acceleration of the belt, which affects a user's stability since it exerts forces on the user that would not be felt during overground walking. Recently, Souman et al. [57] used a position controller combined with a dynamic observer for estimating voluntary walking speed on a 6-meter-long treadmill. A goal of their research is to present realistic vestibular stimulation during acceleration, and consequently their treadmill belt is long in order to allow real acceleration before reaching the front of the belt. If their controller is applied to smaller treadmills, a user would feel undesired large inertial forces [62]. Most recently, Kim et al. [62] proposed an estimation limiter to attenuate the unwanted inertial forces due to acceleration/deceleration of the treadmill belt. Of course, it is not possible to completely eliminate these unwanted forces with any belt of finite length.

Energy expenditure on treadmill devices is another important consideration. Frishberg et al. [63] showed that sprinting on a treadmill requires significantly less energy than sprinting on the ground.

Lee et al. [4] found that global patterns including kinematics and kinetics are similar between overground and treadmill locomotion, however the energy cost, regardless of the method used to compute it, is significantly different. Crétula et al. [64] showed that for computing mechanical work during treadmill locomotion and comparing it with overground, variations in belt speed must be taken into account. Acceleration/deceleration of a treadmill belt due to speed adaptation requires less energy expenditure, which can be compensated using kinesthetic force feedback.

3.3 Control algorithm

The objectives of the Treadport's controller design are to achieve the user's intended self-selected walking speed while mitigating the obtrusive and unnatural effects of belt acceleration on the user, to create a natural walking experience similar to overground locomotion. To fulfill these objectives, two separate controllers have been implemented to work together with the human user as a complete closed-loop system: (1) A recentering controller regulates the user's position to some reference position on the belt (typically near the center), which ultimately provides an instantaneous desired belt velocity command to a low-level belt-speed controller (the low-level belt-speed controller, as well as an adaptive dead zone to improve system behavior when the user is attempting to stand still, are included as supplemental material). (2) A kinesthetic force-feedback controller exerts a horizontal force on the user's torso via a mechanical tether in order to create a stable and energetically realistic walking experience. In this section, we describe our recentering controller and our kinesthetic force-feedback controller. We then analyze the stability of the combined system, with a human user in the loop.

3.3.1 Recentering controller

The principle of self-selected speed, in its most basic form, is quite simple: a user walking on the belt should be kept near some reference position (typically near the center of the belt), and if the user advances beyond the reference position it indicates that the user's intent is to increase walking speed, so the belt speed is increased until the user is brought back to the reference position with a new equilibrium walking speed, with deceleration handled analogously. Any scheme that accomplishes this goal could be a valid self-selected speed controller. It is also necessary on any treadmill belt of finite length that some controller exists to prohibit the user from walking off the edge of the belt. In practice, a well-designed recentering controller also serves as a self-selected speed controller once a human user, with the ability to establish their own self-selected gait pattern, is included in the closed-loop system.

Because human users have their own volition, a user may choose to stop walking by planting their feet instantaneously at any moment, and in that moment the recentering controller must act to

bring the now-riding user to a stop quickly and safely. This is an additional factor that should be considered when designing the recentering controller.

We implement a simple PD controller for recentering that uses the position error between the user and the reference position to set the desired belt acceleration:

$$a_{bd} = K_x(x_{\text{ref}} - x_p) - K_v v_p \tag{3.1}$$

where x_p is the person's position, v_p is the person's velocity, and x_{ref} is the reference position, all in the inertial frame (Fig. 3.2); a_{bd} is the desired belt acceleration; K_x and K_v are proportional and derivative gains, respectively. Note that x_{ref} is static, so its derivative is always zero. We see that the belt tends to be accelerated backward from the user's point of view whenever they are either in front of the reference position (i.e., too close to the front of the belt) or moving forward in the inertial reference frame (i.e., getting closer to the front of the belt), with an analogous and opposite behavior when accelerating the belt forward.

In the Treadport, the position x_p and velocity v_p are measured by a mechanical tether attached to the user, via the system's forward kinematics. The resulting desired acceleration a_{bd} is then numerically integrated to derive the instantaneous desired belt velocity v_{bd}, which is then given to the low-level belt-speed controller. Equation (3.1) is mathematically similar to the "second-order controller" in [57]. The belt velocity v_b can be expressed in terms of the user's speed relative to the belt, $v_{p/b}$, and their speed relative to the inertial frame v_p:

$$v_{p/b} = v_p - v_b \quad \leftrightarrow \quad v_b = v_p - v_{p/b} \tag{3.2}$$

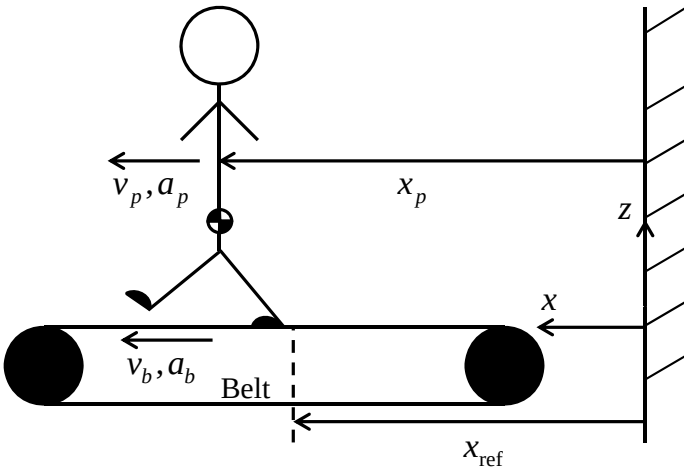

Figure 3.2: A user on the Treadport. The user's position x_p at the tether attachment point and the reference position x_{ref} are measured with respect to the same arbitrary inertial reference frame. The belt's velocity v_b and acceleration a_b are defined as positive in the forward direction.

The user perceives $v_{p/b}$ as their instantaneous walking speed. Assuming that the dynamics of the low-level belt-speed controller are of sufficiently high bandwidth relative to the dynamics of the recentering controller (the bandwidth of our belt-speed controller is an order of magnitude faster than the recentering controllers considered), we can drop the "desired" subscript "*d*" in the desired speed v_{bd} and acceleration a_{bd} for a simplified analysis. Substituting (3.2) into (3.1), the Laplace transform yields:

$$s(v_{p/b} - v_p) = K_x(x_p - x_{\text{ref}}) + K_v v_p \tag{3.3}$$

leading to the transfer function for the user's position:

$$x_p = \left(\frac{K_x}{s^2 + K_v s + K_x}\right) x_{\text{ref}} + \left(\frac{s}{s^2 + K_v s + K_x}\right) v_{p/b} \tag{3.4}$$

We observe that the position of the person on the belt is a function of two independent variables: x_{ref} and $v_{p/b}$. We see that with $v_{p/b} = 0$, which occurs when the user plants their feet and rides the belt, the person will eventually be brought to x_{ref} with no steady-state error, with dynamics given by a simple second-order system response. If we consider a step-input in $v_{p/b}$, corresponding to the person walking at some new self-selected speed, what we will observe is an impulse response of a simple second-order system, which has no steady-state component. Thus, the desired recentering and self-selected-speed components are both achieved.

We can express the characteristic equation of the resulting system in terms of the standard form of a second-order system with damping ratio ζ and natural frequency ω_n as its parameters: $s^2 + 2\zeta\omega_n s + {\omega_n}^2$. Such a representation makes the parameter study more intuitive and facilitates a systematic procedure for choosing gains, rather than choosing them on an *ad hoc* basis. Since ζ and ω_n are positive values, provided our original gains are both positive values, one can easily verify the stability of the system. Both ζ and ω_n influence the transient response of the controller, which in turn significantly affects the perception of realistic walking on a locomotion interface.

To investigate the effect of parameters on walking with self-selected speed, we simulated the behavior of a user on the belt starting at rest and then changing the self-selected speed to $v_{p/b} =$ 1 m/s, and then coming to a stop after a few seconds. In Fig. 3.3 we see the different behaviors of x_p due to changes in the value of ζ, while ω_n is held constant. For $\zeta < 1$ (underdamped), the user's position has an oscillatory transient response. Such a behavior is not desirable since it can disturb the user's sense of balance; we find that it is disconcerting to be brought backward on the belt, come to a complete stop relative to the inertial frame, and then be brought forward again. We initially hypothesized that a critically damped system $\zeta = 1$ would be the most desirable, in that it would eliminate any oscillation, but would still result in a fast system. However, we find that a

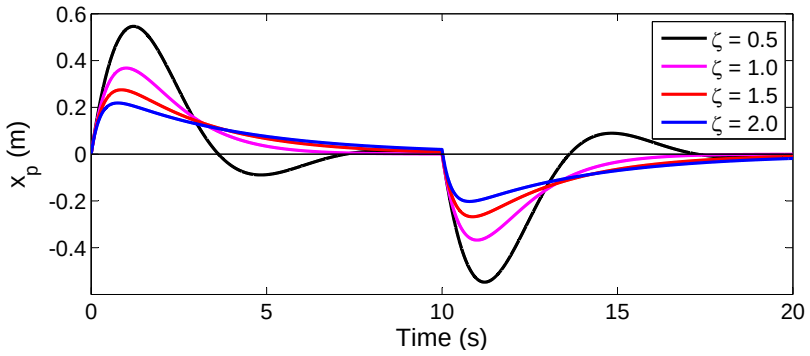

Figure 3.3: The effect of different values of ζ while $\omega_n = 1$ rad/s on a user's position x_p during walking. Starting from rest, $v_{p/b} = 1$ m/s for the first 10 sec, and then $v_{p/b} = 0$ m/s.

higher damping ratio actually results in a more-desirable response, since the user is not allowed to move forward as much on the belt before being recentered.

An additional benefit of adding more damping to the system is to increase stability robustness. The phase margin of the system is related to the damping ratio [65], with phase margin being quite sensitive to ζ in the approximate range $0 < \zeta \leq 1.2$, and with diminishing returns on phase margin for further increases in ζ. In our pilot tests, we found that increasing $\zeta > 1.5$ did not lead to noticeable differences in the controller; this can also be observed in Fig. 3.3 by comparing the responses with $\zeta = 1.5$ with $\zeta = 2$, which are very similar. We also note that these system properties were observed regardless of the value of ω_n used (although that would affect the settling time). From the above considerations, we conclude that a damping ratio value of $\zeta = 1.5$ is a desirable value in terms of system response and stability robustness, and we will use this value throughout the remainder of the experiments.

We can now investigate the effect of ω_n on the response of the system. Having selected a constant $\zeta = 1.5$, rather than using ω_n, we can use a more intuitive parameter: an effective time-constant τ. For an overdamped system, the dominant (i.e., slowest) pole is located at

$$r_{\text{dom}} = -\zeta\omega_n + \omega_n\sqrt{\zeta^2 - 1} \tag{3.5}$$

and the effective time-constant is calculated as

$$\tau = -\frac{1}{r_{\text{dom}}} \tag{3.6}$$

Given any desired combination of damping ratio and time-constant, we can compute the required natural frequency:

$$\omega_n = \frac{1}{\tau(\zeta - \sqrt{\zeta^2 - 1})} \tag{3.7}$$

Finally, we set our gains as $K_x = \omega_n^2$ and $K_v = 2\zeta\omega_n$.

The choice of τ has a significant impact on the behavior of x_p, as shown in Fig. 3.4, and on the user's perception of realistic walking. If τ is chosen too small, then the controller returns the user to x_{ref} quickly, and in pilot testing we observed that this can result in the belt feeling too responsive, almost as if it moves before the user was expecting it to move. If τ is selected too large, then a larger deviation in the user's position from x_{ref} is tolerated by the controller, which can result in the user walking nearer to the edge of the belt (and closer to the screens) before being drawn back to the center, which can be disconcerting. The value of τ is limited on the low end by the belt motor's capabilities, and on the high end by the allowable traveling distance from x_{ref} based on the length of the belt and other similar constraints.

3.3.2 Kinesthetic force feedback

When walking overground, a person must put in mechanical work to accelerate their body, equal to the change in kinetic energy of the person's mass, and this work is ultimately done by the person's feet applying forces to the ground. When walking through a virtual world on a treadmill, it is possible to accelerate through the virtual world by simply increasing the belt speed, without the user putting in the same amount of work that would be required overground; this can negatively impact on the user's sense of balance, and can lead to a locomotion interface that feels unstable (similar to walking on ice). The Treadport utilizes a mechanical tether to apply a force f_t to the user's torso, as shown in Fig. 3.5, and this kinesthetic force feedback can be used to increase the user's sense of balance and stability, and to make the work done by the user to accelerate in the virtual world similar to overground walking.

In prior work with the Treadport [55], the kinesthetic force feedback was set as *inertial force feedback*:

$$f_t = -ma_b \tag{3.8}$$

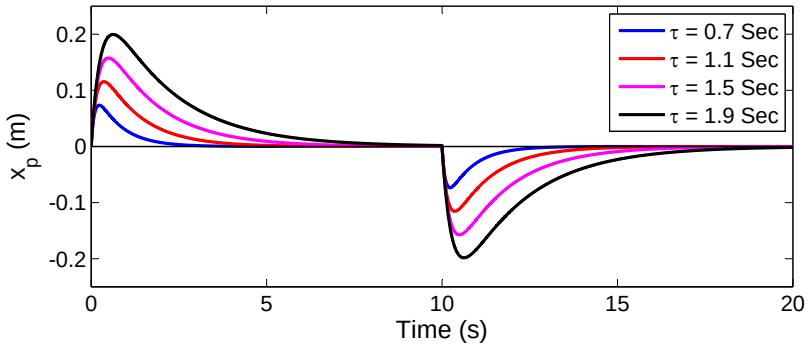

Figure 3.4: The effect of different values of τ while $\zeta = 1.5$ on a user's position x_p during walking. Starting from rest, $v_{p/b} = 1$ m/s for the first 10 sec, and then $v_{p/b} = 0$ m/s.

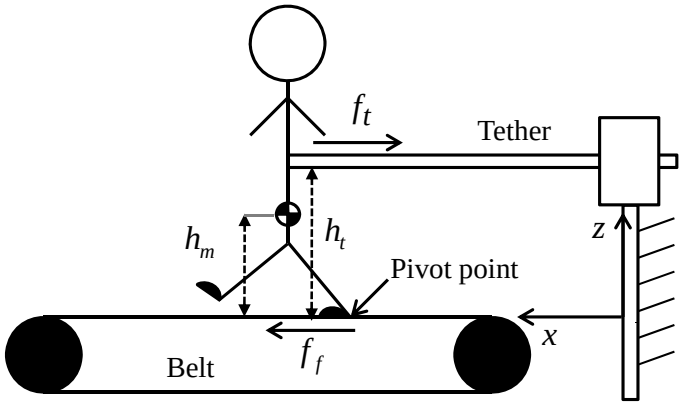

Figure 3.5: The tether force is defined as positive when pulling back on the user (in tension). The foot force is defined as positive when the belt is pushing forward on the user's foot (in compression). The tether attachment point is not assumed to be at the user's center of mass in general.

where m is the mass of the user. The rationale behind inertial force feedback is that if a person were accelerating overground with some acceleration a, it would require the person to generate a net forward force equal to ma to cause that acceleration, so the kinesthetic force feedback in the Treadport should demand such a force from the user. This inertial force feedback results in a reasonably good walking experience for the user, but often with a sense that the effective inertia of the user in the virtual environment seems slightly too high, such that starting from rest and coming to rest both seem slightly too difficult. An *ad hoc* tuning parameter to attenuate the force often results in a more desirable experience for users, and it was hypothesized that this parameter was necessary due to inaccurately modeling the user as a point mass concentrated at the harness contact point rather than considering the whole body [55].

In this section we reconsider the kinesthetic force feedback of the tether, in an attempt to provide a more realistic walking experience. Rather than considering a person walking on a treadmill belt, we instead consider a person standing on a stationary belt, and imagine that the belt is accelerating forward without the user's knowledge. This would feel like the ground was being pulled out from under the user's feet; the inertia of the user's body would not allow the body to accelerate with the feet (we assume no slip between the feet and the belt, due to friction), resulting in an angular rotation of the body in the sagittal plane and a negative impact on the user's balance. However, it is easy to imagine in this scenario that there exists a tether force (pushing forward in this case) that would prevent the user's body rotation and thus prevent the loss of balance (similar to the role played by the handrail on an escalator or moving walkway). Our new *balance-based force feedback* provides such a force.

To calculate the correct tether force f_t for balance-based force feedback, we consider the user

on the Treadport as illustrated in Fig. 3.5. We assume the user to be a rigid body in contact with the ground at some pivot point with a no-slip condition, with a body center of mass at a height h_m, and with a tether applying a force at a height h_t. There is a force f_f that the belt applies to the user's foot (defined positive in the forward direction), but which is unknown to us. Our goal is to set f_t such that the user's center of mass moves forward with the same acceleration as the belt, due to the two applied forces:

$$f_f - f_t = ma_b \tag{3.9}$$

We would also like the the resulting moments of the two applied forces to result in no rotation of the user's body about the center of mass in the sagittal plane:

$$f_f h_m + f_t(h_t - h_m) = 0 \tag{3.10}$$

By combining (3.9) and (3.10) to eliminate the unknown force f_f, we solve for the correct tether force:

$$f_t = -\frac{h_m}{h_t} ma_b \tag{3.11}$$

The value of h_t can be easily measured for a given user after the user dons the harness. The value of h_m is not trivial to measure, but it can be approximated with good accuracy given only a measurement of a user's height H as $h_m = 0.58H$ [66].

This balance-based force feedback is similar to the previous inertial force feedback in that it is proportional to the user's mass and the belt's acceleration, but typically smaller due to the coefficient h_m/h_t, which is typically less than 1. This result explains the need for the previous *ad hoc* tuning parameter to attenuate the inertial force feedback. Although the new balance-based force feedback was derived using a thought experiment that involved a *standing* user, we will show later in this paper that this new method is preferred by users over the previous inertial force feedback when *walking* on the Treadport under a variety of conditions.

Note that the value of f_t in (3.11) is the correct value to apply for a given belt acceleration a_b, regardless of how that value was selected or achieved; in this way, the kinesthetic-force-feedback controller is truly independent of the belt controller. However, the stability of the complete system, including the user and the various distributed Treadport controllers, must still be considered.

3.3.3 Stability analysis

The most commonly used model for human running is

$$v_p = v_{\text{des}}(1 - e^{-t/\tau_{\text{int}}}) \tag{3.12}$$

where v_p is a person's speed overground, v_{des} is their desired speed, and τ_{int} is the person's inherent time constant [67]. We make the assumption that this common running model is a reasonable

approximation for walking and running on the Treadport. As illustrated in Fig. 3.6, this observed behavior can be predicted by modeling a person as a mass m that controls their speed using a proportional feedback controller on velocity. The relationship between the person's internal "gain" K_{int} and the resulting time constant τ_{int} is

$$\tau_{\text{int}} = \frac{m}{K_{\text{int}}} \tag{3.13}$$

In this simple walking model, the ground applies f_f to the person's foot, which is a reaction force to the propulsive force applied by the person to the ground, to accelerate them with a_p.

Walking on the Treadport is similar to overground walking, with two major differences. First, the net force causing the person's acceleration a_p in the inertial frame is obtained by considering both the force f_f from the belt to the person's foot and the force f_t applied by the tether. Second, the person compares their desired walking speed v_{des} with their speed relative to the belt's speed $v_{p/b}$.

The resulting closed-loop system comprising a user in the Treadport is depicted in Fig. 3.7; we have included all of the elements that affect the systems dynamics, including the low-level belt-speed controller and the differentiation filter used. To analyze the stability of the system, we convert the equations into the Laplace domain. To be concise, we use $\psi = h_m/h_t$ in the subsequent

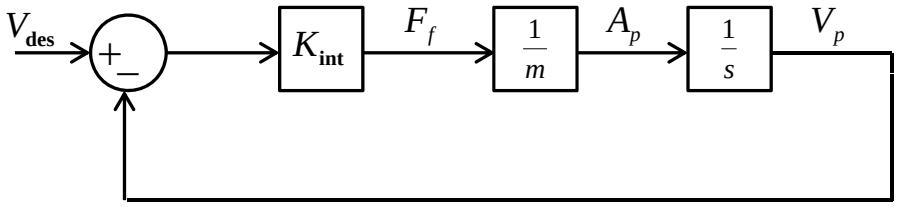

Figure 3.6: Simple human walking model.

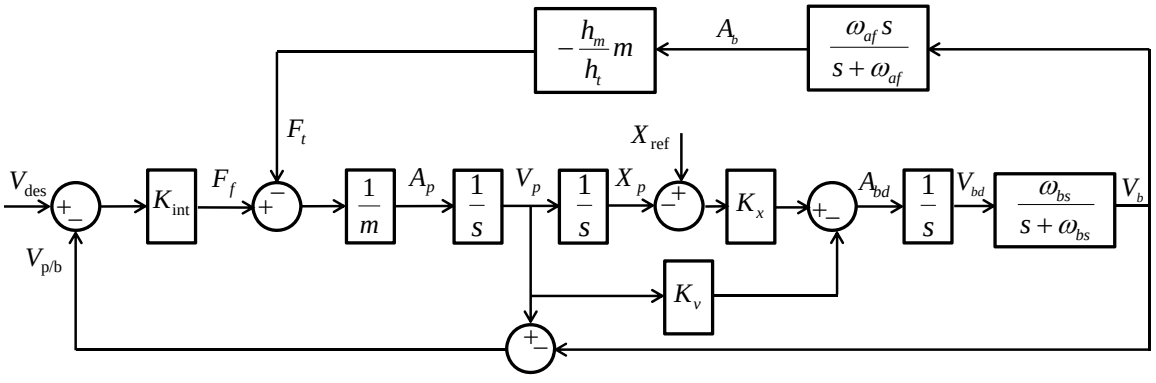

Figure 3.7: Block diagram of a user in the Treadport. The user's desired velocity V_{des} is set internally by their own volition. The reference position X_{ref} is set in the control software and is typically constant.

equations. Note that $\psi = 1$ when the tether applies its force directly at the user's center of mass, and in the Treadport $\psi < 1$ typically.

The belt speed $V_b(s)$ can be expressed as a function of the two exogenous inputs as

$$V_b(s) = \left(\frac{\omega_{\text{bs}} K_x s(ms + K_{\text{int}})(s + \omega_{\text{af}})}{\Delta(s)} \right) X_{\text{ref}}(s) - \left(\frac{\omega_{\text{bs}} K_{\text{int}}(K_v s + K_x)(s + \omega_{\text{af}})}{\Delta(s)} \right) V_{\text{des}}(s) \tag{3.14}$$

where $\Delta(s)$ is the system's characteristic equation:

$$\begin{aligned} \Delta(s) &= ms^5 + (K_{\text{int}} + \omega_{\text{af}} m + \omega_{\text{bs}} m)s^4 \\ &+ (K_{\text{int}}(\omega_{\text{af}} + \omega_{\text{bs}}) + \omega_{\text{bs}} \omega_{\text{af}} m)s^3 \\ &+ \omega_{\text{bs}}(K_{\text{int}}(K_v + \omega_{\text{af}}) + \omega_{\text{af}} m \psi)s^2 \\ &+ \omega_{\text{bs}}(K_{\text{int}}(K_x + \omega_{\text{af}} K_v) + K_x \omega_{\text{af}} m \psi)s \\ &+ \omega_{\text{bs}} \omega_{\text{af}} K_{\text{int}} K_x \end{aligned} \tag{3.15}$$

where ω_{af} is the acceleration-differentiator's filter corner frequency, and ω_{bs} is the bandwidth of the low-level belt-speed controller (see supplemental material). Equation (3.14) indicates that if a user wants to walk with V_{des}, the belt speed asymptotically approaches V_{des}, but in the opposite direction as expected ($V_b \to -V_{\text{des}}$), provided the system is stable.

Something that is not immediately evident from (3.15) is that the user's mass cancels out of the characteristic equation, once the recentering-controller gains are set as described.

To investigate the stability of the system, we first numerically explored the range of specific values being proposed for the Treadport: $\omega_{\text{af}} = 16$ rad/s, $\omega_{\text{bs}} = 9$ rad/s, $\zeta = 1.5$, $\tau_{\text{int}} \in [0.85\text{–}1.29]$ (based on [67]), $\tau \in [0.7\text{–}1.9]$ (time-constants used in the study), and $\psi \in [0.87\text{–}0.92]$ (the range of values measured with our human subjects in this study); we found that all combinations of values are stable. Next, we conducted a sensitivity analysis by fixing all variables but one at their nominal values (using $\psi = 0.9$, $\tau = 1.26\,s$, and $\tau_{\text{int}} = 1$ as nominal) and then varying the remaining parameter from zero to infinity, using root-locus techniques, and examined the effect on stability. We found the stability ranges of the mentioned parameters to be as follows: $\omega_{\text{af}} \geq 3$ rad/s, $\omega_{\text{bs}} \geq 2$ rad/s, $1 \leq \zeta \leq 2.3$, $\tau_{\text{int}} > 0$, $\tau \geq 0.46$, and $0.1 \leq \psi \leq 3.9$. All of the values used in this study safely fall in the stability ranges of these parameters. It is observed that if no force feedback were to be used (i.e., $\psi = 0$) with all other parameters held constant, the system would become unstable. This observation implies that if no force feedback is used during locomotion on the Treadport, the stability of the system should be ensured by changing other parameters prior to any experiment.

3.4 Experiment design and methods

The purpose of the new controller is to enhance the realism of walking on the Treadport in several ways: the belt's response to a user's motion should be such that it does not harm their perception of realistic walking; a user should be able to start walking and come to a stop without feeling excessive pulling/pushing forces; a user should be able to maintain any reasonable self-selected walking speed similar to overground locomotion; and a user should be able to smoothly transition between forward and backward walking without any modification to the controller.

In order to evaluate our proposed changes to the Treadport controller in light of the desired characteristics described above, we conducted three separate human-subjects experiments. The purpose of the experiments were threefold: First, to find the most preferred value for the recentering-controller time constant τ (which we will denote by τ_p). We conducted an experiment to test the hypothesis that the controller's time constant influences users' perception of realistic walking, and that there exists a most-preferred time constant. Second, to compare the proposed balance-based force feedback with the previous inertial force feedback. We conducted a second experiment to test the hypothesis that the proposed method leads to more realistic walking than the previous method. Third, to quantitatively evaluate the ability of subjects to attain any self-selected walking speed and maintain it. We conducted a final experiment to test the hypothesis that subjects would be able to attain and maintain four distinct self-selected speeds denoted qualitatively as "normal" walking, "fast" walking, "jogging," and "backward" walking.

Our goal is to determine the most preferred recentering-controller time-constant and kinesthetic-force-feedback method independently of one another. However, both controllers must be active for the Treadport to function properly, so it is impossible to completely isolate the effects of the two controllers. Pilot testing provided strong evidence that our new kinesthetic-force-feedback controller was significantly superior to the previous controller, whereas pilot testing for the recentering-controller was not as conclusive. Therefore, we structured our experiments as follows. First, we conducted our recentering-controller experiment while always using our new kinesthetic-force-feedback controller (which we hypothesize is superior). Then, after finding the preferred recentering-controller, we conducted our kinesthetic-force-feedback experiment to verify that our original hypothesis was correct, and that the new controller was indeed superior to the previous controller.

We chose twenty healthy subjects with a range of height (1.76 ± 0.07 m) and weight (78.87 ± 13.59 kg). Subjects' ages ranged from 19 to 32 years. Subjects were naïve with respect to the experiment. The inclusion criterion was that a participant could fit well in the harness such that mechanical coupling between the participant and the attached tether was maximized. Subjects were provided with written instructions explaining the experiment.

3.4.1 Recentering-controller time-constant

In pilot testing we determined two extreme values for τ. Enforcing a maximum value of τ prevents a user from getting too close to the Treadport's front edge; this value is set at $\tau = 1.9\,\text{s}$. Enforcing a minimum value of τ prevents commanding belt motions that are too large to actually be achieved by the Treadport hardware; this value is set at $\tau = 0.7\,\text{s}$. The full range was then divided into three equal regions by considering four values of τ: $\tau_A = 0.7\,\text{s}$, $\tau_B = 1.1\,\text{s}$, $\tau_C = 1.5\,\text{s}$, and $\tau_D = 1.9\,\text{s}$.

We designed the experiment based on the two-alternative-forced-choice (2-AFC) method, which is widely used in sensory tests [68]. Within a given trial, subjects were forced to choose between two different conditions, each corresponding to a different τ value unknown to them. Within a given trial, subjects were asked to start walking from rest and then stop walking, and to repeat this process as many times as possible within the time provided. There were no instructions about what their speed should be. They were then asked to simply choose the condition that they preferred. There were no instructions given as to how the subjects should make their determination of preference. We used computerized auditory cues through a speaker to inform subjects about: the trial's number; the beginning and the end of each trial; and the condition's number (i.e., "first" or "second"). After completion of each trial, subjects were prompted to select their preferred condition by saying either "first" or "second."

For the first part of the experiment, there were six possible combinations for all τ pairs to present to the subjects using the 2-AFC method: $\{(\tau_A,\tau_B), (\tau_A,\tau_C), (\tau_A,\tau_D), (\tau_B,\tau_C), (\tau_B,\tau_D), (\tau_C,\tau_D)\}$. We presented each pair twice to improve the power of the experiment, resulting in 12 total trials per subject. The order of these twelve trials was fully randomized, as was the ordering of the two τ values presented within a given trial. Figure 3.8 shows the timing of the experiment within and between trials. Before starting the experiment, subjects had a one-minute period for familiarization with the Treadport.

From the results of the first part of the experiment, we chose the two most preferred τ values (i.e., the two values selected most often). In the event that three τ values were selected equally, we planned to perform an additional six trials (three combinations with two repetitions) to narrow the selection down to the two most preferred values, but this eventuality never occurred in our experiment.

In a second part of the experiment, immediately following the first part, we presented the subject with their two most preferred τ values in six repeated trials, with the order of the conditions within each trial fully randomized. We again used the timing shown in Fig. 3.8. Again, the subjects were asked to state their preference. A value of six trials was chosen because, when using the 2-AFC

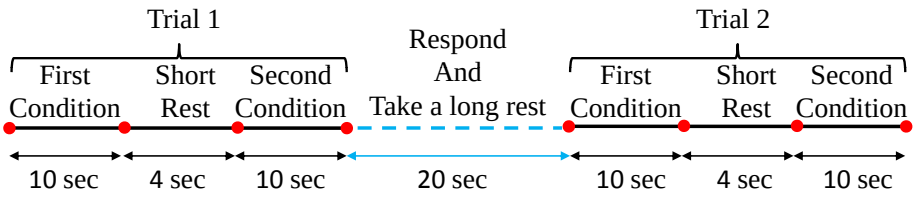

Figure 3.8: The timing used within and between trials in the two-alternative-forced-choice experiments.

method, six is the minimum number required such that if the subject chooses the same condition for all trials we can say with 95% certainty that they prefer that condition. At the end of the experiment, we asked the subjects to fill out a questionnaire comprising a single question: "When selecting the condition that you preferred in a trial, what was your preference based on?"

We utilized the convex combination of the results to estimate the preferred time-constant τ_p for each subject, where the weighting coefficients were the fraction of the times that each of the two τ values were selected in the second part of the experiment. For example, if τ_B was chosen 4 out of 6 trials, and τ_C was chosen 2 out of 6 trials, then τ_p would be calculated as $\tau_p = (4/6)\tau_B + (2/6)\tau_C$. This method essentially performs an interpolation between tested values, with the assumption that there exists an underlying continuous preference function with a local maximum value.

3.4.2 Kinesthetic-force-feedback method

This experiment was carried out after completion of the experiment of Section 3.4.1, on a different day. Participants were presented with the two different force-feedback methods through 12 trials, again using the 2-AFC method, with the order of the conditions randomized within trials. The instructions provided to the subjects were identical to those of the experiment of Section 3.4.1, and the timing within and between trials is again depicted in Fig. 3.8. With 12 trials, a given subject must choose a condition at least 10 times out of 12 in order to say that the subject prefers the condition with 95% confidence. In this entire experiment, the time-constant of the recentering controller was set at the mean value of τ_p across all twenty subjects, obtained as described in Sections 3.4.1.

3.4.3 Ability to walk at self-selected speeds

The final experiment was conducted immediately following the experiment of Section 3.4.2. We asked the subjects to walk with various speeds and to maintain their speed for a given period of time. Four qualitative walking speeds were used: "normal" walking, "fast" walking, "jogging," and "backward" walking. The subjects were not provided with any quantitative definition of these terms, and were asked to self-select the speed that best represented the qualitative terms. For normal walking, we instructed the subjects to walk at their preferred speed as if they were walking down

a hallway. For fast walking, we instructed the subjects to imagine that they were walking down a hallway in a hurry, but to not run. Subjects did not receive any explicit guidance for jogging or backward walking.

For a given subject, the order of the four walking speeds was randomized. The subject was given a verbal instruction of which walking speed they would be attempting, with the instruction to walk at that speed, starting from rest, until they were informed of the end of the trial, at which point they should come to a stop. Before each trial, the subject spent 20 s to practice their assigned walking speed. We then used computerized auditory cues through a speaker to inform subjects about the beginning and the end of each trial. Each trial lasted for 20 s. We continuously recorded the belt's speed during the trials. The wait time between trials was approximately 20 s, but varied from trial to trial and between subjects.

To quantify the ability to maintain a given speed, we consider the standard deviation σ and mean μ of the belt's speed for the final 15 s of data (thus removing the transient effects observed in the first 5 s of data). We use the coefficient of variance in speed when attempting to walk at a constant speed as the quantitative measure for evaluating the Treadport's performance:

$$C_v = \frac{\sigma}{\mu} \tag{3.16}$$

The importance of minimizing variance in self-selected speed has been considered previously [69, 58]. The lower the C_v, the easier it is to maintain a constant speed.

3.5 Experiment results

3.5.1 Recentering-controller time-constant

Throughout the twelve trials in the first part of the experiment, the number of times that a given τ could be preferred could vary from zero (i.e., never preferred) to six (i.e., always preferred). Figure 3.9 depicts that in the first part of the experiment, subjects chose the conditions corresponding to $\tau = 1.1$ s and $\tau = 1.5$ s most often as their preference. Since our results were non-parametric, we used Friedman's test and Dunn-Sidak *post hoc* analysis for multiple comparison [70]. We find a statistically significant difference between either of the two most-preferred time constants and either of the two least-preferred time-constants, but we do not find a statistically significant difference between the two most-preferred time-constants.

The second part of the experiment used the two most-preferred time-constants for each individual subject to determine a more accurate value of the preferred τ_p for that subject. The results of the second part of the experiment are presented in Fig. 3.10. The mean preferred time-constant across all subjects, with a 95% confidence interval, is $\tau_p = 1.26 \pm 0.09$ s. 16 out of 20 subjects had an individual τ_p in the range 1.1–1.5 s, which is sufficient to say with 95% confidence that the

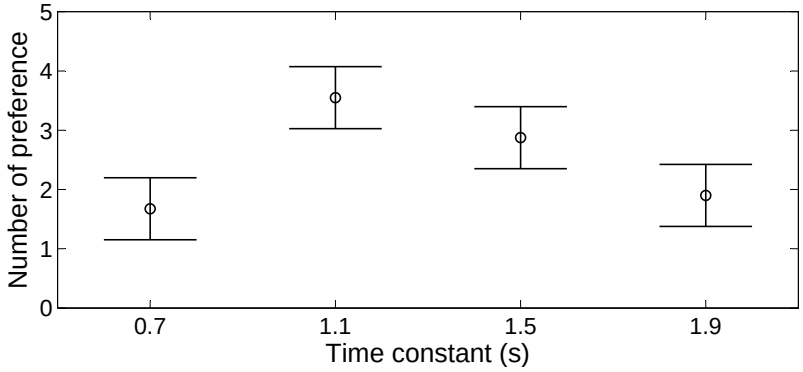

Figure 3.9: Preference mean with 95% confidence interval for each belt-controller time-constant across 20 subjects.

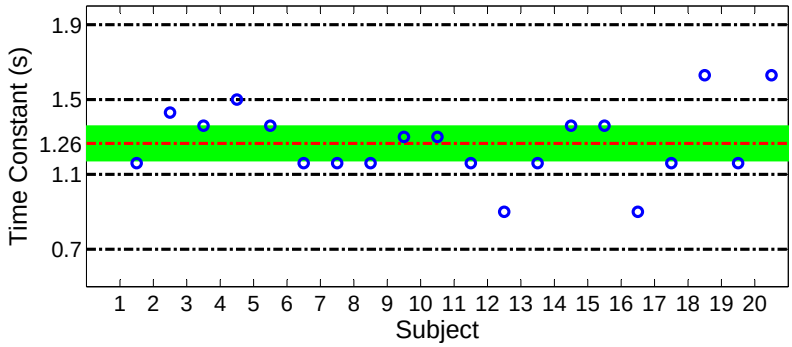

Figure 3.10: Subjects' individual preferred belt-controller time-constants τ_p are given with circles. The mean preferred time-constant across subjects is at $\tau_p = 1.26\,\text{s}$, and the 95% confidence interval is shown as a bar.

entire population as a whole will prefer a τ in this range. In looking at Fig. 3.4, we believe this is a nonobvious result.

We also investigated the effect of subjects' height, weight, self-selected speed, and the tether attachment point encoded by ψ (which is correlated with height) on their preferred time-constant. Statistical analysis using linear regression revealed no statistically significant effect of any of these four parameters on the preferred time-constant. It can be inferred that despite their different heights and weights, the subjects had a similar walking preference on the Treadport, and variance between subjects is likely due to personal preference as opposed to a quantifiable anatomical characteristic.

Based on the results of this experiment, we conclude that it is reasonable to use a time-constant of $\tau = 1.26\,\text{s}$ for all users in the future, and no additional user-specific measurements (i.e., height or weight) can be used to improve the value of τ. Any additional user-specific improvements to τ would essentially require this experiment to be recreated on a user-by-user basis. Fortunately, we see in Fig. 3.10 that the variance between users is relatively small, and most users will be satisfied

with $\tau = 1.26\,\text{s}$.

To see how the subjects perceived the effect of different τ's, we used a questionnaire at the end of the experiment. Their responses to our question about what their preference was based on revealed that subjects typically determined one condition to be inferior to the other condition, and then voted *against* that condition (as opposed to voting *for* the other). Comments typically took one of three forms: (1) Sometimes the belt was too responsive and started moving sooner or faster than I expected. (2) Sometimes the belt was too sluggish and it seemed to take too much effort to accelerate or decelerate. (3) Sometimes the belt seemed to keep moving for too long after I tried to stop walking. From our own experience in pilot testing, we know that the first response is due to τ being too small, and the second and third responses are due to τ being too large.

3.5.2 Kinesthetic-force-feedback method

We compared the previous inertial-force-feedback method to the new balance-based-force-feedback method using the 2-AFC method. Figure 3.11 indicates that the new method is significantly preferred across the 20 subjects (and thus the population). A binomial distribution is the appropriate way to analyze statistical significance of 2-AFC tests [71], and it enables us to analyze each subject's preference individually.

To state with 95% certainty that the new method is preferred over the previous method, we need to show that there is less than a 5% chance that random guessing could have led to the number of preferences of the new method. The probability of choosing the new method in a trial merely by guessing is $p = 0.5$ (there are only two choices). For the n trials of any given subject, the null hypothesis is that the two methods are identical, which means the chance of choosing the new method out of n trials is equal to the chance of choosing the previous method. The alternative hypothesis is that the new method performs differently than the previous method, so that the difference observed in the preferences was not obtained by guessing. We need to choose the

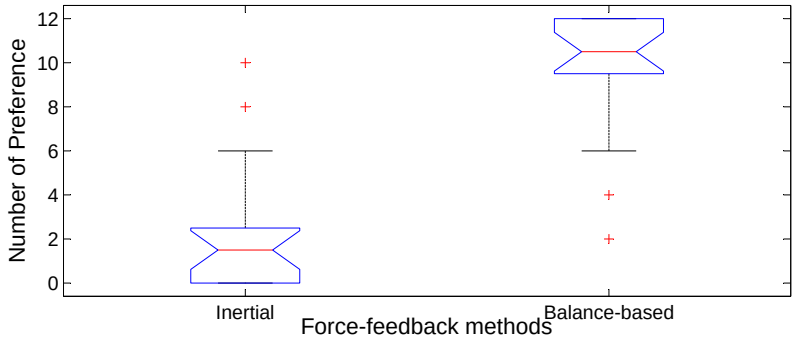

Figure 3.11: Preference of force-feedback methods, shown as a notched-box-whisker plot.

new method in at least T trials out of n trials in order to conclude that the new method is selected significantly more often than it would be by chance. The probability of choosing the new method at least T times out of n just by chance (denoted by $P(X \geq T)$) should be less than α ($\alpha = 0.05$ for 95% confidence). Thus:

$$P(X \geq T) = (1 - P(X \leq T-1)) \leq \alpha \tag{3.17}$$

where the cumulative distribution function of a binomial distribution can be expressed as:

$$P(X \leq T-1) = \sum_{i=0}^{T-1} \binom{n}{i} p^i (1-p)^{n-i} \tag{3.18}$$

With $p = 0.5$, $\alpha = 0.05$, and $n = 12$ (i.e., 12 trials for a given subject), we calculate $T = 10$, meaning that the new method must be preferred in at least 10 out of 12 trials to be 95% confident in the preference. Fifteen subjects chose the new method in at least 10 out of 12 trials. One subject chose the new method with 90% confidence, and three subjects did not have any significant preference. Only one subject preferred the previous method with 95% confidence. The fact that 15 out of 20 subjects preferred the new method with 95% confidence is sufficient for us to also conclude that the *population* will prefer the new method with 95% confidence. That is, if we consider $p = 0.5$, $\alpha = 0.05$, and $n = 20$ (i.e., the total number of subjects), we calculate that $T = 15$. This confirms the results shown in Fig. 3.11.

We considered the effect of the tether attachment point relative to the center of mass of the user, through the variable ψ, on the preference of the balance-based force feedback over inertial force feedback. The results are shown in Fig. 3.12. We find that there is a statistically significant effect of ψ on preference, with lower values of ψ (i.e., the tether being attached farther above the user's center of mass) resulting in more likely preference for the balance-based method. We will return to this result in Section 3.6.

In the post-experiment questionnaire, the subjects mentioned several reasons for their preference. Again, they tended to vote *against* one method, rather than voting *for* the other. Comments typically took one of three forms: (1) Sometimes I was too aware of the tether pushing/pulling on my back. (2) Sometimes it required too much effort to get the belt to move. (3) Sometimes my balance was disturbed when I tried to come to a stop. These comments echo our own observations that led us to reconsider the kinethetic-force-feedback method in the first place.

3.5.3 Ability to walk at self-selected speeds

In the final experiment, we used each subject's preferred kinesthetic-force-feedback method (whether or not it was significantly different from the other method), and used $\tau = 1.26\,\text{s}$ for all

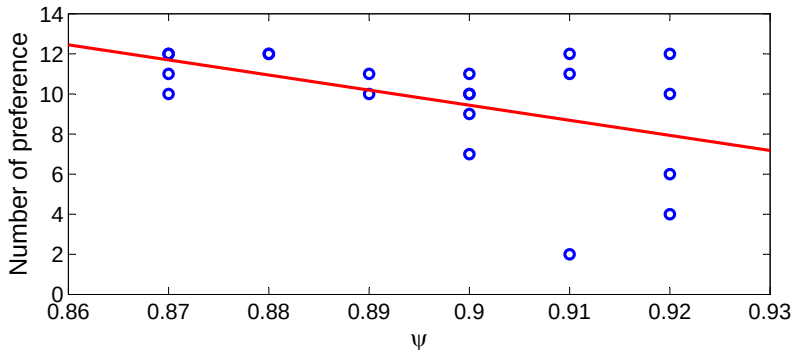

Figure 3.12: Preference of balanced-based force feedback (out of a possible 12) as a function of ψ. Note that there are two data points at each of (0.87,12), (0.88,12), and (0.9,10). The effect of ψ is statistically significant.

subjects. Figure 3.13 depicts the self-selected speeds of each subject for each of the four qualitative speed types. Each of the means and standard deviations shown are the result of experimental data of the type shown in Fig. 3.14, after removing the transient effects of the first 5 s of data. We can readily see that subjects are able to achieve self-selected speeds and maintain those speeds. We see that the user's perceived walking speed $v_{p/b}$ has more variance than the speed of the belt itself, indicating the periodic (rather than constant) walking speed reminiscent of natural walking. We also observe that the speed profiles are in agreement with the standard first-order model [67].

The mean (with 95% confidence interval) of C_v values from (3.16) for the four different qualitative speeds are presented in Fig. 3.15. It can be observed that C_v is less than 5% for normal walking, fast walking, and jogging, and there is no significant difference between them. Although C_v of backward walking is significantly larger than the other three cases, it is still relatively small. Backward walking seems to be not as intuitive as forward walking, so this result is not surprising; we observe that users usually have more difficulty in keeping a constant pace. Thus, it is critical that a locomotion interface provides a stable and safe condition for a user to experience backward walking.

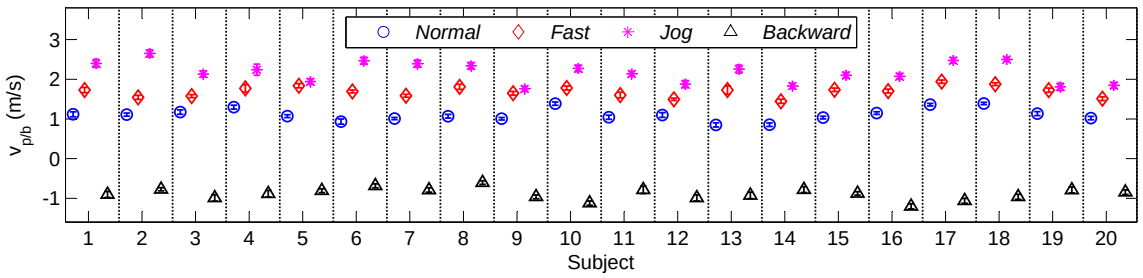

Figure 3.13: Subjects' mean walking speed with standard deviation for the four qualitative speeds.

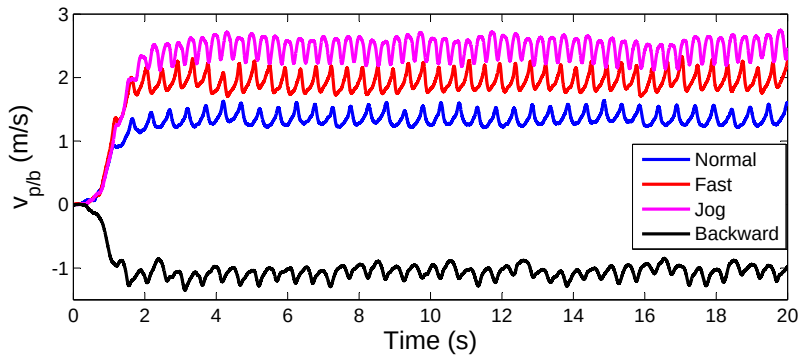

(A)

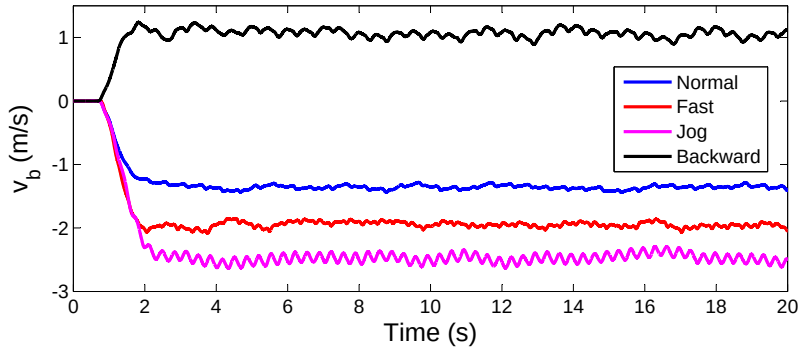

(B)

Figure 3.14: Four different self-selected qualitative speeds for a typical user. (A) Walking speed of the user relative to the belt $v_{p/b}$. (B) The belt's speed v_b.

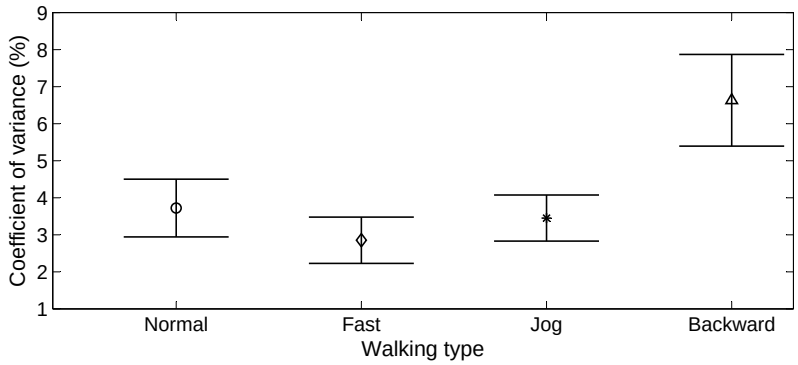

Figure 3.15: Mean value of C_v with 95% confidence interval for different walking types.

Walking on the Treadport is similar to overground walking. All subjects could perform all of the four qualitative walking types, as well as starting from rest, coming to stop, and standing still, with smooth transitions between these modes. Figure 3.16 demonstrates all of the above mentioned tasks carried out on the Treadport for a typical user. The ability to come to a stop and stand still can be observed around 60 s. A quick transition from backward walking to forward walking can be

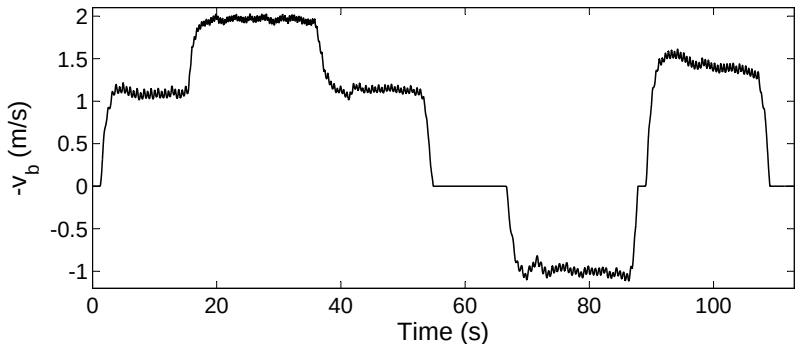

Figure 3.16: Walking speed while transitioning between different walking types for a typical user.

observed around 90 s. We plot $-v_b$ rather than $v_{p/b}$ so that the perfectly motionless condition can be clearly seen during the standing-still portions ($v_{p/b}$ exhibits the user's natural sway).

3.6 Discussion

For further analysis of the new controller, we consider the energy expended by a user to change their walking speed. This expended energy can be thought of as the work done by the user's feet when pushing the ground away, or alternatively, as the work performed on the user's center of mass (COM) by the ground. The relationship used for COM work is given by [72]:

$$w = \int f_f \cdot v_{COM} dt \tag{3.19}$$

where $w(t)$ is equal to the user's expended energy as a function of time, f_f is the force applied between the ground or belt and the user's feet (positive in compression), and v_{COM} is the speed of the user's COM. In overground walking, $v_{COM} = v_p$. In the Treadport, $v_{COM} = v_{p/b}$ [64]. Using numerical simulations, the value of $w(t)$ in Treadport walking is evaluated by using the block diagram in Fig. 3.7 for different values of ψ, and $w(t)$ in overground walking is evaluated from the block diagram of Fig. 3.6. Figure 3.17 depicts the energy expenditure $w(t)$ for a typical human with the mass of 80 kg, starting from rest and reaching a steady-state walking speed of 2 m/s.

The results indicate that using both inertial and balance-based force feedback results in energy expenditure on the Treadport that is similar to overground. However, inertial force feedback results in more energy expenditure than overground, whereas balance-based force feedback for all the values of ψ used in this study results in less energy expenditure than overground. This trend is independent of the user's mass and walking speed. For the preferred time-constant and the full range of ψ from our studies, users would expend 5.3% more energy than overground with inertial force feedback, whereas they would expend 3.7–9.4% less energy than overground with the balance-based force feedback, depending on ψ. It is possible to modify the tether attachment point to result in a

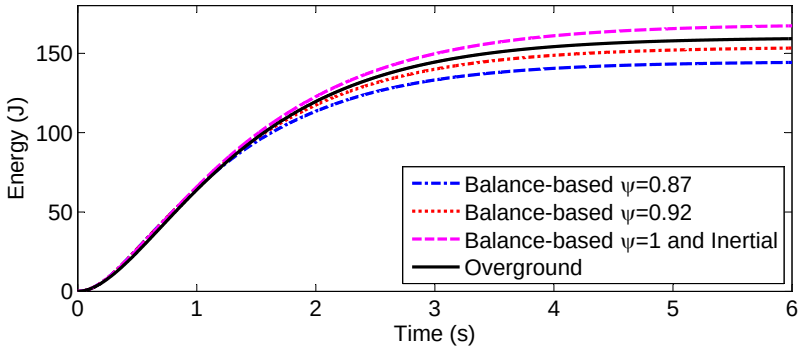

Figure 3.17: Energy expenditure in overground walking and the Treadport walking of a typical user during different force-feedback methods.

perfect energy expenditure when using balance-based force feedback ($\psi = 0.95$, for the recentering-controller parameters used here, independent of user mass and steady-state speed). However, with inertial force feedback, even if we consider modifying the recentering-controller time-constant over the range of reasonable values found in our study, the inertial force feedback would always result in 5.0–5.5% more energy expenditure than overground.

Regardless of the tether attachment point, once ψ is set, the balance-based force controller is the correct force in terms of the user's sense of balance, and we believe that this is the primary reason for subjects' preference of the method. The improvement in balance and feeling of safety is particularly noticeable when coming to a stop, during the brief period after the feet are firmly planted on the belt but before the belt has come to a complete stop. The improvement is also noticeable when starting from rest, removing the need of the user to lean forward slightly during the acceleration phase. It seems likely that energy expenditure is also contributing to the subjects' preference, with users preferring to expend less energy. The dependence of user preference on ψ, seen in Fig. 3.12, provides evidence of this dependence, in light of the results shown in Fig. 3.17. Even if energy expenditure were the only factor determining user preference, the balance-based method would still be the preferred method with $\psi = 0.95$, since the inertial method would require 5.3% more energy.

3.7 Conclusion

In this paper we described an improved control system for the Treadport immersive locomotion interface, with results that should generalize to any treadmill that utilizes an actuated tether to enable self-selected walking speed. A new controller for the belt was implemented to regulate the user's position to some reference position (typically near the center); when combined with the user's volition, this same controller also enables the user to naturally self-select their walking speed as they would when walking over ground. We found that a simple proportional-derivative controller is

effective at regulating the user's position, and it is most natural feeling when it has a damping ratio of approximately 1.5 and a time constant of approximately 1.26 s. A new kinesthetic-force-feedback controller was designed for the tether that applies forces to the user's torso. This new controller was derived based on maintaining the user's sense of balance during belt acceleration, rather than by rendering an inertial force as was done in prior work. Based on the results of our human-subjects study, both the belt controller and the kinesthetic-force-feedback controller significantly contribute to an improved perception of realistic walking on the Treadport. Our improved controllers use intuitive dynamic-system and anatomical parameters, rather than gains that require *ad hoc* tuning. Our controller simply requires three measurements to be made for a given user—the user's mass, the user's height, and the height of the tether attachment point on the user's torso—and all other controller parameters can be set constant for the entire population.

3.8 Acknowledgments

We would like to thank Dr. Ed Colgate, Dr. Robert Riener, and Dr. Mark Minor for their constructive comments that led to this redesign of the Treadport control system, as well as the anonymous reviewers for their helpful suggestions. This work was supported by the National Science Foundation through grant 1208637.

CHAPTER 4

AN UNDERACTUATED WEARABLE ARM-SWING REHABILITATOR FOR GAIT TRAINING

The following chapter is aimed at design and fabrication of an Underactuated Wearable Arm-swing Rehabilitator (UWEAR) that swings the arms for use in gait rehabilitation.

4.1 Abstract

This paper presents the design concept and fabricated prototype of a device that swings the arms for use in gait rehabilitation. The device is designed to be used in conjunction with a body-weight-support treadmill. The device is backdrivable, wearable, capable of assisting the user's arm swing in the sagittal plane, and has unhindered kinematics in the remaining unactuated degrees of freedom. Tests are performed to validate the shoulder-angle prediction equations based on the non-collocated motor-angle sensor measurements, to validate the device's ability to provide adequate torque to induce arm-swing in a passive user, and to investigate whether or not the user's active involvement can be determined by examining sensor data. The results show that the device does provide sufficient torque to move the arms with a factor of safety, but that the model-based shoulder-angle estimates obtained from the motor measurements have non-negligible error with the current prototype. It is shown that the controlled device generates low RMS tracking error and is able to diagnose user-assistance level (i.e., if the user is passive or actively assisting arm swing) online by observing shoulder-angle amplitudes and peak motor torques.

4.2 Introduction

The walking gait of those who have had strokes or spinal-cord injury (SCI) is often altered so that it is no longer healthy, but these people can undergo physical therapy in order to improve gait. Rehabilitation is done through exercises that help stimulate muscles and exploit neuroplasticity for the diminished functions [73]. Gait rehabilitation is often focused on the legs and de-emphasizes the role of arms. However, studies show that there is neural coupling between the upper and lower limbs [9] and that it can be exploited for rehabilitative purposes [13]. Research also shows that upper-limb muscle activity can actually induce lower-limb muscle activity [15, 74] and that the effect is most pronounced when the arms move in phase with the legs [75]. Additionally, arm swing contributes to balance [9], regulates rotational body motion [18], and metabolic efficiency of the walker [12]. Therefore, more effective rehabilitation can be performed as the patient exerts effort to naturally swing their arms.

One method of gait rehabilitation involving arm swing was shown in a study in which SCI subjects walked on a treadmill with their arms being manually assisted by a therapist with poles [9]. This type of rehabilitation enabled the subject to exercise both the upper and lower limbs. However, according to [76], rehabilitation is activity-dependent, and using devices (especially ones with arm supports) can alter the input interpreted by the spinal cord, thus leading to the learning of incorrect muscle firing patterns. Although the arm weight that is supported by the therapist's poles may be little, depending on the therapist's skill, it may be enough to cause the learning of incorrect muscle

firing patterns. Therefore, it is important to allow the arms to swing as naturally as possible without gripping or supporting weight. Additionally, this method of rehabilitation requires several physical therapists to assist the patient during the exercise.

Many robotic technologies have been developed for performing gait rehabilitation [35, 37, 38, 16, 77], but the vast majority are focused on the legs with no active assistance for arm swing. One example of a robotic orthosis includes arm-swing assistance [16]. The robot consists of swinging prismatic links with handholds that interact with the user's hands and arms, combined with sliding height- and pitch-adjustable foot pads. Since the robotic system constrains the user's feet and arms kinematically, it is likely that what the user experiences is dissimilar to natural, over-ground walking.

The need for a device that properly swings the arms during gait training for neurorehabilitative purposes has led to the development of the Underactuated WEarable Arm-swing Rehabilitator (UWEAR), shown in Fig. 4.1. The device is powered in just one degree of freedom (DOF) to assist in flexion/extension of the user's shoulder, while allowing relatively uninhibited motion of the user's arms in the remaining DOFs. The UWEAR is worn like a backpack on the user while they are walking on a treadmill. Body-weight-support is already provided for the user, which can also be used to compensate the additional weight of the UWEAR. Its arm links move in flexion/extension and abduction/adduction. The range of motion is large (-40° extension, 90° flextion, and 20° abduction), and covers the motions necessary for both natural gait and relatively free movement while not performing rehabilitative tasks. Our goal was not to design a fully powered portable exoskeleton, but rather a therapeutic device that assists the patient's arms in following a healthy gait at their own walking pace. The UWEAR comprises three key subassemblies: a military All-purpose Lightweight Individual Carrying Equipment (ALICE) frame with additional supporting structures, underactuated arm-swing mechanisms to induce arm swing in the shoulder joint, and a power train to convert torque generated by DC motors located near the user's hips to amplified torque near the user's shoulders for the arm-swing mechanisms.

The underactuated arm-swing mechanism applies power to the user's arms in the sagittal plane without constraining the arms in the other unactuated DOFs. The assemblies are located lateral to the user's arms. They start above the user's shoulders, near the user's head, from the UWEAR's supporting structures, and extend to the user's arms via arm cuffs. The assemblies comprise five joints each, all with one DOF. Only the shoulder flexion/extension DOF is actuated. The underactuated arm-swing mechanism was designed, and is described here, independently of the power train that powers its single actuated DOF.

A military ALICE backpack frame provides both a foundation for the rest of the mechanism

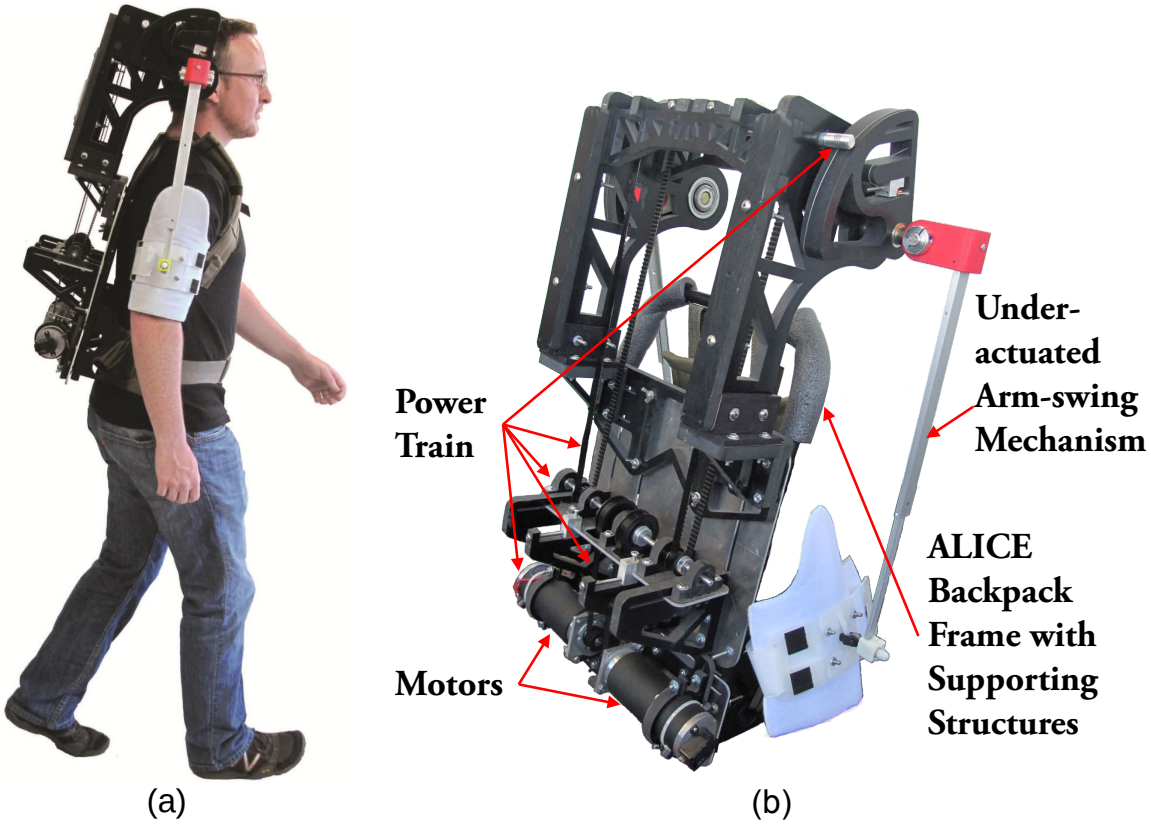

Figure 4.1: (a) The UWEAR is worn like a backpack, and provides active arm-swing assistance for flexion/extension of the shoulder, while being unconstraining in the other degrees of freedom. (b) The UWEAR comprises several subassemblies: a backpack frame with additional supporting structures, an underactuated arm-swing mechanism, and a power train that transmits motor torque to torque for the arm-swing mechanism.

and a secure fit on the user. The ALICE frame is made of aluminum and steel. The strength and rigidity of the metals along with the adjustable shoulder and waist straps accomplish two objectives. They provide adequate reaction forces to ensure that power is spent in moving the arms, rather than moving the frame relative to the user's body. Additionally, the strength and rigidity of the frame prevent the structure from flexing from the torques generated by the motors.

Additional structural components support the underactuated arm-swing mechanism and power train. ABS is chosen for its strength and weight. Screws fasten two slotted aluminum plates to the ALICE frame. The slots enable positioning the device's components and enable modular additions (e.g., the power train's tensioning shelf and motor mounts). Several bolts and slots in the structure provide adjustability for the UWEAR so that it fits a large population.

The power train—comprising motors, a timing-belt system, and capstan drives—is located on the back of the ALICE frame. The timing-belt system transfers torque from the motors, which sit by the user's hips, up to the input of the underactuated arm-swing mechanism, located above the user's

shoulders. The timing-belt assembly has stages of pulleys that amplify the motor torques. After the first stage of pulleys there is a tensioning device, and by adjusting its positioning screws, it can eliminate slack in the timing-belts. Large motors with no gearhead provide relatively high torque while being backdrivable. The power train's final stage is the capstan drive, which further amplifies the torque while maintaining the backdrivability of the power train.

4.3 Design of the UWEAR

4.3.1 Underactuated arm-swing mechanism

Fig. 4.2(a) shows the underactuated arm-swing mechanism comprising a 2-DOF shoulder joint, a 1-DOF sliding prismatic link, and a 2-DOF cuff joint. The shoulder joint is made of two custom 1-DOF joints. They enable powered flexion/extension and free abduction/adduction.

The prismatic arm link is a 1-DOF sliding joint. Because there is an offset between the user's shoulders and the mechanism's shoulder joint, as well as movement that can occur from the user's scapulothoracic joint, as well as to accommodate users of varying size, an arm link made of sliding rails is used to account for necessary change in link length as the user flexes/extends and abducts/adducts their arm. Otherwise, the user would experience constrained kinematics. Telescopic slide rails from MISUMI (#SAR230) are used for the prismatic arm links; they cover the necessary range of lengths encountered in flexion/extension and abduction/adduction in normal walking.

The cuff joint is made of three components: a small bearing housing, a pin joint formed by an eyelet and clevis rod end, and an arm cuff. The small bearing housing accommodates rotational differences between the user's upper arm and the mechanism's arm link in flexion/extension. The eyelet and clevis rod end pin joint accommodate angular differences between the user's upper arm and the mechanism's arm link in abduction/adduction. The arm cuff has sheet plastic attached to it that passes through the clevis rod end. This prevents the rod end from rotating about an axis normal to the arm cuff's surface, which prevents the clevis rod end's abduction/adduction axis from changing orientations that would cause awkward and uncontrollable pulling motions. The arm cuff is worn firmly on the user's upper arm so that forces generated by the UWEAR are transmitted to the user.

4.3.2 Power train and supporting structures

The power train is made of motors, a timing-belt system, and a capstan drive. Its purpose is to amplify and transmit motor torque to the arm-swing mechanisms. The DC motors (Brush Type DC Servo Motor from Servo Systems #23SMDC-LCSS-500) are direct-drive and backdrivable. The motors are sufficiently short such that they do not obstruct the user's arms as the arms swing past

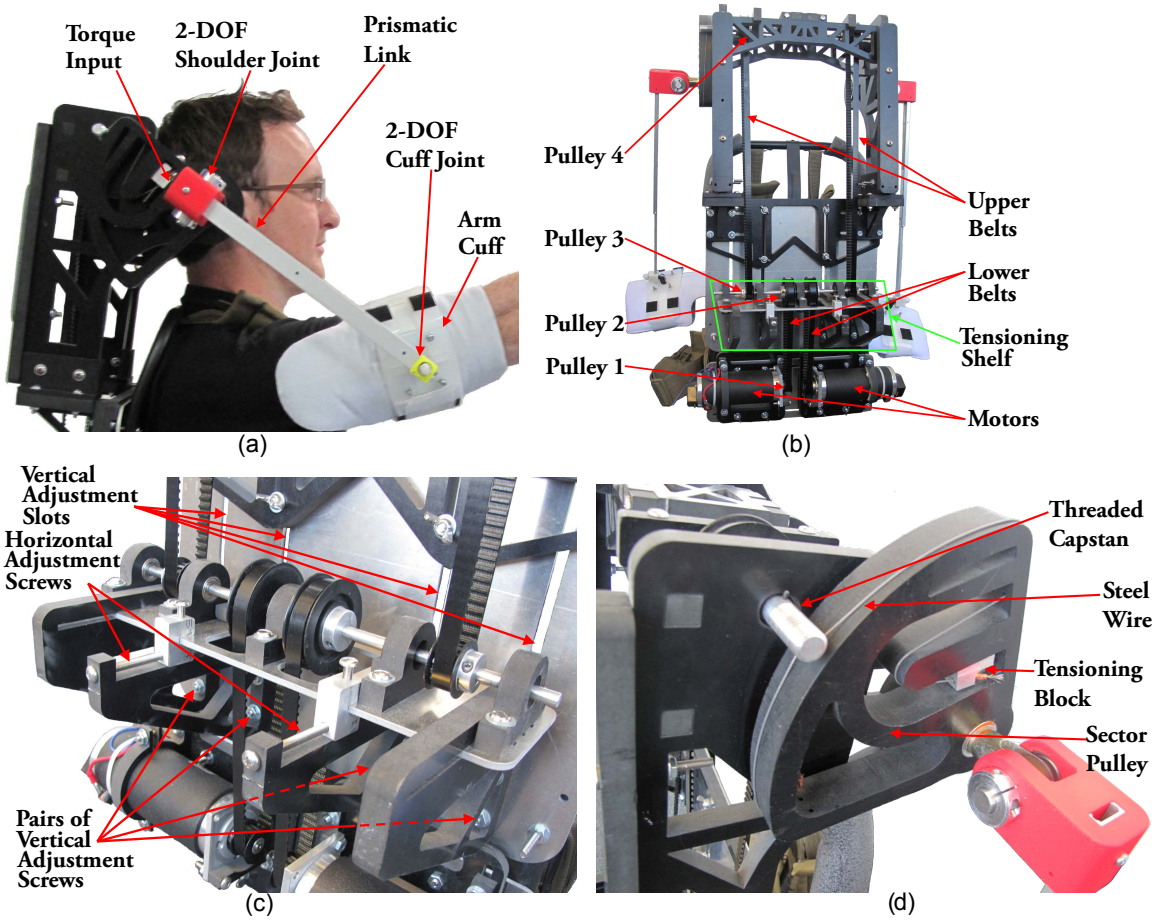

Figure 4.2: Several images of the UWEAR prototype. (a) highlights the underactuated arm-swing mechanism, (b) highlights the timing-belt system, (c) focuses on the timing-belt system's tensioning shelf, and (d) highlights the capstan drive.

the motor's location. The motors have a maximum continuous stall torque of 0.388 N·m, which is sufficient for generating arm swing when combined with the additional torque amplification of the drive train. The backdrivability of the motors and drive train make the UWEAR unconstraining when it is unpowered, which is desirable for fail-safe operation and easy donning/doffing of the device. The motors are placed near the user's hips with the goal of mitigating additional rotational inertia on the user.

The timing-belt system comprises two stages of timing-pulleys and timing-belts that span the distance between the motor shaft and input shaft of the capstan drive (Fig. 4.2(b)). The timing-pulleys are of two different pitch diameters, 46.89 mm and 22.63 mm, which result in a total timing-belt system gear ratio of $k_{TB} = 4.30$. The timing-belts span the stages of pulleys, and have a belt-width of 9.53 mm, which prevents belt skipping from potential timing-belt teeth deflections. The timing-belt system includes an adjustable device for tensioning the belts called the "tensioning

shelf" (Fig. 4.2(c)), which ensures good torque transmission as well as facilitates the timing-belt system's assembly.

The last member of the power train is the capstan drive (Fig. 4.2(d)). The capstan drive draws inspiration from various "haptic paddle" designs [78, 79]. It provides one final stage of torque amplification. It is made of a threaded capstan, which transmits torques via a steel wire (diameter=0.94 mm) that rotates the sector pulley, which is the input to the arm-swing mechanism. The capstan drive assembly also includes a tensioning block to eliminate slack in the steel wire. The threaded capstan has a radius of 6.35 mm, a length of 25.4 mm, and thread count of 13 threads-per-inch such that the steel wire does not unravel from the capstan during operation (from overrunning either the length of the capstan or the wire over the individual threads from poor steel-wire diameter sizing). The sector pulley is designed to be large in radius (12.29 cm) so that a large gear ratio for the capstan drive is obtained ($k_{CD} = 19.36$). The gear ratio for the entire power train is the product of the timing-belt system's and capstan drive's gear ratios; it is $k_{PT} = 83.2$.

The ALICE frame and its straps serve the important purpose of providing a foundation to mount the rest of the UWEAR components and providing a stable connection between the UWEAR and user, so that minimal relative motion between them occurs. The rigidity of the ALICE frame as well as the lateral supports and truss bridge insure that the generated torques are applied to the user's arm, rather than causing the device to deflect.

The total weight of the UWEAR is about 10 kg, however, a standard body-weight-support system can compensate the total weight of the device. A rehabilitation harness can be worn underneath the ALICE frame, such that the UWEAR to be worn simultaneously with a body-weight-support system, as depicted in Fig. 4.3, which shows the UWEAR being worn by a mannequin combined with a standard body-weight-support system. In this way, the weight of the UWEAR can be compensated along with the weight of the user.

4.4 Geometry of the arm-swing mechanism

The arm-swing mechanism can be described geometrically in order to create a relationship between the user's shoulder angle and the mechanism's arm-link angle. Fig. 4.4 presents the geometry used, in two different configurations: when the upper arm is vertical (the "zero" position) and when the upper arm is flexed to an arbitrary shoulder angle θ_s. Parameters O_s and O_m represent the user's shoulder axis and the arm-swing mechanism's powered axis, respectively. The distance between O_s and O_m is described by D. The angle between the line measured by D and vertical is described by γ. The relative angle of the prismatic arm link is represented by θ_m. O_c is the connection point between the mechanism and the user's upper arm at an arbitrary shoulder angle. O_{c0} is the connection point's location at the "zero" position. R represents the distance between the

Figure 4.3: The UWEAR was designed to be worn in conjunction with a weight-support system.

user's shoulder axis and the connection point. The length of the mechanism's prismatic link, $L(\theta_s)$, is a function of θ_s. At the "zero" position ($\theta_s = 0^\circ$), the initial length of the prismatic arm link is represented by L_0. The angle α describes the angle between the user's upper arm and the prismatic link in the "zero" position and ϕ represents the angle between D and L_0. A number of additional useful relationships follow:

$$\alpha = \arctan\left(\frac{D\sin\gamma}{D\cos\gamma + R}\right) \tag{4.1}$$

$$\phi = \gamma - \alpha \tag{4.2}$$

$$L_0 = \frac{R\sin(\pi-\gamma)}{\sin\phi} = \frac{R\sin(\gamma)}{\sin\phi} \tag{4.3}$$

It is now possible to find the relationship between the shoulder angle and the mechanism angle. First, the length of the prismatic link is calculated as:

$$L = D\cos(\theta_m - \phi) + \sqrt{R^2 - D^2\sin^2(\theta_m - \phi)} \tag{4.4}$$

The Law of Cosines can then used, first on the triangle $O_m O_{c0} O_c$ and then on the triangle $O_s O_{c0} O_c$,

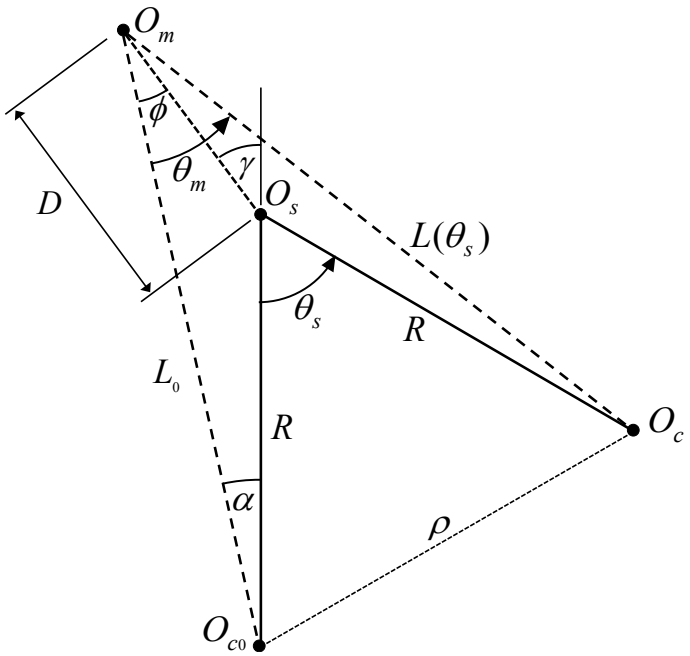

Figure 4.4: Geometry of the powered DOF of the arm-swing mechanism, shown in two different configurations: with the upper arm vertical, which we refer to as the "zero" position, and with the upper arm flexed to an arbitrary shoulder angle. The parameters that are used for calculating the relationship between the arm-swing mechanism and the user's shoulder angle are shown.

which share the side ρ, to find the cosine of the user's shoulder angle:

$$\cos(\theta_s) = 1 - \frac{L^2 + L_0^2 - 2LL_0\cos(\theta_m)}{2R^2} \tag{4.5}$$

However, use of the arccos function to solve for θ_s can be poorly conditioned numerically. Equation (4.5) is rearranged to a more numerically robust form using a trigonometric half-angle formula involving the tangent and cosine of the same angle:

$$\theta_s = \pm 2\arctan\sqrt{\frac{1-\cos(\theta_s)}{1+\cos(\theta_s)}} \tag{4.6}$$

Substituting the solutions for $\cos(\theta_s)$ from (4.5) into (4.6) gives the final relationship to calculate the user's shoulder angle based on the measured angle of the arm-swing mechanism:

$$\theta_s = \pm 2\arctan\sqrt{\frac{L^2 + L_0^2 - 2LL_0\cos(\theta_m)}{4R^2 - L^2 - L_0^2 + 2LL_0\cos(\theta_m)}} \tag{4.7}$$

The positive solution for θ_s is used when θ_m is positive, the negative solution is used when θ_m is negative, and θ_s is zero when θ_m is zero

The geometric model here assumes that the shoulder joint is a static pin joint. However, the shoulder joint is capable of moving due to its scapulothoracic degrees of freedom. Therefore,

(4.7) is not a relationship that will predict the shoulder angle with high accuracy, but rather it will approximate it. This result is seen in the experiments of Section 4.5.

4.5 Experimental results

In the experiments, the UWEAR is worn by four healthy male subjects with heights {1.71, 1.77, 1.71, 1.91} in meters and masses of {80, 65, 70, 94} in kilograms. Only four subjects were used here because we are only interested in validating the performance of the UWEAR prototype, not in conducting any human-subjects study *per se*.

After the UWEAR is donned and has its straps tightened so that it is secure, measurements are made to obtain values for R, D, L_0, and γ, which are used to estimate the user's shoulder angle from the mechanism's angle.

4.5.1 Validation of the relationship between the sector pulley and shoulder angle

An experiment was performed to evaluate the accuracy of the geometrical relationship provided in (4.7), which uses motor encoder data combined with the total power-train gear ratio to estimate the user's shoulder angle, compared against angles obtained by using motion-capture cameras to accurately measure the relative angle between the user's upper arm and torso without any assumptions about the shoulder's kinematics. One test subject donned the UWEAR and was fitted with motion-capture markers in standard locations. The subject, after starting from a relaxed position with his arms at his side, moved his arms periodically between the range-of-motion limits (approximately from -40° extended to 90° flexed) for a trial time of 60 seconds. The absolute errors between the motion-capture and encoder-based trajectories are shown in Fig. 4.5(a). It is seen that the error of the shoulder-angle prediction equations are not larger than 12°, with maximum errors that occur at a position outside the normal range of arm-swing motion (-30° extension to 10° flexion [12]). Additionally, errors appear to decrease as arm-motion speeds increase toward those of natural arm swing. The error is non-negligible, and it is believed that this is largely due to the subject's shoulder movement (Fig. 4.5(b)), which is also non-negligible, since (4.7) assumes that the user's shoulder is an immovable pin joint. Thus, we conclude that the UWEAR, in its current form, cannot be used for high-accuracy position measurement.

4.5.2 Inducing arm-swing

4.5.2.1 Experiment design

Another experiment is performed to characterize the UWEAR's ability to induce arm-swing in its users under a variety of different factors including arm-swing frequency (0.6 Hz or 1.0 Hz, which correspond to a slow or a brisk walking pace, respectively [80]), and user assistance level (*passive*,

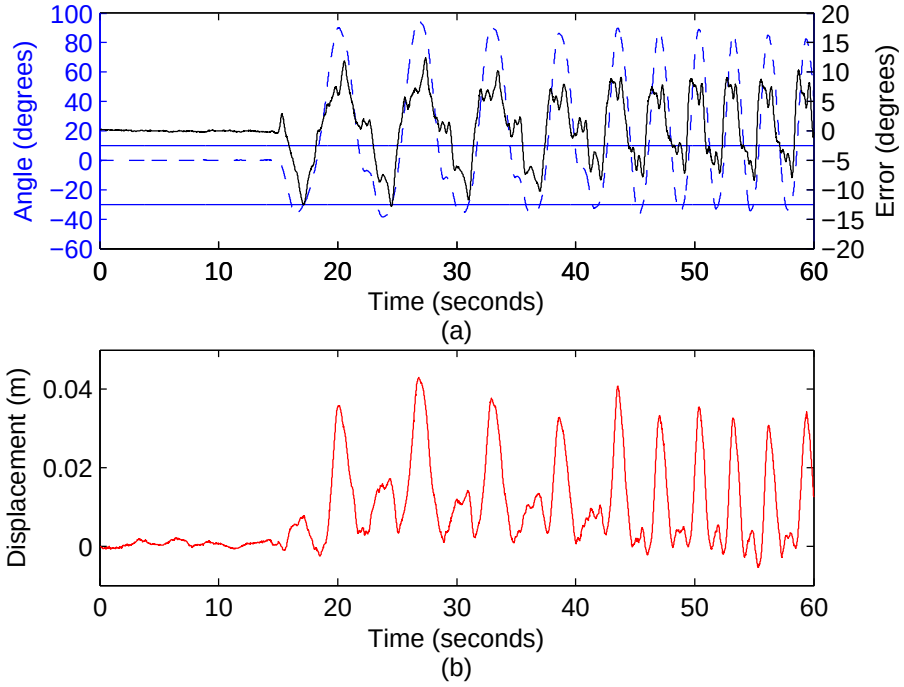

Figure 4.5: (a) Errors between the motion-capture and encoder-based data for the shoulder-angle, in black (right vertical axis), compared against the motion-capture data for the shoulder angle, in dashed blue (left vertical axis). Blue horizontal reference lines at 10° and -30° show the expected range of arm swing during normal gait. (b) Vertical displacement of the shoulder joint, obtained from the motion-capture data.

in which the user relaxes their arms, and *assistive*, in which the user attempts to swing their arms as being directed by the UWEAR, using only haptic information). The desired sinusoidal shoulder-angle trajectory for inducing arm-swing is precalculated based on the limited information in [81]. A position tracking PD servo controller with gains of $k_p = 2.0\,\text{N·m/rad}$ and $k_d = 0.3\,\text{N·m·s/rad}$ is implemented in the UWEAR to track the desired trajectory. The gains are tuned to be stiff yet stable to minimize tracking error.

Each of the four subjects stand with their arms initially at their sides. The UWEAR is then activated and it swings their arms through 20°-amplitude sinusoidal motion (-30° extension to 10° flexion) while motor-torque and optical-encoder data is recorded. To test all the factors and levels, the subjects perform 4 trials each with randomized order. The trials are evaluated by examining the peak motor torques, RMS tracking error, and shoulder-angle amplitudes once the transient from the beginning of the trial has decayed (after 5 seconds).

4.5.2.2 Results and discussion

Fig. 4.6 contains the data for the experiment. Fig. 4.6(a) shows the peak motor torques required by the UWEAR for different frequencies and assistance levels. The required peak motor torque for any case is not higher than 0.12 N·m, which is approximately one-third of the continuous stall torque that the chosen motor can provide. Thus, we see that the selected motors are oversized, and that they could be chosen to be less powerful, with the potential benefit of being more lightweight.

Fig. 4.6(b) shows the shoulder-angle amplitudes created by the UWEAR for different frequencies and assistance levels. With increasing frequency, the shoulder-angle amplitude increases, and the assistive user case creates shoulder-angle amplitudes larger than the passive case. At 1.0 Hz, it is seen that the assistive user case has a median shoulder-angle amplitude larger than the desired of 20°.

The RMS tracking errors of the UWEAR are shown in Fig. 4.6(c). The errors increase with increasing arm-swing frequency, but there appears to not be a difference between RMS error for the user assistance level. The RMS errors are not larger than approximately 1.6°.

The UWEAR can diagnose the level of user assistance by examining the peak motor torque and shoulder-angle amplitudes. When examining the motor torques, significant differences exist between the user assistance levels for motor torque at both frequencies. At 0.6 Hz, the assistive level requires less motor torque than the passive; however, at 1.0 Hz, the assistive level requires more motor torque. This may be due to the user's errors in following the desired trajectory, which requires more torque, since the PD controller is error based. The user assistance level can also be diagnosed by observing the shoulder-angle amplitudes at both tested arm-swing frequencies. For both frequencies, the assistive user case achieves significantly greater shoulder-angle amplitudes than the passive user case. As discussed previously, the errors for predicting the shoulder angles are non-negligible, but they do not prevent the shoulder-angle amplitudes from being used to monitor user involvement for rehabilitation for the same therapy session, since the movement of the shoulder joint appears fairly repeatable for a given user during a given session. The RMS errors have no significant differences between user assistance levels and cannot be used to diagnose user involvement.

4.6 Conclusions

The UWEAR has promise of being a successful device for inducing arm-swing. It is a therapeutic device designed to be used along with a body-weight-support during gait rehabilitation on a treadmill. Its design makes it free of kinematic constraints for the user's arms. The error associated with the geometric relationship between the sector pulley and user's shoulder angle (due to unmodeled shoulder-joint movements) is non-negligible at the lower and upper limits of

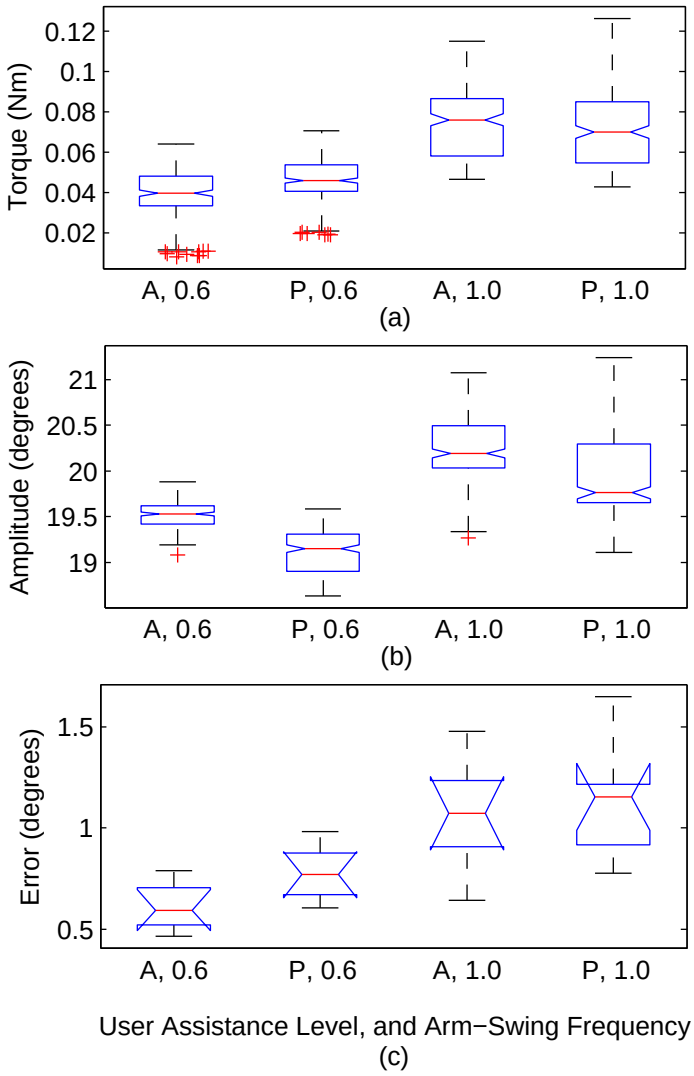

Figure 4.6: Box plots showing the results of the human-subject experiments. The subfigures contain the data for (a) the maximum motor torques, (b) shoulder-angle amplitude, and (c) RMS error. The individual boxes are coded by the user assistance level (A=assistive, P=passive), and arm-swing frequency (1.0=1.0 Hz, 0.6=0.6 Hz). Note that the desired shoulder-angle amplitude is 20°. In a box plot, the red line in the center indicates the median of the data. The upper and lower blue edges that bound the box indicate the 75th and 25th percentile of the data, respectively. The dashed black lines above and below the boxes—the whiskers—extend to the most extreme data points that are not considered outliers. Outliers are plotted as red crosses, if they are present. The notches centered around the medians of the box plots indicate the 95% confidence interval for the median, and indicate whether the median is significantly different from that of another box, depending on if the boxes' notches overlap or not.

the UWEAR's motion range; the device is not to be used for high accuracy positioning. The UWEAR induces arm swing in its users and can diagnose the user assistance level via motor torque and shoulder-angle amplitudes. A remaining open problem is how to generate proper arm-swing trajectories, to be tracked by UWEAR, in real-time based on the user's self-determined walking.

4.7 Acknowledgments

The authors would like to thank Dr. John Hollerbach and Dr. Andrew Merryweather for their helpful comments.

CHAPTER 5

COMPREHENSIVE QUANTITATIVE INVESTIGATION OF ARM SWING DURING WALKING AT VARIOUS SPEED AND SURFACE SLOPE CONDITIONS

The following chapter, under review by the journal Human Movement Science, is aimed at presenting a comprehensive look at the effects of a variety of conditions on arm-swing patterns during walking. The results describe the effects of surface slope, walking speed, and physical characteristics on arm-swing patterns in healthy individuals. Data-driven mathematical models are proposed to quantify the changes in arm-swing patterns and to describe arm-swing trajectories.

B. Hejrati, S. Chesebrough, K. B. Foreman, J. J. Abbott, and A. S. Merryweather, "Comprehensive quantitative investigation of arm swing during walking at various speed and surface slope conditions," *Human Movement Science*, Under Review, 2016

5.1 Abstract

Previous studies have shown that inclusion of arm swing in gait rehabilitation leads to more effective walking recovery in patients with walking impairments. However, little is known about the correct arm-swing trajectories to be used in gait rehabilitation given the fact that changes in walking conditions affect arm-swing patterns. In this paper, we present a comprehensive look at the effects of a variety of conditions on arm-swing patterns during walking. The results describe the effects of surface slope, walking speed, and physical characteristics on arm-swing patterns in healthy individuals. We propose data-driven mathematical models to describe arm-swing trajectories. Thirty individuals (fifteen females and fifteen males) with a wide range of height ($1.58\,\mathrm{m} - 1.91\,\mathrm{m}$) and body mass ($49\,\mathrm{kg} - 98\,\mathrm{kg}$), participated in our study. Based on their self-selected walking speed, each participant performed walking trials with four speeds on five surface slopes while their whole-body kinematics were recorded. Statistical analysis showed that walking speed, surface slope, and height were the major factors influencing arm swing during locomotion. The results demonstrate that data-driven models can successfully describe arm-swing trajectories for normal gait under varying walking conditions. The findings also provide insight into the behavior of the elbow during walking.

5.2 Introduction

Arm swing, which is characterized primarily by arm flexion/extension in the sagittal plane, contributes to balance [9, 83], regulates rotational body motion [18], and increases metabolic efficiency [12] during locomotion of humans. Most clinical and modeling studies on gait tend to ignore arm swing altogether [84]. Gait rehabilitation is often focused on the legs and neglect the role of the upper limbs. However, studies show that there are neural couplings between the upper and lower limbs [9] that can be exploited and may improve gait rehabilitation [15, 85, 86]. New findings also capitalize on the significant role of exaggerated arm swing in improving dynamic stability during walking, which can be utilized for gait rehabilitation of patients with walking impairments [10, 11, 87]. The effect of arm-swing integration in gait rehabilitation becomes more pronounced when patients practice correct arm-swing patterns [86]. However, such patients may have impaired or abnormal arm-swing patterns [84, 23, 14, 88, 89, 90, 91, 92], and may require assistance to attain a more natural arm-swing pattern. Thus, the integration of arm swing in gait rehabilitation may lead to more effective walking recovery for patients with walking impairments [15, 86, 23, 93]. Robotic or other devices for gait rehabilitation should take this integration into account in their design [15, 86].

Although the integration of arm swing in gait rehabilitation has been attempted by previous studies [15, 16, 17], a fundamental question still needs to be answered: What are the correct and

normal arm-swing trajectories that should be utilized for gait rehabilitation and assessment during various conditions? Most studies that propose models for describing arm swing during walking have been motivated to answer the question of whether arm swing is passive or active. Elftman [18] and others [12, 19, 20, 21] have reported shoulder moment peaks using inverse dynamics and motion capture. Since shoulder moments vary significantly in these studies, mechanisms other than the acceleration of the shoulder and gravity likely contribute to arm swing [84]. Goudriaan et al. [22] used a musculoskeletal model in OpenSim and found that muscle activity is needed to obtain correct arm swing amplitude and relative phase. Arms have also been modeled as double pendulums in which the muscle activities have been excluded from the model. Jackson et al. [94] utilized the double pendulum model for the first time to explain arm swing; however, their model lacked proper estimation of several key parameters. The interlimb coordination and transition from 2:1 to 1:1 in arm-to-leg swing frequency ratio were investigated, where a driven pendulum model was used to explain arm movements [95, 96, 97, 98]. Also, a multibody model was developed for simulation of human locomotion by capitalizing on the relationship between arm swing and foot reaction moments [99]. Although arm swing can be partially explained by passive dynamics, the finding of EMG activities in arm muscles suggests that passive models alone cannot adequately represent arm swing during normal walking [100, 101]. Since further investigation is still required to determine the extent to which arm swing is passive, most current models may not rely on valid assumptions for describing arm swing during locomotion.

As mentioned earlier, current models try to provide an insight into the mechanism of arm swing, but they may not be appropriate to generate normal arm-swing trajectories for integrating arm swing into gait rehabilitation. Typical models currently used have been derived using small samples of human subjects performing a limited number of experimental conditions, and they require the measurement of the arms' and joints' mechanical properties, which are not straightforward to obtain. In addition, gait rehabilitation that includes walking on different surface slopes has been recommended as a preferred rehabilitation strategy for improving balance and walking ability to prepare patients for functioning in the community [102, 103]. Arm swing should be considered in slope-walking gait rehabilitation due to its important role in balance and walking ability. Although the effect of surface slope on lower-limb movements has been reported in many studies [104, 105, 106, 107, 108], to the best of our knowledge, the effect of surface slope on arm swing has not been investigated. Therefore, previous models may not capture the variations in arm swing caused by walking in various conditions (i.e., walking at different speeds on different surface slopes).

The purpose of this study is to provide tools for enabling the integration of arm swing in gait rehabilitation by quantifying normal arm-swing trajectories. This study quantitatively investigates

the effect of variations in both walking condition and an individual's physical characteristics on arm-swing patterns during walking. We propose data-driven mathematical models to describe arm-swing trajectory parameters given the mentioned variations. To the best of our knowledge, this is the first time that the effect of surface slope, along with walking speed, on arm swing is reported. We account for the variations between individuals by studying individuals with a wide range of height and body mass who represent a relatively large sample of healthy people with an equal number of male and female participants. Furthermore, this is the first time that the elbow joint angle during various walking conditions is investigated. These findings may help to provide a deeper insight into the mechanism that controls the forearm motion during human locomotion.

The data-driven models can be used to generate arm-swing trajectories in rehabilitative devices aiming to integrate arm swing in gait rehabilitation of patients with walking disabilities [23, 16, 17]. Furthermore, the elbow joint range of motion and its relative phase with respect to the ipsilateral shoulder joint angle during walking may be useful in the design and control of powered-elbow prostheses [109, 110].

5.3 Methods

Thirty healthy subjects participated from a large sample of young individuals with healthy gait. This study was approved by the Institutional Review Board of the University of Utah. We used an equal number of female and male subjects (fifteen males and fifteen females) to account for the effect of gender on arm-swing patterns and to make the results generalizable across genders. The inclusion criteria were the absence of walking disability and gait-related injuries. The age range of our male subjects was 20–35 years with the mean and standard deviation (SD) of (26.00 ± 4.85 years) reported as (mean $\pm$ SD), and the age range of our female subjects was 18–37 years (24.13 ± 5.16 years). Male subjects' body mass ranged from 64–98 kg (77.98 ± 11.59 kg), and female subjects' body mass ranged from 49–71 kg (61.23 ± 7.51 kg). The male subjects' height ranged from 1.70–1.91 m (1.80 ± 0.06 m), and the height range of female subjects was from 1.58–1.76 m (1.67 ± 0.04 m).

5.3.1 Subjects

5.3.2 Experimental protocol

Subjects were required to find their self-selected "normal" and "fastest" walking speeds. Based on each subject's "normal" and "fastest" walking speeds, we used linear interpolation and calculated the midpoint between "normal" and "fastest" speeds to represent the "fast" speed; to calculate "slow" speed, we used linear extrapolation, such that "normal" speed is the midpoint between "slow" and "fast" speeds. Each subject tried four walking speeds as "slow", "normal", "fast", and

"fastest" based on their own self-selected walking speeds, while the overall walking speeds spanned the range of 0.22–2.2 m/s, comparable to the range used in previous studies [97, 90, 23, 92].

To investigate the effect of walking surface slope on arm swing, we utilized five slope levels in our experiments. The slope grades included -15%, -7.5%, 0%, +7.5%, 15%, corresponding to $-8.5^\circ, -4.2^\circ, 0^\circ, +4.2^\circ, +8.5^\circ$, respectively, where negative grades indicate decline walking and positive grades indicate incline walking. Figure 5.1 shows experimental trials with various surface-slope conditions. Overall, each subject tried twenty experimental trials as the combination of four walking speeds on five surface slopes in a randomized order.

5.3.3 Experimental setup and data collection

During a given trial, participants walked at one of their four subject-specific walking speeds, and were instructed to walk naturally on a given slope grade for approximately 1 min. Whole-body kinematic data were recorded during the entire length of each trial by means of a ten-camera motion analysis system (NaturalPoint, Corvallis, OR) operating at 120 Hz sampling frequency. We used thorax, arm, and forearm segments based on a modified clinical model proposed by other researchers [111, 112]. Thorax, arm, and forearm segments and their coordinate systems were defined using markers on the sternum, C7 and T10 spinous processes, clavicle, left/right acromions, left/right medial and lateral epicondyles, and left/right distal radius and ulna landmarks. For tracking the segments during walking, marker clusters were attached to the arms and forearms. All the trials were carried out on a PrecoreC956 treadmill, which has a 3.2 HP motor and is capable of providing a wide incline range of 0%–15%. Since the treadmill had a powerful motor and sturdy structure, it could handle a 181.43 kg (400 lb) user with the maximum speed of 5.36 m/s (12 mph). We utilized adjustable car jack stands under the rear side of the treadmill's frame to provide the decline walking

(a) (b) (c)

Figure 5.1: A subject is performing the experimental trials during (a) decline walking, (b) level walking, and (c) incline walking.

condition.

5.3.4 Data processing

Marker trajectories were labeled and data were imported into Visual3D (C-Motion, Germantown, MD) where raw kinematic data were low-pass filtered (4th-order zero-lag Butterworth with cut-off frequency of 6 Hz using residual analysis [113]). Right-hand rule was followed to form the coordinate systems such that X directed laterally to the right, Y directed forward (anteriorly), and Z axis directed upward (superiorly). Joint angles were calculated in Visual3D using Cardan sequence $XY'Z''$ in which joint angles in the sagittal plane (flexion/extension) were around the X-axes of the proximal segments' coordinate systems. We also extracted the heel-strikes of both left and right feet utilizing the heel markers' trajectories and an algorithm proposed by Zeni et al. [114]. Calculated joint angles and heel-strikes were imported into Matlab (MathWorks, Natick, MA) for further analysis and modeling.

5.4 Results

5.4.1 Shoulder-angle modeling

Shoulder joint angles θ_{sh} in the sagittal plane during subjects' steady-state walking were considered for representing gait-related arm swing. Each shoulder-angle trajectory within an experimental trial was segmented by the contralateral foot's heel-strikes (i.e., the right shoulder angle was segmented by the left foot's heel-strikes, and the left shoulder angle was segmented by the right foot's heel-strikes) as illustrated in Fig. 5.2. The shoulder angle between each two consecutive heel-strikes was considered as the shoulder angle of a gait cycle, which we refer to as a shoulder-angle cycle throughout this paper.

At least five shoulder-angle cycles that had only one peak and one valley in a gait cycle were chosen for each right and left shoulder. Then, all the chosen shoulder-angle cycles were normalized to 100% of their corresponding gait cycles, which enabled superimposing of the chosen cycles within an experimental trial. The mean trajectory of all the shoulder-angle cycles were calculated to represent the mean arm-swing trajectory of a trial. We approximated the mean trajectory of a trial by means of a sinusoid using the Fourier series; the first harmonic (i.e., the fundamental frequency) of the Fourier series was utilized to fit a sinusoid to the mean trajectory. Figure 5.3 shows all of the shoulder-angle cycles from a typical subject and the mean trajectory with its Fourier fit within a trail. The Fourier fit of the mean shoulder-angle trajectory is given by:

$$\theta_{sh} = A_{sh}\cos(2\pi f_{sh}t + \phi_{sh}) + \theta_{0sh} \tag{5.1}$$

where A_{sh} is the amplitude in degrees, f_{sh} is the frequency in Hz, ϕ_{sh} is the relative Fourier phase

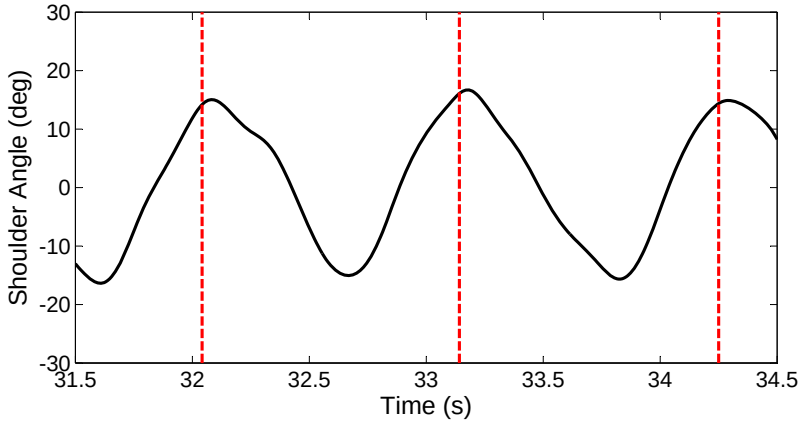

Figure 5.2: Right shoulder joint angle (solid black line) of a typical subject is segmented by the left foot's heel-strikes (dashed red lines) during an experimental trial.

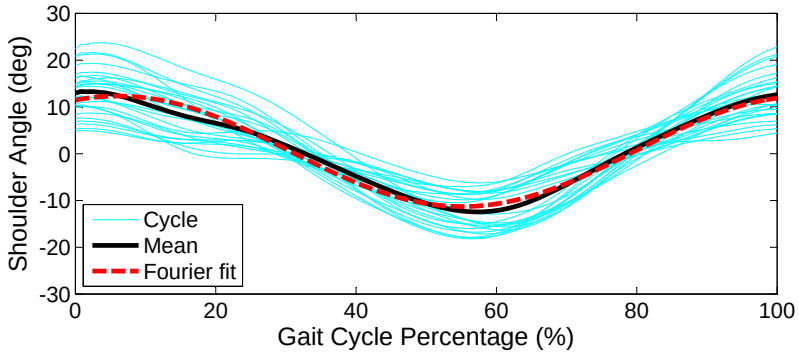

Figure 5.3: Shoulder-angle cycles and the mean cycle with its Fourier fit of a typical subject within a trial.

between the shoulder angle and the contralateral foot's heel-strikes in radians, and θ_{0sh} is the offset value of the shoulder angle, which is the value that the shoulder-angle trajectory oscillates about, in degrees. To provide a better insight into the relative Fourier phase, ϕ_{sh} is presented in degrees throughout this paper, but must be converted to radians for use in Equation 5.1. A positive value of θ_{sh} corresponds to shoulder flexion, and a negative value of θ_{sh} corresponds to shoulder extension, relative to θ_{0sh}. We quantitatively investigated the effect of walking conditions (i.e., walking speed v and surface slope s) and subjects' physical characteristics (i.e., height h, mass m, and gender g) on the shoulder-angle trajectories by examining their effect on each of the Fourier fit's parameters.

A 1:1 arm-to-leg frequency coordination (i.e., one shoulder oscillation per gait cycle) in human walking is a stronger attractor pattern [88], and only 6% of our data, corresponding to very slow walking, followed a 2:1 arm-to-leg frequency pattern. Due to the importance of a 1:1 frequency pattern for gait rehabilitation [9, 15, 86, 92], we only considered cases with a 1:1 arm-to-leg fre-

quency ratio. At least five shoulder-angle cycles from each left and right shoulder-angle trajectories were chosen. The chosen shoulder-angle cycles were normalized to 100% of their corresponding gait cycles to superimpose the cycles within an experimental trial. The mean trajectory of the superimposed cycles were calculated to represent the mean arm-swing trajectory of a trial.

5.4.1.1 Shoulder-angle frequency f_{sh}

The independent variables in our statistical analysis included: height h in meters, mass m in kilograms, gender g with $g = 0$ for females and $g = 1$ for males, walking speed v in meters per second, and surface slope s in degrees; the dependent variable was the frequency of the mean shoulder-angle trajectory f_{sh} in Hertz. We carried out hierarchical multiple regression to investigate the contribution of each individual independent variable to the prediction of f_{sh} using SPSS software package (IBM Corp, Armonk, NY).

The overall multiple regression model comprised of all the independent variables was statistically significant ($p<0.05$). An independent variable was considered significant when the amount of unique variance that it accounted for was statistically significant (i.e., the unique variance is greater than zero with $\alpha = 0.05$). The significant independent variables shown in Table 5.1 are presented in the order of their importance; the importance of independent variables were based on several measures such as R^2-change, F-change, and standardized coefficient. The R^2-change of each significant independent variable indicates the proportion of the variance that the variable accounts for after removing all other variables. The independent variables with larger R^2-change, F-change, and standardized coefficient have larger effect size than other variables. In order to avoid multicollinearity among the independent variables in a model, variance inflationary factor (VIF), which is the inverse of tolerance, should be less than 10 [115] or less than 5 [116]. All the VIF's in Table 5.1 are less than 5, indicating that there was no multicollinearity among the significant independent variables.

Although the significant variables include speed v, slope s, and height h, the effect size of v is

Table 5.1: Statistical analysis for f_{sh} where variables are organized by decreasing R^2-change

Independent Variable	R^2 Change	F Change	Standardized Coefficients	Collinearity Statistics Tolerance	VIF
Speed (v)	56.8%	703.92	0.76	0.98	1.02
Slope (s)	10.8%	211.00	-0.34	1.00	1.00
Height (h)	2.7%	23.69	-0.24	0.34	2.94
Mass (m)	0.2%	1.06	-0.13	0.43	2.32
Gender (g)	0.02%	0.12	0.10	0.42	2.38

substantially larger than the effect size of the others. The shoulder-angle frequency f_{sh} increased by walking speed v, whereas it decreased by an increase in subjects' height h and surface slope s. We developed a mathematical model for calculating the dependent variable f_{sh} based on the significant independent variables. To avoid including unimportant terms in the model and to enhance the usability and conciseness of the model, we did not consider variables with R^2-change less than or equal 1%; thus, m, g, hv, and hs were not included in the model. A linear model was used to represent the relationship between f_{sh} and each of the independent variable v, s, and h since quadratic and cubic polynomials did not improve R^2 of the fits. The proposed model containing an intercept, main effects, and a two-way interaction is expressed by:

$$F_1(h,v,s) = 0.361v - 0.0141s - 0.561h + 0.00340vs + 1.46 \tag{5.2}$$

where $F_1(h,v,s)$ represents the data-driven model for calculating f_{sh} with coefficients obtained by solving the system of linear equations in Matlab. Table 5.2 shows the importance of each variable in the model based on its R^2-change.

5.4.1.2 Shoulder-angle amplitude A_{sh}

To create a model for the amplitude of the mean shoulder-angle A_{sh}, we followed a similar approach to what we described for f_{sh}. All of the significant independent variables shown in Table 5.3 were included for creating the model.

The significant variables include height h, speed v, mass m, and slope s; the effect size of h and v are similar and much larger than the effect size of m and s. The amplitude of the mean shoulder-angle trajectory decreased with an increase of h, whereas it increased by an increase in

Table 5.2: R^2-change due to the use of each variable in Equation 5.2

Variable	v	s	h	vs
R^2-change	56.8%	10.8%	2.70%	1.90%

Table 5.3: Statistical analysis for A_{sh} where variables are organized by decreasing R^2-change

Independent Variable	R^2 Change	F Change	Standardized Coefficients	Collinearity Statistics Tolerance	VIF
Height (h)	22.00%	142.10	-0.63	0.34	2.94
Speed (v)	20.05%	185.33	0.45	0.98	1.02
Mass (m)	2.00%	13.50	0.19	0.43	2.32
Slope (s)	1.10%	10.31	0.10	1.00	1.00

v, m, and s. A quadratic polynomial fits the relationship between A_{sh} and h better than a linear fit, whereas linear fits were best-fitting functions between A_{sh} and the rest of the variables. The proposed model in Equation 5.3 includes variables whose R^2-change was greater than 1%.

$$F_2(h,m,v,s) = -359h + 74.07v + 107h^2 + 0.289mv - 0.267m - 50.1hv + 0.0995s + 323 \tag{5.3}$$

where $F_2(h,m,v,s)$ represents the data-driven model for calculating A_{sh} and Table 5.4 shows the importance of each variable in the model based on its R^2-change.

5.4.1.3 Shoulder-angle offset value θ_{0sh}

The offset value of the mean shoulder-angle trajectory θ_{0sh} was most significantly influenced by the walking surface slope s. Subjects leaned forward during incline walking, thus their arm swing occurred in more flexed angle (i.e., $\theta_{0sh}>0$), whereas subjects leaned backward during decline walking and their arm swing occurred in more extended angle ($\theta_{0sh}<0$). Height h, speed v, and mass m also had statistically significant impact on the offset value; however, they had smaller effect size compared to slope s as shown in Table 5.5.

Linear fits were used to represent the relationships between θ_{0sh} and the independent variables used for modeling since other higher-order polynomials did not improve the fits in terms of R^2. The proposed model in Equation 5.4 includes an intercept, main effects, and two-way interactions with R^2-change greater than 1%:

$$F_3(h,v,s) = 0.160s - 12.3h - 2.28v + 0.246vs + 25.2 \tag{5.4}$$

Table 5.4: R^2-change due to the use of each variable in Equation 5.3

Variable	h	v	h^2	mv	m	hv	s
R^2-change	22.0%	20.05%	2.40%	2.10%	2.00%	1.15%	1.10%

Table 5.5: Statistical analysis for θ_{0sh} where variables are organized by decreasing R^2-change

Independent Variable	R^2 Change	F Change	Standardized Coefficients	Collinearity Statistics Tolerance	VIF
Slope (s)	36.70%	325.11	0.60	1.00	1.00
Height (h)	4.50%	28.49	-0.30	0.34	2.94
Speed (v)	2.80%	14.82	-0.19	0.98	1.02
Mass (m)	0.60%	2.99	0.10	0.43	2.32

where $F_3(h,m,v,s)$ represents the data-driven model for calculating θ_{0sh} and Table 5.6 shows the importance of each variable in the model based on its R^2-change.

5.4.1.4 Shoulder-angle relative Fourier phase ϕ_{sh}

Relative Fourier phase is an advantageous measure for determining the relative phase between two segments compared to other common measures [117, 118]. The relative Fourier phase of the mean shoulder-angle trajectory is the phase between the shoulder angle and contralateral foot's heel-strikes. When $\phi_{sh}>0^\circ$, it indicates that maximum flexion of the shoulder angle precedes the contralateral foot's heel-strike in a cycle, whereas $\phi_{sh}<0^\circ$ indicates the opposite sequence. Table 5.7 shows that walking speed v, surface slope s, and gender g are significant independent variables.

At slower walking speeds, $\phi_{sh}>0^\circ$, meaning that the maximum shoulder flexion preceded the contralateral foot's heel-strikes, and as walking speed increased, the mentioned pattern became reversed ($\phi_{sh}<0^\circ$); the opposite trend exists for the relationship between ϕ_{sh} and s such that as the slope increased from decline walking ($s<0^\circ$) to incline walking ($s>0^\circ$), the value of ϕ_{sh} changed from negative to positive. Gender g had a small effect size compared to the effect size of speed v and slope s. The proposed model expressed in Equation 5.5 utilizes linear fits for explaining the relationships between ϕ_{sh} and the significant independent variables, and it contains only the variables with R^2-change greater than 1%; thus mass m and two-way interactions were not used in the model.

$$F_4(g,v,s) = -40.2v + 1.55s + 8.26g + 41.2 \tag{5.5}$$

where $F_4(g,v,s)$ represents the model for calculating ϕ_{sh} and Table 5.8 shows the importance of each variable in the model based on its R^2-change.

Table 5.6: R^2-change due to the use of each variable in Equation 5.4

Variable	s	h	v	vs
R^2-change	36.70%	4.50%	2.80%	2.00%

Table 5.7: Statistical analysis for ϕ_{sh} where variables are organized by decreasing R^2-change

Independent Variable	R^2 Change	F Change	Standardized Coefficients	Collinearity Statistics Tolerance	VIF
Speed (v)	38.00%	299.05	-0.62	0.98	1.02
Slope(s)	15.60%	167.00	0.39	1.00	1.00
Gender(g)	1.80%	8.67	0.12	0.42	2.38

Table 5.8: R^2-change due to the use of each variable in Equation 5.5

Variable	v	s	g
R^2-change	38.00%	15.60%	1.80%

5.4.1.5 Shoulder-angle model analysis

We utilized two approaches to evaluate the proposed models in Section 5.4.1 for calculating the shoulder-angle parameters (f_{sh}, A_{sh}, θ_{0sh}, ϕ_{sh}); first, we analyzed the relationship between the shoulder-angle parameters predicted by the models and the same parameters obtained from kinematic measurements; second, we assessed the residual errors between the predicted values and the actual measurements for checking the validity of the proposed models. The predicted parameters are denoted by ($f_{sh,p}$, $A_{sh,p}$, $\theta_{0sh,p}$, $\phi_{sh,p}$), and the actual measured parameters are denoted by ($f_{sh,m}$, $A_{sh,m}$, $\theta_{0sh,m}$, $\phi_{sh,m}$).

Figure 5.4 depicts the measured parameters versus the predicted ones, where each data point in the plots represents a pair of predicted and measured values, i.e., ($f_{sh,p}$,$f_{sh,m}$), ($A_{sh,p}$,$A_{sh,m}$), ($\theta_{0sh,p}$,$\theta_{0sh,m}$), ($\phi_{sh,p}$,$\phi_{sh,m}$). The thick line in each plot indicates the best-fit line that explains the relationship between predicted and measured values; the use of high-order polynomials instead of a line did not improve the goodness of the fit. The equation of the best-fit line in each plot is expressed by $y_m = ax_p + b$, where (x_p,y_m) could take any of the paired values mentioned earlier, and a and b are the line's slope and intercept, respectively. Ideally, the best-fit line's slope should be $a = 1$ and its intercept should be $b = 0$, indicating that the predicted values greatly match the measured ones. The thin lines in each plot, which are parallel with the thick lines, illustrate 95% prediction bands for the best-fit lines. The prediction band sizes for f_{sh}, A_{sh}, θ_{0sh}, and ϕ_{sh} are (± 0.18 Hz), ($\pm 7.8^\circ$), ($\pm 6.3^\circ$), and ($\pm 31^\circ$), respectively. The prediction bands in each plot cover an area into which we expect future data points in the form of (prediction,measured) to fall. Therefore, Fig. 5.4 can be used as a tool to decide if an individual's shoulder-angle parameters fall inside or outside the normal ranges. Residual analysis was used to asses whether the errors between the predicted and measured values (residuals) are consistent with a random pattern. The residuals of the proposed models do not demonstrate any particular pattern, and they are centered around zero throughout the range of the predicted values.

Table 5.9 shows the goodness of the fit in terms of R^2 and root-mean-squared error (RMSE) of the proposed models in Section 5.4.1; it also represents the mean value and 95% confidence interval of each best-fit line's slope and intercept (Fig. 5.4), and the mean value and (min,max) of the residuals. The coefficient of determinations R^2 in Table 5.9 indicate that the models sufficiently explain the variations in the shoulder-angle parameters. The slope a and intercept b of the best-fit

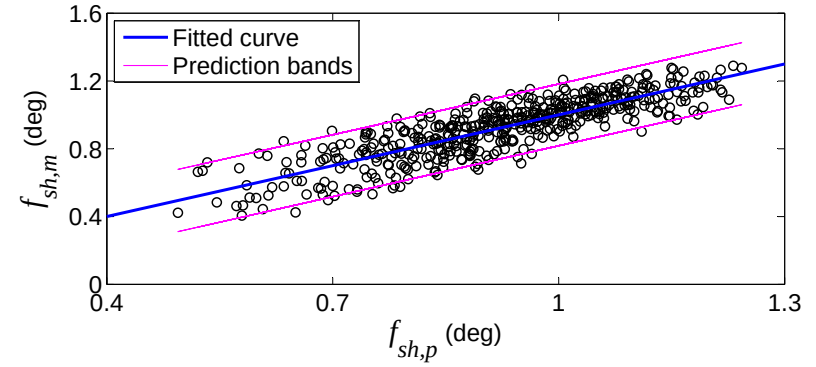

(a)

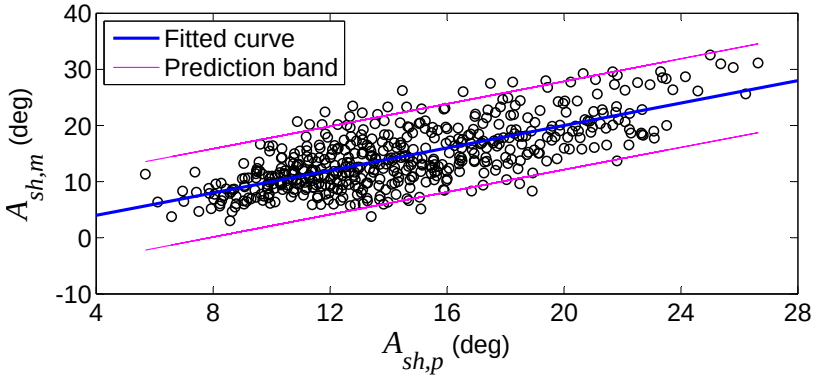

(b)

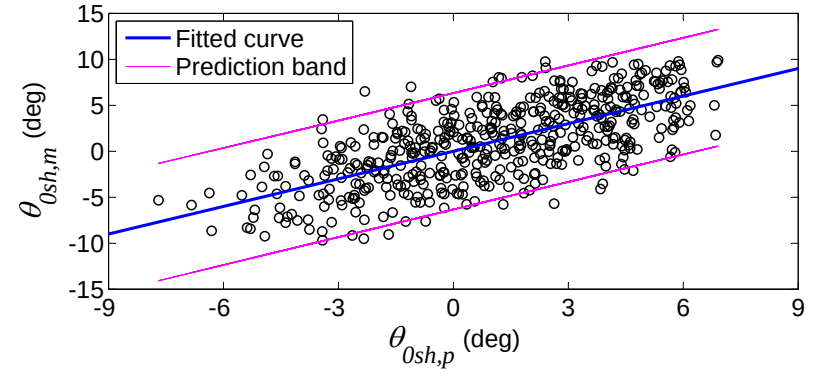

(c)

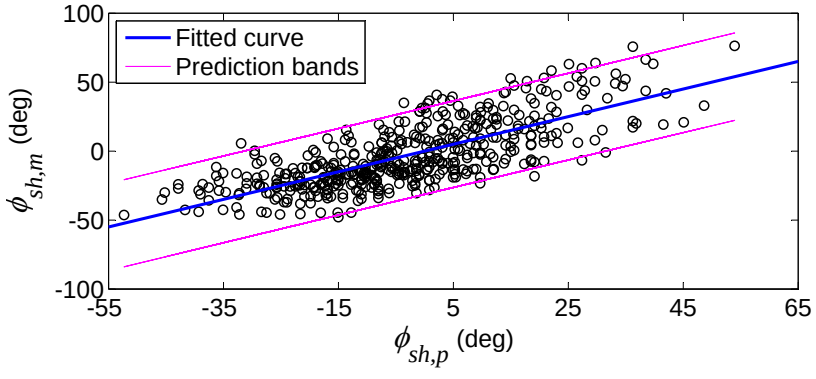

(d)

Figure 5.4: Predicted and measured values for (a) f_{sh}, (b) A_{sh}, (c) θ_{0sh}, and (d) ϕ_{sh}. Data are shown for all subjects. Each data point represents an individual trial.

Table 5.9: Quantitative analysis of the proposed models in terms of coefficient of determination, prediction-measurement relationship, and residual analysis.

Model (variables)	R^2 (%)	RMSE (Units)	a (CI)	b (CI)	Residual mean (min,max)
$F_1(h,v,s)$	72.2%	0.09 (Hz)	1(0.94,1.05)	0(-0.05,0.05)	0(-0.23,0.20)
$F_2(h,m,v,s)$	50.8%	3.98 (deg)	1(0.91,1.08)	0(-1.26,1.26)	0(-10.6,11.7)
$F_3(h,v,s)$	46.0%	3.20 (deg)	1(0.90,1.09)	0(-0.30,0.30)	0(-8.33,8.81)
$F_4(g,v,s)$	55.4%	15.90 (deg)	1(0.92,1.07)	0(-1.46,1.46)	0(-37.35,39.45)

lines for each plot are almost equal to one and zero, respectively, implying that models F_1, F_2, F_3, and F_4 adequately describe the kinematic measurements. The residual mean value of each model was zero and the minimum and maximum errors across the range of predictions were almost symmetric. Residual analysis suggested that the prediction errors were random, thus there was no need to improve the proposed models by including extra variables, using higher-order terms, or considering more complex interaction terms. A leave-one-out cross-validation procedure [119] was used to estimate the true achieved coverage of the prediction bands. The cross-validation analysis demonstrated that the true coverage probabilities for f_{sh}, A_{sh}, θ_{0sh}, and ϕ_{sh} were 94%, 94%, 96%, and 95%, respectively. Since the true coverage probabilities were close to the desired value of 95%, we conclude that the prediction bands were able to capture the normal ranges of shoulder joint angles' parameters, and they can be generalized to the population of people with normal gait [120].

We used the proposed models in Section 5.4.1 to describe the shoulder-angle trajectories as follows:

$$\theta_{sh,p}(h,m,g,v,s) = F_2 cos(2\pi F_1 t + F_4) + F_3 \tag{5.6}$$

Equation 5.6 utilizes the subject's physical characteristics along with walking conditions to describe the shoulder-angle trajectory during locomotion. Figure 5.5 illustrates a few examples of the shoulder-angle trajectory described by Equation 5.6 together with the actual mean shoulder-angle trajectory for an individual participant and walking condition.

The coefficient of determination R^2 was used as the goodness of the model in Equation 5.6, where the described angles were compared with the actual angles obtained by kinematic measurements. The mean value of R^2 and RMSE between described and measured trajectories (with their 95% confidence intervals) are 68.20% (65.57%,70.83%) and 4.80° (4.60°, 4.99°), respectively. Also, the range of motion of the described shoulder trajectories with the mean value of 28.93° (28.21°, 29.66°) were similar to the range of motion of the actual shoulder angles with the mean value of 29.64° (28.60°, 30.69°) with no statistically significant difference ($p = 0.27$) between their

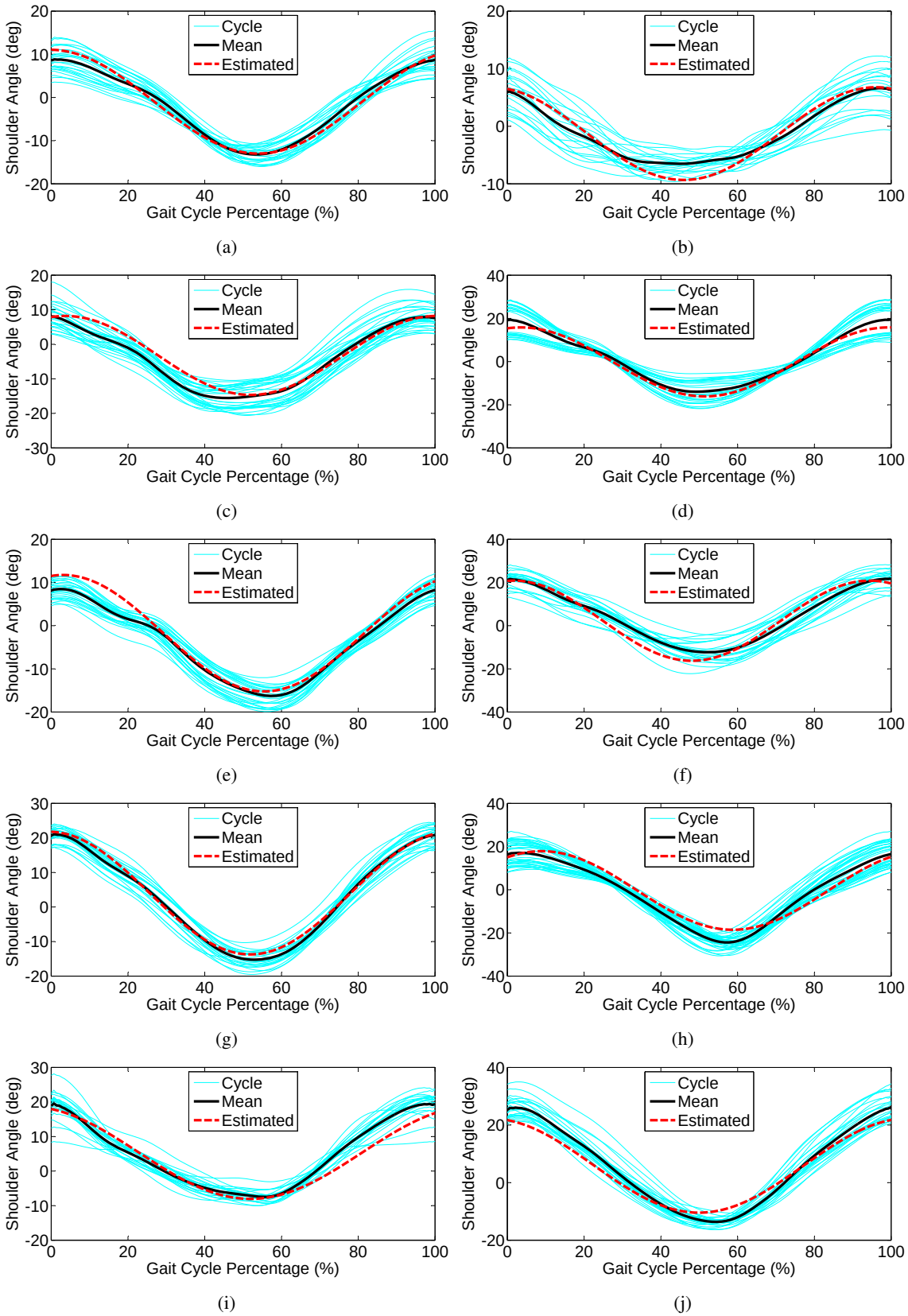

Figure 5.5: Comparison between the described and measured shoulder-angle trajectories for the values of (h,m,g,v,s) as follows: (a) (1.70,74,1,0.88,-8.5), (b) (1.85,72,1,0.52,-8.5), (c) (1.87,84,1,1.40,-4.2), (d) (1.68,65,0,1.18,-4.2), (e) (1.91,98,1,1.5,0),
(f) (1.64,60,0,1.2,0), (g) (1.66,67,0,1.14,4.2), (h) (1.91,97,1,2.2,4.2),
(i) (1.71,71,0,0.88,8.5), and (j) (1.66,67,0,0.96,8.5).

mean values. The obtained results indicate that the proposed models properly describe shoulder-angle trajectories for our study population across all conditions.

To summarize the effect of walking speed and surface slope on the shoulder-angle parameters, we considered a scenario in which hypothetical average male and female individuals performed experiments with different walking conditions. We assumed that the body mass and height of the individuals were equal to the average of our male and female participants' mass and height (i.e., for the male individual $h = 1.80\,\mathrm{m}$ and $m = 78\,\mathrm{kg}$, and for the female individual $h = 1.67\,\mathrm{m}$ and $m = 61\,\mathrm{kg}$). For considering only the effect of walking speed v, we assumed that the individuals walked on a level surface ($s = 0^\circ$) with v ranging from $0.22\,\mathrm{m/s}$ to $2.2\,\mathrm{m/s}$ for the male individual and $0.44\,\mathrm{m/s}$ to $1.7\,\mathrm{m/s}$ for the female individual; these ranges cover our male and female participants' ranges of walking speeds. For considering only the effect of walking surface slope s, we assumed that the individuals walked with our male and female participants' average "normal" walking speeds on a level surface ($s = 0^\circ$) (i.e., $v_{male} = 0.9\,\mathrm{m/s}$ and $v_{female} = 1\,\mathrm{m/s}$), but on the surface slopes ranging from -8.5° to 8.5°. Figure 5.6 demonstrates the changes in shoulder-angle parameters for both hypothetical average individuals as either walking speed or surface slope varies independently. Figure 5.6 makes it possible to quickly visualize the trends on each of the individuals' four shoulder-angle-trajectory parameters as a function of walking speed or surface slope. Gender only directly affects ϕ_{sh} as given by Equation 5.5; the differences between the males and females trends in the other three parameters are caused entirely by the differences in their height, walking speed, and body mass.

5.4.2 Elbow-angle modeling

The elbow joint is a hinge joint that allows the elbow to reach a full flexion of $\theta_{el} \approx 150^\circ$ and a neutral position of $\theta_{el} \approx 0^\circ$. However, the elbow range of motion is typically limited to the neutral position and a small flexion angle during walking. We studied the effect of walking conditions and subjects' physical characteristics on the elbow joint angles θ_{el} in the sagittal plane. Each elbow joint angle's trajectory within an experimental trial was segmented by the ipsilateral shoulder joint angle's local maxima (i.e., the right elbow angle was segmented by the right shoulder angle's local maxima, and the left elbow angle was segmented by the left shoulder angle's local maxima) as illustrated in Fig. 5.7. The elbow joint angle between each two consecutive local maxima of the ipsilateral shoulder joint angle was considered as the elbow angle of a gait cycle, which we refer to as the elbow-angle cycle throughout this paper.

At least five elbow-angle cycles that had only one peak and one valley in a gait cycle were chosen for each right and left elbow. Then, all the chosen elbow-angle cycles were normalized to 100% of their corresponding gait cycle, which enabled superimposing of the chosen cycles

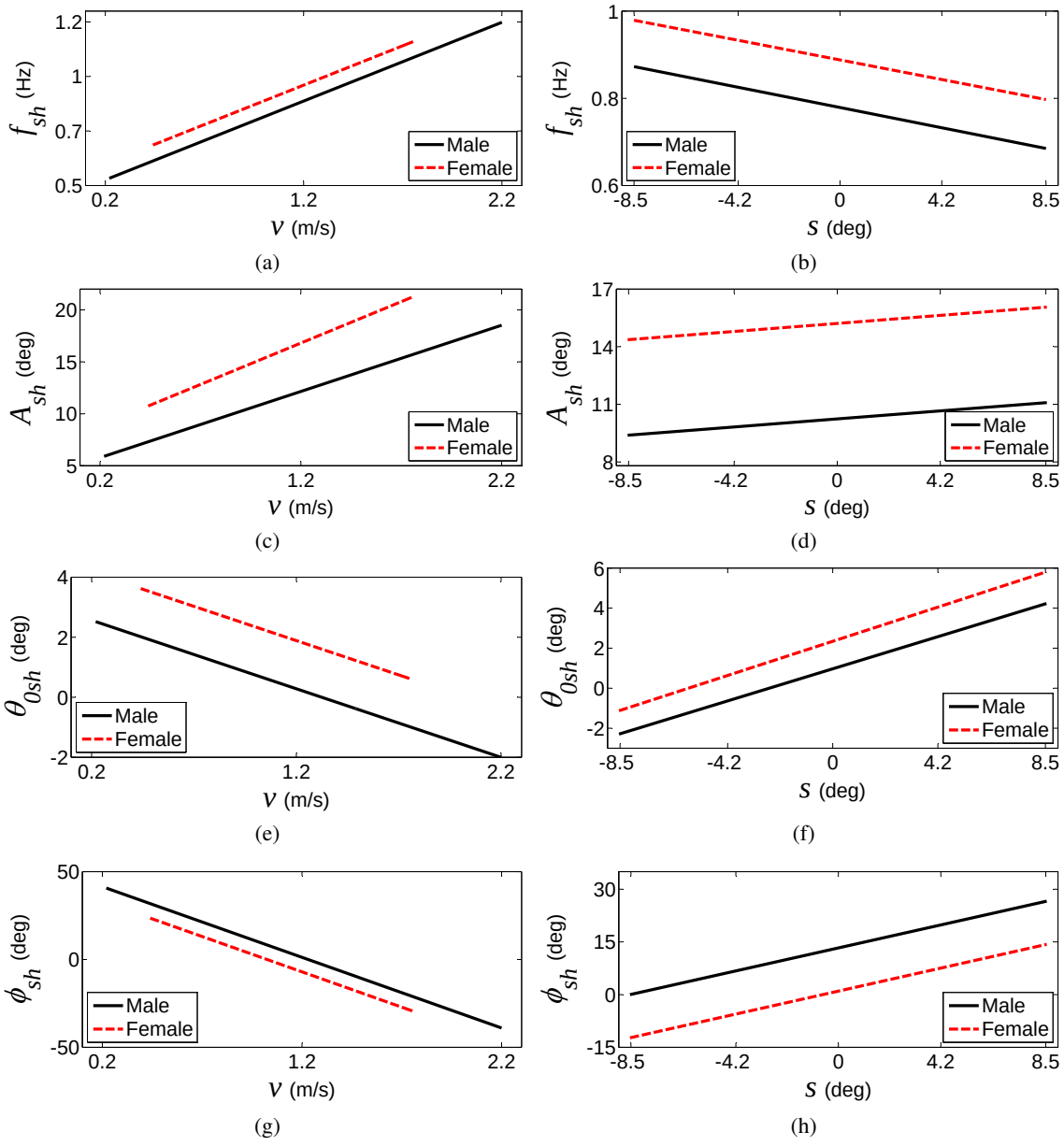

Figure 5.6: Changes in shoulder-angle parameters versus walking speed v and surface slope s are presented in the left and right column, respectively, for typical average male ($h = 1.80\,\text{m}$, $m = 78\,\text{kg}$) and female ($h = 1.67\,\text{m}$, $m = 61\,\text{kg}$) participants performing the conditions with a nominal $v_{male} = 0.9\,\text{m/s}$, $v_{female} = 1\,\text{m/s}$, and $s = 0^{\circ}$.

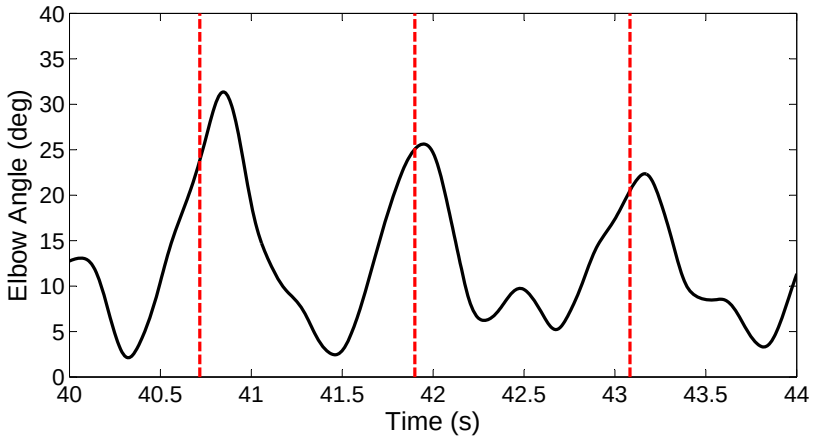

Figure 5.7: The right elbow joint angle of a typical subject (solid black line) is segmented by the right shoulder angle's local maxima (dashed red lines) during an experimental trial.

within an experimental trial. The mean trajectory of all the elbow-angle cycles were calculated as shown in Fig. 5.8. The mean elbow-angle trajectory could not be sufficiently approximated by the first harmonic of the Fourier series. Therefore, we calculated the amplitude, offset value, and relative phase of the mean elbow-angle trajectory in a different manner from the method used for the shoulder-angle trajectory.

5.4.2.1 Elbow-angle amplitude A_{el}

To determine the amplitude A_{el} of the mean elbow-angle trajectory, we divided the range of motion of the elbow joint angle by two:

$$A_{el} = \frac{\theta_{el,max} - \theta_{el,min}}{2} \tag{5.7}$$

where $\theta_{el,max}$ and $\theta_{el,min}$ indicate the maximum and minimum, respectively, of the mean elbow-joint angle in an experimental trial. Statistical analysis showed that walking speed v, gender g, and slope

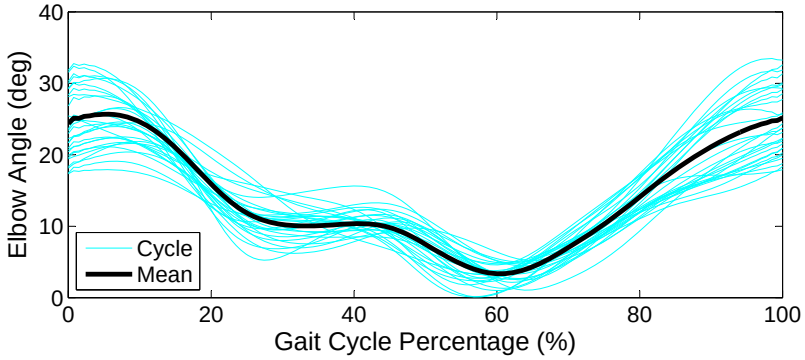

Figure 5.8: Elbow-angle cycles and the mean cycle of a typical subject during an experimental trial.

s were the significant independent variables influencing A_{el} (Table 5.10). Although g and s were found significant, their effect size was considerably smaller than the effect size of v. The amplitude A_{el} increases significantly as walking speed v increases, and A_{el} decreases as the surface slope s changes from decline to incline condition; female subjects (i.e., $g = 0$) has slightly larger A_{el} than male subjects.

Although all the significant variables were considered in developing the mathematical model, only one two-way interaction with R^2-change greater than 1% was used. Linear fits were used to describe the relationships between A_{el} and the significant independent variables. The model, which consists of an intercept, main effects, and a two-way interaction, is expressed by:

$$F_5(g,v,s) = 6.39v - 1.59g + 0.117s - 0.182vs + 0.101 \tag{5.8}$$

where $F_5(g,v,s)$ is the model that explains the changes in A_{el} and Table 5.11 shows the importance of each variable in the model based on its R^2-change.

5.4.2.2 Elbow-angle offset value θ_{0el}

We determined the mean elbow-angle offset value θ_{0el} by:

$$\theta_{0el} = \frac{\theta_{el,max} + \theta_{el,min}}{2} \tag{5.9}$$

Table 5.12 shows that walking speed v, gender g, and slope s were the significant independent variables; however, the effect size of v is considerably larger than the effect size of g and s. θ_{0el} increases significantly as walking speed v increases, and it decreases as the surface slope s changes from decline to incline condition; female subjects (i.e., $g = 0$) has slightly larger θ_{0el} than male subjects. The offset values of the mean elbow angles, unlike the offset values of the mean shoulder

Table 5.10: Statistical analysis for A_{eh} where variables are organized by decreasing R^2-change

Independent Variable	R^2 Change	F Change	Standardized Coefficients	Collinearity Statistics Tolerance	VIF
Speed (v)	40.40%	384.53	0.64	0.98	1.02
Gender (g)	5.90%	31.72	-0.28	0.42	2.38
Slope (s)	2.50%	24.87	-0.15	1.00	1.00

Table 5.11: R^2-change due to the use of each variable in Equation 5.8

Variable	v	g	s	vs
R^2-change	40.40%	5.90%	2.50%	1.78%

Table 5.12: Statistical analysis for θ_{0el} where variables are organized by decreasing R^2-change

Independent Variable	R^2 Change	F Change	Standardized Coefficients	Collinearity Statistics Tolerance	VIF
Speed (v)	40.50%	389.78	0.64	0.98	1.02
Gender (g)	6.20%	33.74	-0.29	0.42	2.38
Slope (s)	2.40%	24.08	-0.15	1.00	1.00

angles, were always greater than zero, since the elbow joint angles were always flexed during locomotion.

All the significant variables and vs (R^2-change greater than 1%) were considered in the mathematical model. Linear fits were used to describe the relationships between θ_{0el} and the significant independent variables. The model, which consists of an intercept, main effects, and a two-way interaction, is expressed by:

$$F_6(g,v,s) = 26.4v - 6.69g + 0.458s - 0.722vs + 2.155 \tag{5.10}$$

where $F_6(g,v,s)$ is the model that explains the changes in θ_{0el} and Table 5.13 shows the importance of each variable in the model based on its R^2-change.

5.4.2.3 Point relative phase between elbow and shoulder $PRP_{el/sh}$

We determined the relative phase between the ipsilateral shoulder and elbow joint angles because it provides insight into the coordination of the shoulder and elbow angles during walking. Since the mean elbow-angle trajectory could not be properly represented by the first harmonic of the Fourier series, we could not use relative Fourier phase for determining the relative phase between the ipsilateral shoulder and elbow joint angles. Instead, we calculated the point relative phase (PRP) based on the moments that local maxima in the shoulder and the ipsilateral elbow joint angles occurred [23]. PRP, in degrees, for gait cycle j was calculated as:

$$PRP_{el/sh}(j) = \frac{t_{max\theta_{el}}(j) - t_{max\theta_{sh}}(j)}{t_{cycle}(j)} \times 360^\circ \tag{5.11}$$

where the gait cycle j was determined by two consecutive shoulder joint angle's local maxima (i.e., maximum flexion angles) as shown in Fig. 5.7, $t_{cycle}(j)$ represents the time duration of gait cycle j in

Table 5.13: R^2-change due to the use of each variable in Equation 5.10

Variable	v	g	s	vs
R^2-change	40.50%	6.20%	2.40%	1.13%

seconds, $t_{max\theta_{el}}(j)$ is the time at which the elbow's maximum flexion in cycle j occurs, and $t_{max\theta_{sh}}(j)$ is the time at which the ipsilateral shoulder's maximum flexion in cycle j occurs. A positive value of $PRP_{el/sh}$ indicates that maximum flexion of the elbow occurred after the maximum flexion of the ipsilateral shoulder, whereas a negative value indicates the opposite sequence.

The mean $PRP_{el/sh}$ for all the gait cycles within an experimental trial was calculated based on the mean elbow joint-angle trajectory as depicted in Fig. 5.8. The results of statistical analysis in Table 5.14 show that height h, speed v, and mass m were significant independent variables. The overall multiple regression model had a small coefficient of determination ($R^2 = 18.4\%$). Although h, v, and m were statistically significant, their effect sizes were small.

5.4.2.4 Elbow-angle model analysis

As discussed previously, the first harmonic of the Fourier series could not sufficiently fit the mean elbow-joint trajectories, so we calculated the amplitude, offset values, and $PRP_{el/sh}$ of the elbow-joint trajectories by using their local maxima and minima. The elbow parameters described by Equations 5.8 and 5.10 are denoted by $A_{el,p}$ and $\theta_{0el,p}$; the values of the parameters evaluated by Equations 5.7 and 5.9 from the measured data are denoted by $A_{el,m}$ and $\theta_{0el,m}$. Figure 5.9 shows the measured elbow-angle parameters versus the predicted ones as ($A_{el,p}$,$A_{el,m}$) and ($\theta_{0el,p}$,$A_{el,m}$), along with their best-fit lines and 95% prediction bands. The prediction band sizes for A_{el}, and θ_{0el} are ($\pm 5.3^\circ$), and ($\pm 22^\circ$), respectively. Residual analysis indicates that the prediction errors of A_{el} and θ_{0el} are centered around zero with patterns consistent with random errors.

Table 5.15 presents the quantitative analysis of the proposed models for A_{el} and θ_{0el} based on the best-fit lines and residual errors of the predictions. The models F_5 and F_6 sufficiently explain the variations in the elbow-angle amplitude and offset value, respectively. The slope a and intercept b of the best-fit lines were close to one and zero, respectively, indicating the predicted values adequately matched the measured ones. The residual mean values were zero and the minimum and maximum errors in the ranges of prediction were approximately symmetric. Since the patterns of residuals were random, we conclude that there is no need to improve the proposed models by including extra variables, using higher-order terms, or considering more complex interaction terms. A leave-one-out

Table 5.14: Statistical analysis for $PRP_{el/sh}$ where variables are organized by decreasing R^2-change

Independent Variable	R^2 Change	F Change	Standardized Coefficients	Collinearity Statistics Tolerance	VIF
Height (h)	13.30%	83.49	-0.21	0.34	2.94
Speed (v)	3.70%	24.26	0.19	0.98	1.02
Mass (m)	1.10%	6.83	-0.16	0.43	2.32

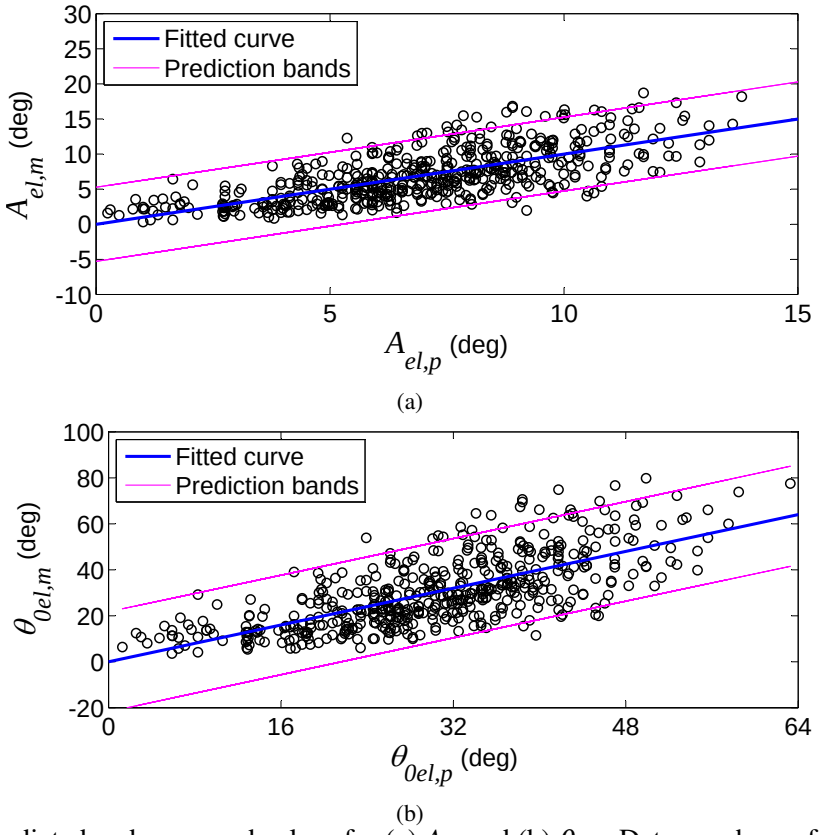

Figure 5.9: Predicted and measured values for (a) A_{el} and (b) θ_{0el}. Data are shown for all subjects. Each data point represents an individual trial.

Table 5.15: Quantitative analysis of the proposed models for A_{el} and θ_{0el} in terms of goodness of the fit, prediction-measurement relationship, and residual analysis.

Model (variables)	R^2 (%)	RMSE (Units)	a (CI)	b (CI)	Residual mean (min,max)
$F_5(g,v,s)$	50.5%	2.66 (deg)	1(0.91,1.08)	0(-0.64,0.64)	0(-7.24,7.92)
$F_6(g,v,s)$	50.2%	10.95 (deg)	1(0.91,1.08)	0(-2.78,2.78)	0(-28.21,33.07)

cross-validation analysis showed that the true coverage probabilities for A_{el} and θ_{0el} were both 94%. Since the true coverage probabilities were close to the desired value of 95%, it is concluded that the prediction bands were able to capture the normal ranges of elbow joint-angles parameters. As discussed earlier for the shoulder-angle parameters, Fig. 5.10 demonstrates the changes in the average individuals' elbow-angle parameters as either walking speed or surface slope varies, similar to what was presented for shoulder-angle parameters in Fig. 5.6. Gender and walking speed account for the differences between the individuals' parameters.

Statistical analysis of $PRP_{el/sh}$ did not indicate any significant independent variable with a

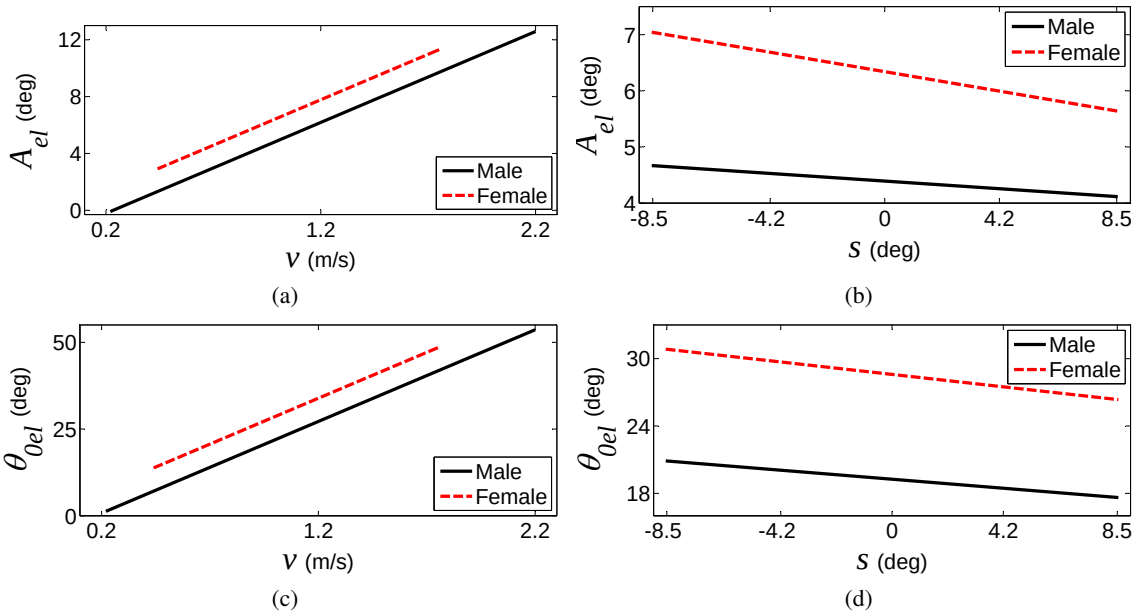

Figure 5.10: Changes in elbow-angle parameters versus walking speed v and surface slope s are presented in the left and right column, respectively, for typical average male ($h = 1.80\,\text{m}$, $m = 78\,\text{kg}$) and female ($h = 1.67\,\text{m}$, $m = 61\,\text{kg}$) participants performing the conditions with a nominal $v_{male} = 0.9\,\text{m/s}$, $v_{female} = 1\,\text{m/s}$, and $s = 0^\circ$.

considerable effect size, thus the multiple linear regression could not explain an acceptable portion of variations in $PRP_{el/sh}$ (i.e., $R^2 = 18.4\%$). The residual analysis of $PRP_{el/sh}$ shown in Fig. 5.11 indicated that two distinct patterns exist in the data. These two patterns could be separated by labeling the residuals located on a straight line in Fig. 5.11 as Pattern 1 and labeling the rest of the residuals as Pattern 2. Figure 5.12a illustrates an example of the elbow joint angle during Pattern 1, in which $PRP_{el/sh}$ is very close to zero, indicating that the maximum elbow flexion occurred at approximately the same time as the maximum ipsilateral shoulder flexion. Figure 5.12b shows an example of the elbow joint angle during Pattern 2, in which $PRP_{el/sh}$ is significantly greater than zero, indicating that there was a significant time lag in the occurrence of the maximum elbow flexion relative to the maximum ipsilateral shoulder flexion.

Patterns were observed across walking conditions and participants' physical characteristics; however, Pattern 2, where significant lag exists, was observed more frequently (67% of trials) than Pattern 1 (33% of trials). The results show our subjects demonstrated both $PRP_{el/sh}$ patterns during walking at various conditions; thus both patterns can be considered as normal elbow movement during locomotion. Since a multiple linear regression model could not sufficiently account for the presence of both patterns, we present $PRP_{el/sh}$ with two distributions. The mean values ($\pm$ standard deviation) of Pattern 1 and Patterns 2 are $3.25^\circ(\pm 0.65^\circ)$ and $23.66^\circ(\pm 8.22^\circ)$, respectively.

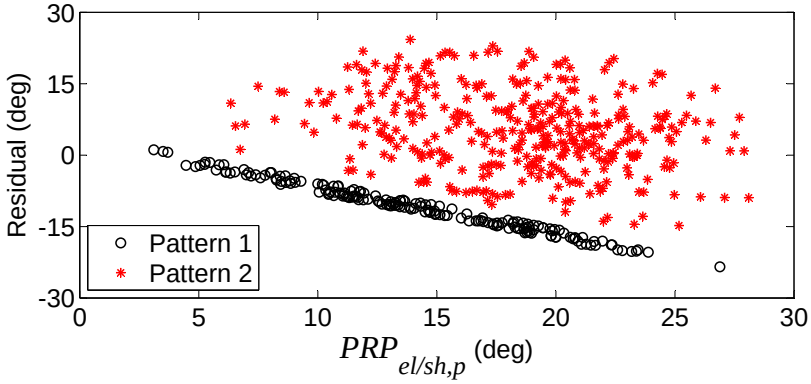

Figure 5.11: Residual plot of the multiple linear regression model for $PRP_{el/sh}$. The black circles demonstrate Pattern 1, and the red asterisks demonstrate Pattern 2.

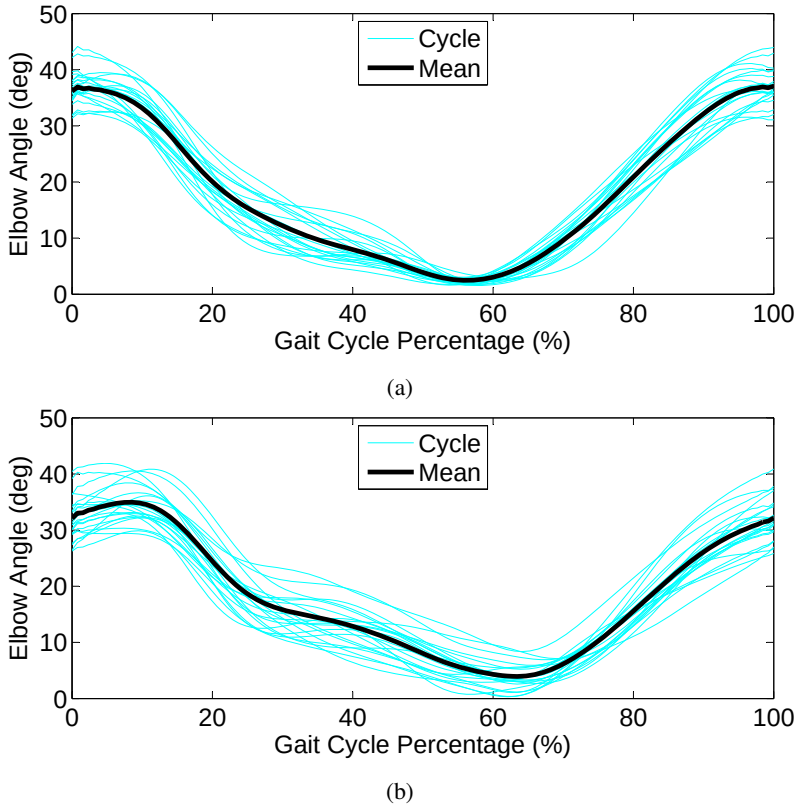

Figure 5.12: The two observed patterns in the point relative phase between elbow and shoulder angles, where (a) $PRP_{el/sh}$ is close to zero, and (b) $PRP_{el/sh}$ is significantly greater than zero.

5.5 Discussion

To address the limitations of existing arm-swing models, we proposed data-driven models based on statistical analyses of the upper-extremities during various walking conditions. The data-driven models simply require five independent variables—height, mass, gender, walking speed, and surface slope—to describe the shoulder-angle parameters such as frequency, amplitude, offset value, and phase, as well as the elbow-angle amplitude and offset value. The trajectories generated by Equation 5.6 may be useful for robotic [16, 17] or other rehabilitation devices [15, 23] that integrate arm swing in gait rehabilitation. Equation 5.6 can use a patient's physical information as primary inputs, and walking speed and surface slope can be measured during walking or be provided as predetermined values to generate desired shoulder-angle trajectories. These trajectories can be applied to the patient by means of devices similar to what is proposed in [16, 17] to correct the patient's arm swing for more effective gait rehabilitation.

In addition, given the fact that analyzing arm-swing patterns in terms of their amplitude and coordination with lower limbs (interlimb coordination) have become increasingly important in rehabilitation of patients with different walking disabilities [23, 121, 90], the plots in Fig. 5.4 and 5.9 may serve as guidelines for diagnosis and assessment of a patients' arm swing.

We also studied the effect of various walking conditions and participants' physical characteristics on elbow-angle parameters. Although walking speed, surface slope, and gender were statistically significant variables, walking speed had a larger effect size than surface slope and gender. We observed two patterns in the point relative phase between ipsilateral shoulder and elbow angles. These two patterns were present across all participants and walking conditions, and both can be considered normal. These results may be helpful for providing a deeper insight into the mechanism that controls the forearm motion during locomotion. However, more studies are required to consider the muscle activities of upper limbs for better understanding of this mechanism.

Our results may be particularly useful for rehabilitation of patients with spinal cord injury since the age group of our participants closely matches those experiencing spinal cord injury [122]. Furthermore, with the addition of older subjects to this study, the results could be expanded to help rehabilitate older individuals who have experienced upper-extremity involvement due to injuries such as stroke and Parkinson disease.

5.6 Conclusion

We investigated the effect of several key factors that influence arm-swing patterns during walking. Although the effect of slope on human walking has been studied in the literature [107, 108], to our knowledge, this work is the first to report the effect of slope on arm swing. Our participants performed a wide range of walking speeds (0.22–2.2 m/s) based on their own self-selected speeds

during the experiments. In this study, we used a large number of participants who represented a wide range of height and mass. Equal numbers of male and female participants were used in the experiments to account for any possible effect of gender on arm swing during walking.

We found that walking speed, surface slope, and individuals' height were the most important factors influencing arm swing during walking. These factors most frequently appeared as significant independent variables with a large effect size in statistical analyses. The shoulder-angle frequency and amplitude increased directly as walking speed increased. Participants' mass and gender were not as influential as height and their effect sizes were small in the statistical analyses.

Our results show that data-driven models can successfully describe arm-swing for normal gait under varying walking conditions. The data-driven models can be used to generate arm-swing-like trajectories for integration of arm swing in gait rehabilitation, for gait assessment of patients with walking disabilities, or for the control of powered-elbow prostheses. The findings also provide a better insight into how the forearm moves during walking in various conditions.

5.7 Acknowledgments

The authors would like to thank Dr. John M. Hollerbach for his support and Alexandra M. Shamir for her assistance in data processing. This work was supported by the National Science Foundation through grant 1208637.

CHAPTER 6

GENERATING ARM-SWING TRAJECTORIES IN REAL-TIME USING A DATA-DRIVEN MODEL FOR GAIT REHABILITATION WITH SELF-SELECTED SPEED

The following chapter, which will be submitted to IEEE Transactions on Neural Systems and Rehabilitation Engineering, is aimed at generating arm-swing trajectories in real-time for gait rehabilitation applications. The results show that the proposed method successfully generates smooth trajectories similar to actual healthy arm-swing trajectories at various walking speeds.

B. Hejrati, A. S. Merryweather, and J. J. Abbott, "Generating arm-swing trajectories in real-time using a data-driven model for gait rehabilitation with self-selected speed," *IEEE Transaction on Neural Systems and Rehabilitation Engineering*, To be submitted, 2016

6.1 Abstract

Gait rehabilitation is often focused on the legs, and overlooks the role of the upper limbs. However, a variety of studies have demonstrated the importance of proper arm swing both during healthy walking and during rehabilitation. In this paper, we describe a method for generating proper arm-swing trajectories in real-time using only measurements of the angular velocity of a person's thighs, to be used during gait rehabilitation with self-selected walking speed. A data-driven linear time-invariant transfer function is developed, using frequency-response methods, which captures the frequency-dependent magnitude and phase relationship between the thighs' angular velocities and the arm angles (measured at the shoulder, in the sagittal plane), using a data set of 30 healthy adult subjects. We show that the proposed method generates smooth trajectories for both healthy individuals and patients with mild to moderate Parkinson disease. The method is verified on gait data gathered from patients with Parkinson disease, and even their pathological thigh trajectories results in proper arm-swing trajectories. The proposed method can be used in future robotic devices that integrate arm swing in gait rehabilitation of patients with walking impairments to improve the efficacy of their rehabilitation.

6.2 Introduction

Gait rehabilitation is often focused on the legs, and overlooks the role of the upper limbs. However, studies show that there is a neural coupling between the upper and lower limbs [9], and this coupling effect can be exploited for rehabilitation of patients with walking impairment [15, 85, 86, 124]. In addition, arm swing contributes to balance [83, 11, 10], regulates rotational body motion [18], and increases metabolic efficiency [12]. The positive effect of arm-swing integration in gait rehabilitation becomes more pronounced when patients practice correct arm-swing patterns [86]. Since it is beneficial for patients with walking impairment to combine rhythmic arm and leg movements [15, 86, 23, 93], gait rehabilitation should take the integration of arm swing into consideration.

Currently, there exist several methods and technologies that attempt to include arm swing in gait rehabilitation. In one study, spinal cord injury patients walked on a treadmill with their arms being manually assisted by a therapist with poles [9]. In other research, sliding handrails were used for stroke patients to enable them to achieve arm swing at a faster walking speed [23]. Other studies have used recumbent stepper machines to show that active upper-limb movements increase neuromuscular activation of the lower limbs during seated recumbent stepping [24, 25]. A robotic device that involves both lower and upper limbs is presented by Yoon et al. [16]. In their device, the walking speed for the robot is updated based on the interactions of the robot with the user's upper

limbs. In all the devices discussed thus far, upper and lower limbs are kinematically constrained with respect to one another; it is likely that what the user experiences is dissimilar to natural overground walking. More recently, our group developed a wearable robotic backpack-type device that is capable of inducing arm swing during gait rehabilitation with a body-weight-support treadmill [17].

The key open problem for the use of robotic devices that induce arm swing for gait rehabilitation is how to generate proper arm-swing trajectories in real-time when patients are allowed to naturally self-select their walking speed. The generated arm-swing trajectories should be periodic (approximately sinusoidal) and have the following key features: First, the generated trajectories should have the same fundamental frequency as the lower limbs (i.e., the stepping frequency) [16, 15, 86, 92]. Second, the generated trajectories need to maintain a correct phase relationship with lower-limb movements [92, 125, 95, 98]. Third, the generated trajectories should be smooth to avoid causing discomfort for the patients when the trajectories are applied to them by a robot; in addition, applying jerky trajectories could lead to learning incorrect muscle firing patterns and an undesired gait [14]. Fourth, the amplitude of generated trajectories should change as a function of the self-selected walking speed and stepping frequency [92, 98].

In order to generate a trajectory with its period matching the walking period at any self-selected walking speed, one may consider measuring the lower-limb movement frequency in real-time, and use it to generate a sinusoidal signal for the arms. A method based on the use of a weighted Fourier linear combiner (WFLC) adaptive filter has been used to estimate lower trunk angle from gyroscope sensors data [126, 127]. Others have used a band-limited multiple Fourier linear combiner (BMFLC) to estimate pathological tremor parameters from gyroscope and accelerometer sensor data [128, 129]. Although the mentioned studies provide a means to estimate the current frequency of the input signals, both WFLC and BMFLC methods have been developed primarily to enable the analytical integration of inertial measurement unit (IMU) sensor data for a drift-free estimation of 3D orientation. Also, an adaptive oscillator can be used to provide an estimation of the fundamental frequency of a quasi-sinusoidal signal in real-time [130, 131]. However, if the input signals are not smooth and quasi-sinusoidal, the frequency estimation is not adequately accurate. Although the extraction of spatio-temporal gait parameters such as step frequency in real-time has been recently considered in a number of studies [132, 133], there is an inherent delay in the methods due to the detection of gait events such as heel strike. The mentioned limitations lead to either generating non-smooth signals or smooth signals with significant time lags, both of which are undesirable. Moreover, merely knowing the walking frequency is not sufficient to generate proper arm-swing trajectories because the correct phase and amplitude relationship between the generated signals and lower-limb movements has to be taken into account.

We recently conducted a study with 30 healthy adults (15 male, 15 female; body mass 49–98 kg; height 1.58–1.91 m; age 18–37 years) in which we characterized arm-swing in the sagittal plane (i.e., the amplitude, phase, and DC offset of the best-fit sinusoidal trajectory) relative to contralateral heel strike [82]. We characterized the effect of walking conditions (walking speed and surface slope) and the subjects' physical characteristics (gender, height, and weight) on arm-swing trajectory parameters. Although the results of this study enable us to predict the arm-swing-trajectory parameters for an average healthy adult (as well as the variance in the parameters across healthy adults) as a function of the aforementioned independent variables, the results still begged the question: How can arm-swing trajectories be generated in real-time during walking at self-selected speed?

In this paper, we propose a simple solution to generate proper arm-swing trajectories in real-time. Our fundamental conjecture is that the knowledge of the thighs' angular velocities, measured by an IMU or motion-capture system, is sufficient to generate arm-swing trajectories in real-time that will be representative of a healthy adult's arm swing. We develop a data-driven mathematical model based on the data set from [82], embodied as a linear time-invariant (LTI) transfer function, which takes a thigh's angular velocity as its input and generates a proper arm-swing trajectory as its output in real-time. With our method, we avoid the inaccuracies and complexities associated with frequency estimation in real-time, and the amplitude and phasing is handled seamlessly. We verify our method using the 30-healthy-subject data set of [82], as well as data collected from nine Parkinson patients from [134], both of which measure the thighs' angular velocities using optical motion tracking. We also verify that our method works with measurements taken from an IMU worn on the thigh.

6.3 Method

We used kinematic data collected from 30 healthy subjects using an optical motion-tracking system during walking on a level treadmill with four equally spaced walking speeds (i.e., "slow", "normal", "fast", and "fastest") based on the subject's self-selected "normal" and "fastest" speeds as described in [82]. The arm angle θ_a and thigh angular velocity ω_t in the sagittal plane (as illustrated in Fig. 6.1) were calculated as a function of time for each of the subjects' left and right arms and legs, respectively.

Our goal is to find a transfer function that takes as its input the angular velocity of the thigh $\omega_t(t)$, and generates as its output an arm trajectory $\theta_a(t)$ that is consistent with what would be expected from a typical healthy adult with the same thigh angular velocity. The transfer function should capture the correct amplitude and phase relationship at the frequencies of interest for walking at self-selected speed. Furthermore, we want the transfer function to be "well behaved", such that high-

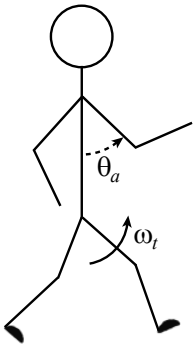

Figure 6.1: A schematic representation of arm joint angle θ_a and thigh angular velocity ω_t in the sagittal plane during walking.

frequency noise in the incoming angular-velocity signal is attenuated, and low-frequency signals that are below the frequency at which humans walk are attenuated. In this regard, we want our transfer function to behave like a band-pass filter, but with specific magnitude and phase behavior in the passband.

We utilize the first harmonic (i.e., the fundamental frequency) of the Fourier series to fit sinusoids to the thigh angular velocity of a given leg, and to the angle of the contralateral arm, as follows:

$$\omega_t = A_t \sin(ft) \tag{6.1}$$

$$\theta_a = A_a \sin(ft + \phi) \tag{6.2}$$

$$M = \frac{A_a}{A_t} \tag{6.3}$$

where we define T as the period of the gait cycle in seconds and $f = 2\pi/T$ as the gait frequency in rad/s. A_t and A_a are the amplitudes of thigh and arm trajectories, respectively, in consistent units of either rad/s and rad, or deg/s and deg. At each gait frequency f, ϕ is the phase shift in the arm angle trajectory relative to the contralateral thigh angular-velocity trajectory. M is the amplitude ratio, with units of seconds. Both M and ϕ significantly depend on the gait frequency f with $R^2 = 9.2\%$ and $R^2 = 42.2\%$, respectively.

The magnitude ratio M and phase shift ϕ, illustrated in Fig. 6.2 versus the gait frequency f, are used to obtain a data-driven transfer function $G(s)$ between the thighs' angular velocities and the contralateral arms' angles. Although subjects' height was found to be a significant independent variable for both M and ϕ, it only accounted for small portions of variances (i.e., $R^2 = 5.9\%$ for M and $R^2 = 1.7\%$ for ϕ). Thus, we neglected the effect of subjects' height when obtaining $G(s)$, which avoided developing an unnecessarily complicated model. Also, the offset values of the arms' angle trajectories were found to significantly dependent on subjects' height; however, the effect size

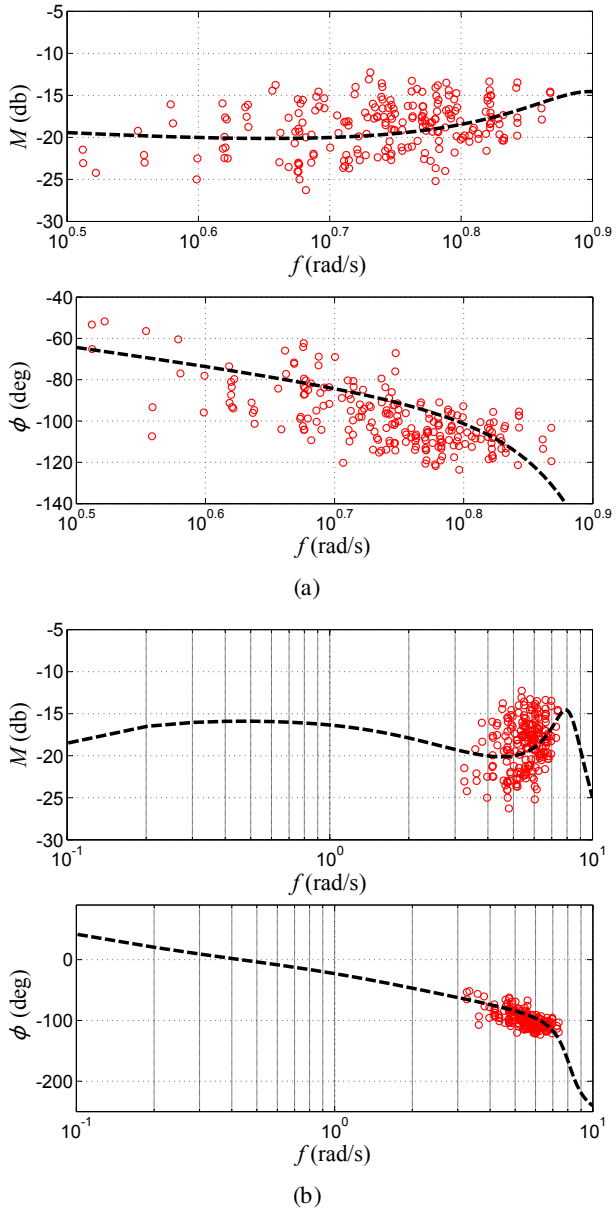

Figure 6.2: Bode diagram of $G(s)$ (black dashed line) within the walking frequency range (a), and over a wider range (b), in which red circles represent experimental amplitude ratios M and phase shifts ϕ between arms' angles and their corresponding contralateral thighs' angular velocities.

of height was found to be small ($R^2 = 2.3\%$). The mean value (with 95% confidence interval) of the arm-trajectories' offset values were found to $0.47^\circ(0.13^\circ, 0.81^\circ)$; since the mean value is small, we neglected the offset value for generating the arm-swing trajectory (we subsequently neglected to include an offset term in (6.2)). By neglecting the small effect of subjects' height, and by neglecting the offset in the arm-swing trajectory, we are able to obtain the simple "one size fits all" LTI transfer function.

Our initial candidate transfer function had a zero at the origin to filter DC signals and two poles to filter high-frequency noise. We found that to perform proper filtering of noisy thigh angular-velocity sensors, our transfer function required a sharp roll-off at frequencies only slightly above the maximum walking frequencies. We used the MATLAB (Mathworks, Natick, MA) System Identification Toolbox to increase the number of poles until we achieved the desired specifications while simultaneously creating a frequency response similar to that of experimental data in the walking frequency range. We prioritized achieving the full set of design specifications over achieving a "best fit" of the data. The transfer function represents the data-driven model in Laplace form:

$$G(s) = \frac{1200s}{s^5 + 58s^4 + 280s^3 + 3900s^2 + 7700s + 730} \tag{6.4}$$

To implement the transfer function, we used MATLAB to convert $G(s)$ to a discrete state-space form using the Tustin discretization method for real-time implementation.

The arm-swing trajectory for a given arm can be directly generated using the contralateral thigh's angular velocity:

$$\theta_a(s) = G(s)\omega_t(s) \tag{6.5}$$

Since the phase difference between the two arms is 180° (since we neglect the offset term), the trajectory for the other arm can be generated simply by using the negative of the trajectory already generated; this method would only use the angular velocity of a single thigh to generate arm-swing trajectories for both arms. Alternatively, the trajectory for a given arm can be generated as the average of trajectories generated by each of the contralateral and ipsilateral thighs' angular velocities:

$$\theta_a(s) = G(s)\left(\frac{\omega_{tc}(s) - \omega_{ti}(s)}{2}\right) \tag{6.6}$$

We will show that this averaging method is more robust to pathological gait, and is the method that should be used during gait rehabilitation.

6.4 Results

To evaluate the performance of the proposed method, we apply the method in (6.6) to the thighs' angular velocities from the collected data to generate arm-swing trajectories. As demonstrated in Fig. 6.3, the generated trajectories have strong correlations with the motion-capture reference trajectories. The phase and frequency of the generated signals closely match the reference trajectories, and despite the non-smooth nature of the thigh angular-velocity signals, the generated trajectories are adequately smooth. The magnitude of generated trajectories is close to the reference trajectories, and has reasonable error when we consider the variance observed in this parameter across the population of healthy adults (see Fig. 6.2).

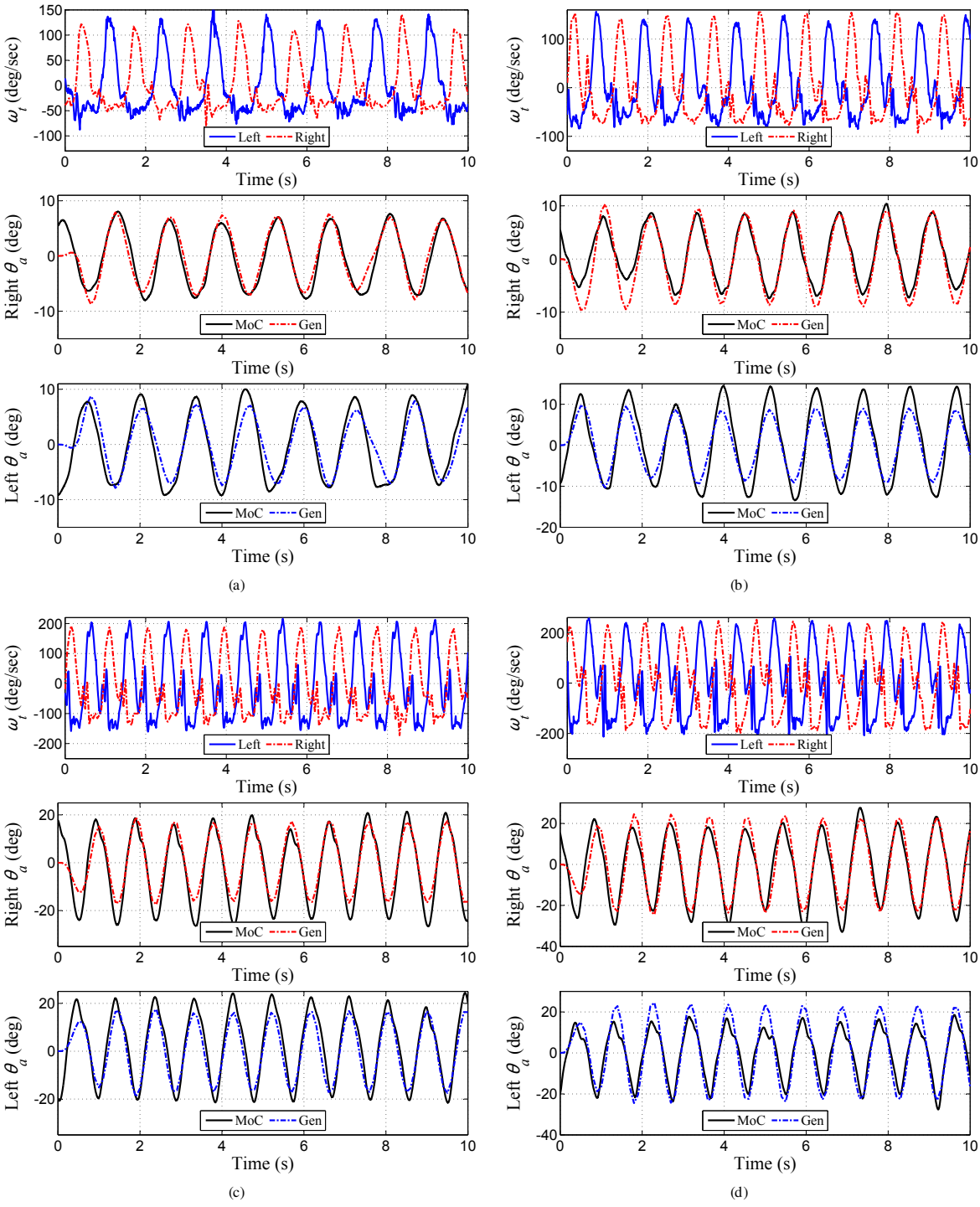

Figure 6.3: Left and right thigh angular velocities from motion-capture, and the resulting generated arm trajectories (using (6.6)) and actual arm trajectories (from motion-capture), of four healthy subjects with walking speeds of: (a) 0.5 m/s, (b) 0.8 m/s, (c) 1.5 m/s, and (d) 2.2 m/s. The motion-capture trajectories correspond to steady-state walking, whereas the generated arm trajectories are initialized at zero to demonstrate a transient response.

We used the coefficient of determination R^2 and correlation coefficient r as metrics to assess the similarity between the arm-swing trajectories generated using our method and the actual trajectories observed with the motion-capture system. The coefficient of determination R^2 and correlation coefficient r between the generated and motion-capture trajectories for the right arm, presented as mean with 95% confidence intervals, are 66.53% (62.65%,70.41%) and 91.10% (89.8%,92.4%), respectively; for the left arm, R^2 and r are 68.64% (64.94%,70.41%) and 90.90% (89.80%,92.40%), respectively. Additionally, although arm-swing is not symmetric in healthy adults, statistical analysis did not reveal significant differences ($\alpha = 0.05$) when applying our method on the left and right arms motion-capture and the generated trajectories in terms of R^2 ($p = 0.43$) or r ($p = 0.82$).

IMUs are commonly used to measure human-body-segment angular velocities in real-time. Since IMUs have different noise properties than motion-capture systems, we tested our proposed method using thigh angular velocities measured by an IMU. We conducted an experiment with 6 healthy adult subjects, with the approval of the Institutional Review Board of the University of Utah. The subjects wore an IMU (a triple axis accelerometer and gyroscope (MPU-6050)) either on their left or right thigh (3 subjects each) during walking. Since each subject only used one IMU, we generated an arm-angle trajectory for the contralateral arm by applying (6.5), and then applying the negative trajectory to the ipsilateral arm. Figure 6.4 demonstrates a few examples of arm-angle trajectories in which the thigh's angular velocity was measured by an IMU. The generated trajectories again have strong correlations with the motion-capture reference trajectories.

Although we can observe the transient response of our LTI transfer function $G(s)$ in Fig. 6.3, in those experiments, the subject is already walking at a steady-state speed at the beginning of data collection. We want to ensure that our method works equally well when the subject begins walking when starting from rest. Figure 6.5 shows a typical generated arm-angle trajectory when a subject starts walking from rest and then reaches a steady-state walking speed. The generated trajectory starts at approximately 0° during the standing phase, and it increases in a well-behaved pattern as the contralateral thigh's angular velocity increases while the subject approaches a steady-state walking speed. We observe that the generated trajectory actually anticipates arm swing a full cycle before it is actually observed in the motion-capture data.

Up to this point, only thigh movements of healthy subjects have been considered for generating arm-swing trajectories (both in terms of generating our data-driven model, and in terms of validating the model). However, it is important to evaluate our proposed method when applied to patients with pathological gait, whose thigh movements are themselves pathological. We applied the method in (6.6) to the gait data of 9 Parkinson patients collected by Merryweather et al. [134]. Table 6.1 shows the demographics for the patients, in which patients' physical characteristics, unified

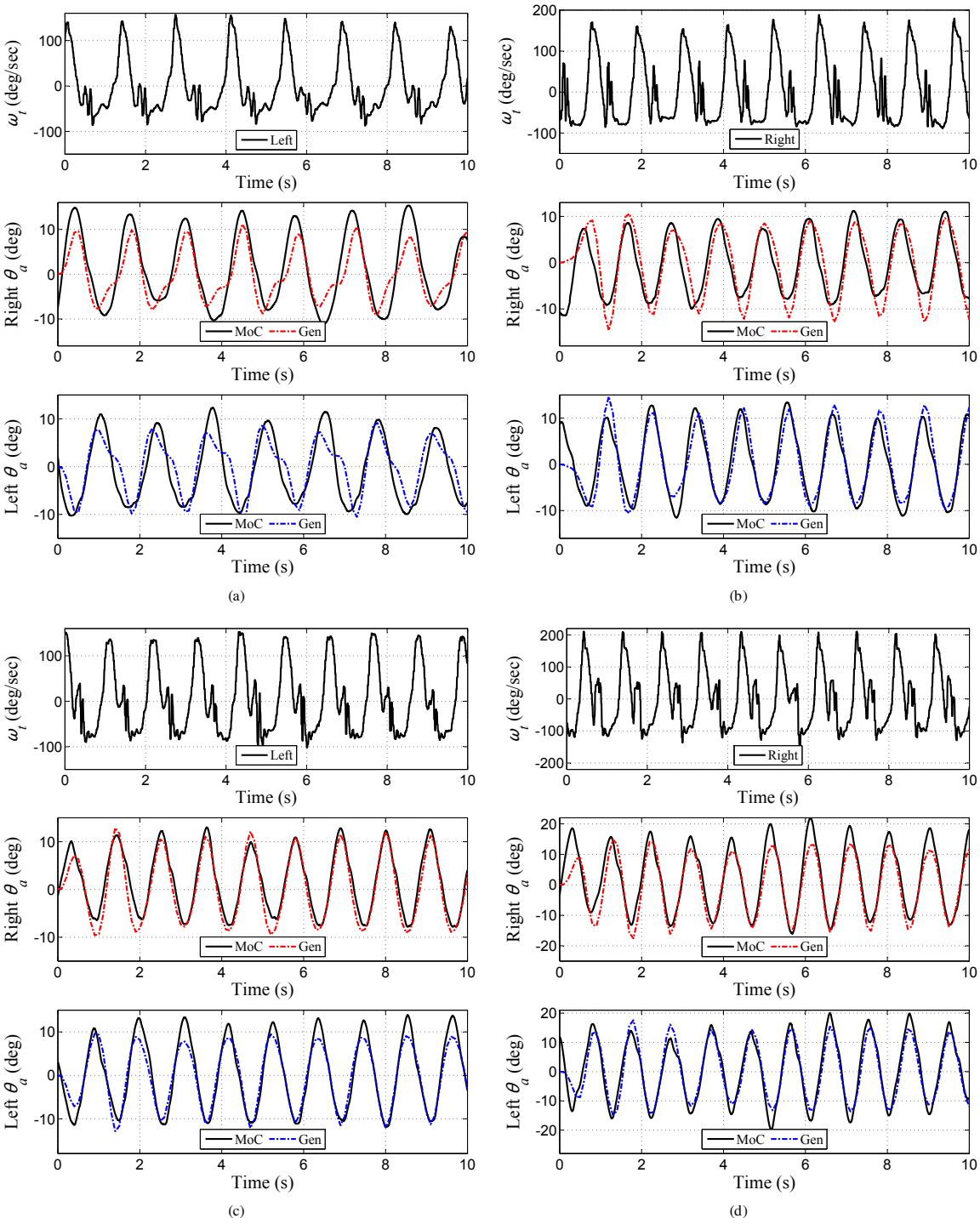

Figure 6.4: Left or right thigh angular velocity from IMU, and the resulting generated arm trajectories (using (6.5)) and actual arm trajectories (from motion-capture), of four healthy subjects with walking speeds of: (a) 0.6 m/s, (b) 1.1 m/s, (c) 1.2 m/s, and (d) 1.4 m/s. The motion-capture trajectories correspond to steady-state walking, whereas the generated arm trajectories are initialized at zero to demonstrate a transient response.

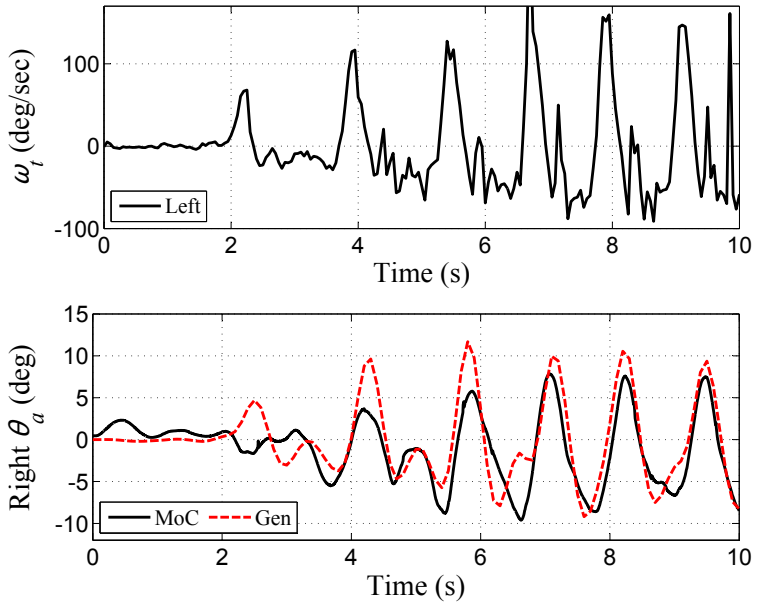

Figure 6.5: Generating the arm-swing trajectory while a subject transitions from standing to steady-state walking.

Table 6.1: Demographics of Parkinson patients with values reported as mean (standard deviation).

Female	3
Male	6
Age	67.67 (7.05)
Mass (kg)	80.98 (20.58)
Height (m)	1.66 (0.16)
UPDRS score	36.13 (11.78)
H&Y score	2.39 (0.31)

Parkinson's disease rating scale (UPDRS), and Hoehn and Yahr scale (H&Y) are presented. Figure 6.6 shows the generated trajectories for the right and left arms of the patients given their thighs' angular velocities, obtained from motion-capture. The proposed method could successfully generate smooth trajectories for the patients at their self-selected walking speeds.

Due to their pathological gait, we should not use the patients' actual arm trajectories as the ground truth for evaluating the generated trajectories. However, we substituted the patients' thigh angular velocities and their corresponding generated arm trajectories in (6.1), (6.2), and (6.3) to compare the magnitude and phase response of the patients' generated trajectories with those of subjects with healthy gait at the same stepping frequency. Figure 6.7 shows that the magnitude of the generated trajectories and their relative phases with respect to the contralateral thigh's angular

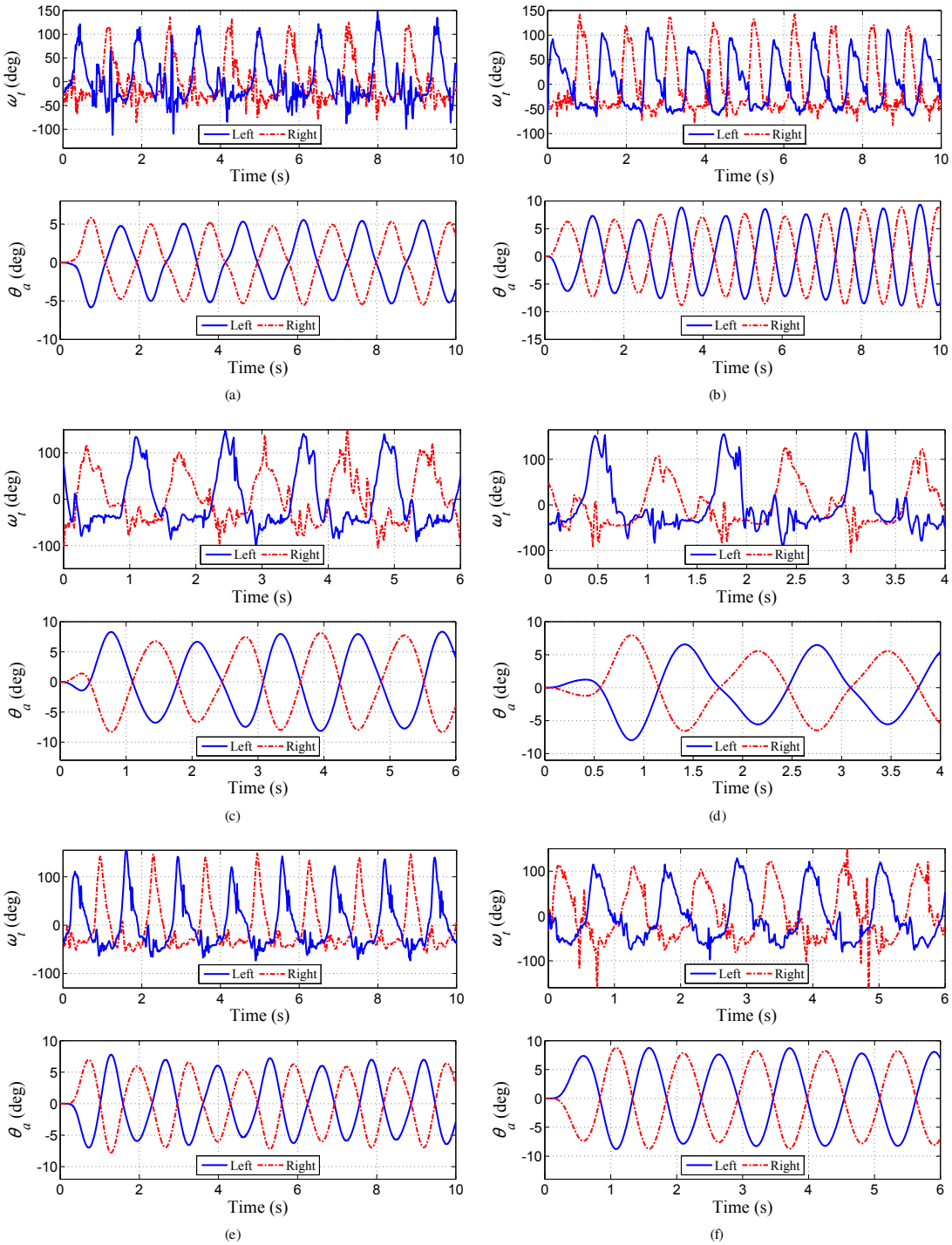

Figure 6.6: Left and right thigh angular velocities from motion-capture, and the resulting generated arm trajectories (using (6.6)) for six Parkinson patients with walking speeds of approximately 0.5 m/s.

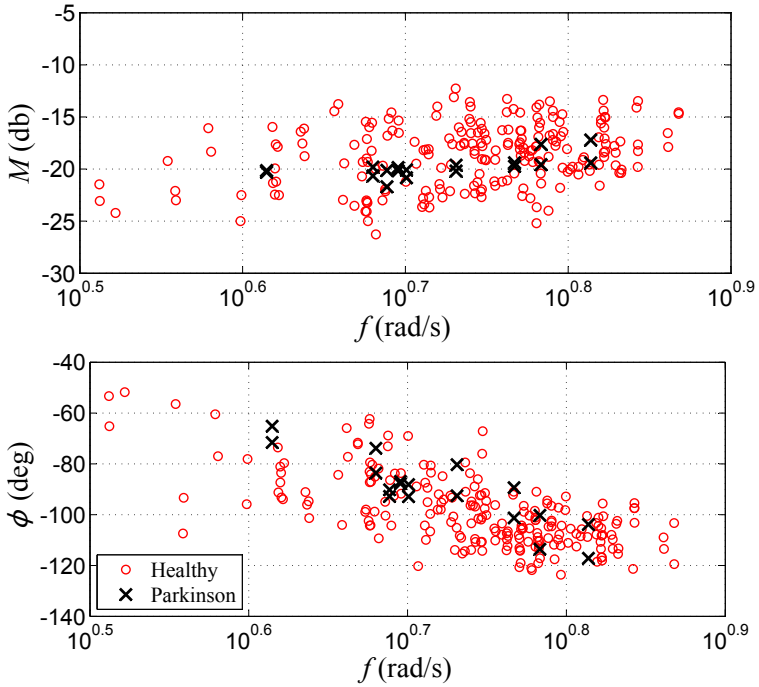

Figure 6.7: Magnitude M and phase ϕ of generated arm-angle trajectories relative to thigh-angular-velocity trajectories for Parkinson patients (black crosses) compared to the data for healthy subjects (red circles).

velocities for Parkinson patients are within the variance of subjects with healthy gait. Thus, we conclude that the pathological thigh angular velocities of Parkinson patients generate a proper arm-swing trajectory.

We found that using only one thigh's angular velocity using (6.5) to generate arm-swing trajectories works satisfactorily for many cases, including most healthy subjects and some pathological subjects. However, Fig. 6.8 shows an example where the generated arm trajectory for a Parkinson patient using only one thigh was qualitatively less smooth than the trajectory generated by measuring both thighs and using (6.6). We observed a similar response in the healthy-subject experiment shown in Fig. 6.4(a). We conclude that measuring both thighs' angular velocities and using (6.6) is the preferred method for use during rehabilitation of pathological gait.

6.5 Discussion

The application of the proposed method is in devices that attempt to integrate arm swing in gait rehabilitation [17]. The reason for choosing thigh angular velocities rather than other gait parameters is that thigh angular velocities can be simply and directly measured by an IMU during walking without any additional processing. The results of this study show that the generated arm-

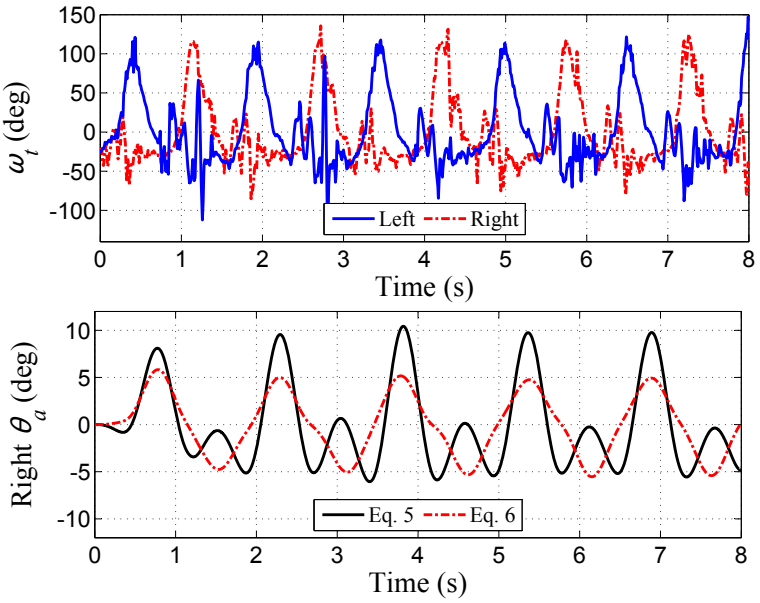

Figure 6.8: Left and right thigh angular velocities of a Parkinson patient, and right arm trajectories generated by using only the left thigh angular velocity using (6.5), and generated by using both left and right thigh angular velocities using (6.6).

swing trajectories satisfied our desired criteria. By using a data-driven LTI transfer function, the generated arm trajectories inherently have the same frequency as the lower-limbs at any self-selected speed, which is essential for coordinated walking. The proposed method generates trajectories that have the proper phase relationships with respect to the gait cycle throughout the full range of walking frequencies. Despite the non-smooth nature of thigh angular velocities, our transfer function's inherent filtering of high-frequency noise, combined with the averaging implemented in (6.6), results in smooth signals that can be applied to patient's arms during gait rehabilitation by robotic or other rehabilitation devices without causing discomfort.

Given that various walking impairments may result in different pathological gait patterns, one method may not be sufficient to generate arm-swing trajectories for patients with different walking impairments. Future work should apply our method to a variety of gait pathologies, such as spinal cord injury and stroke, to determine which pathological gaits can be addressed by our proposed method directly. In addition, future research may consider the relationship between arm trajectories and the motion of other body segments, such as torso rotation or heel-strike, during walking with self-selected speed. It may be possible to apply the techniques used in this paper to generate a new LTI transfer function whose input is one of the aforementioned signals, and this new transfer function may be a better generator of proper arm swing for patients with other gait disorders. But to reiterate, it may be that the method proposed in this paper can be applied, without modification,

to a variety of gait pathologies.

6.6 Conclusions

We proposed a method for generating proper arm-swing trajectories in real-time using only measurements of the angular velocity of a person's thighs, to be used during gait rehabilitation with self-selected walking speed. A data-driven linear time-invariant transfer function was developed, using frequency-response methods, which captures the frequency-dependent magnitude and phase relationship between the thighs' angular velocities and the arm angles (measured at the shoulder, in the sagittal plane), using a large data set of healthy adult subjects. The proposed method generates smooth trajectories that have high correlations with the actual measured arm trajectories of the healthy individuals. The method was verified on gait data gathered from patients with Parkinson disease, and even their pathological thigh trajectories resulted in proper arm-swing trajectories. The proposed method can be used in future robotic devices that integrate arm swing in gait rehabilitation of patients with walking impairments.

6.7 Acknowledgments

The authors would like to thank Dr. Kam K. Leang for his valuable advice regarding frequency-response methods. This work was supported by the National Science Foundation through grant 1208637.

CHAPTER 7

RECOMMENDATIONS FOR FUTURE WORK

Robot-assisted gait rehabilitation can be more effective and less laborious than traditional gait-rehabilitation procedures performed by physical therapists. Therefore, it offers great promise for helping patients with walking difficulties. Considerable effort has been made to improve the state-of-the-art rehabilitation robotics to better prepare patients for dealing with challenges in real-world walking scenarios and to increase their engagement during gait rehabilitation.

In Chapters 2 and 3, the Treadport is proposed as a promising tool for simulating overground walking experience in a virtual environment with applications in gait rehabilitation. Our results in Chapter 2 show that walking on the Treadport may lead to gait patterns that are beneficial for the walking recovery of patients with walking impairments. The Treadport has three unique key features that can be exploited for more effective gait rehabilitation. These features include self-selected speed capability, a relatively large belt, and a CAVE-like visual display. Since SCI patients in Chapter 2 have experienced all of these three features simultaneously while walking on the Treadport, it is not clear how each feature has affected their gait. It is important to determine how each key feature contributes to the patients' gait performance. This knowledge can lead to more effective and optimal designs for the next generation of locomotion interfaces that will be used particularly for rehabilitation applications.

To create real-world scenarios on a locomotion interface, it is necessary to consider new designs and control methods to render three-dimensional force feedback to the user. For instance, to render walking at various slope conditions or hitting into a virtual wall, it is required to apply horizontal forces to the users. Sideway forces are required to create scenarios for balance rehabilitation and perturbation studies of patients with walking impairments [135, 136]. More advanced designs for vertical force display will provide partial body weight support, while allowing the patients to comfortably roam around in a wide workspace.

Currently, patients interact with assistive robots, such as the Treadport, mainly through physical contacts. Interactive forces and displacements of the patients are measured, and then this information is utilized for controlling the robot to adopt to the patient's motion. However, the

pathological gait of patients may result in misleading information that can adversely affect the robot-patient interactions. Therefore, an EEG-based locomotion interface will hold great promise for gait rehabilitation of patients with walking impairments. Future studies should focus on finding an optimal method to fuse EEG and physical contact data to create a natural and robust patient-robot interaction.

Moreover, future locomotion interfaces should focus on providing whole-body gait rehabilitation by integrating arm swing in gait rehabilitation. The UWEAR offers great possibilities to include arm swing to achieve a whole-body gait rehabilitation. Although the UWEAR is primarily designed to induce arm-swing trajectories that follow the patient's leg movements for creating a coordinated walking experience, it is shown that rhythmic arm movements can also evoke leg movements [16, 93]. So, arm movements may be used as the leading movements to drive the legs during rehabilitation. The UWEAR can be used as a gait-modulator device such that by applying arm-swing trajectories to patients with various frequencies and amplitudes, the patients' gait patterns are modified to achieve a better walking recovery. Although the UWEAR is designed to be used along with a body-weight-support system, lighter components may still be considered for the next UWEAR prototype. Subject-study results in Chapter 4 indicate that a considerable amount of torque is required to induce arm swing. This torque requirement may be even more when dealing with patients who do not demonstrate any observable arm swing during walking. Thus, there has to be a compromise between the weight of the device and its power capability in future designs and prototypes.

The results in Chapter 5 may be particularly useful for rehabilitation of patients with SCI since the age group of our participants closely matches those experiencing SCI [122]. With the consideration of older subjects, the results could be expanded to help rehabilitate older individuals who have experienced upper extremity involvement due to injuries such as stroke and Parkinson disease.

The proposed method in Chapter 6 can be used as a "building block" in the controller of robotic devices such as the UWEAR to create desired trajectories for inducing proper arm swing in patients. Given that various walking impairments may result in different pathological gait patterns, a single method may not be adequate to generate arm-swing trajectories. Future research may consider the relationships between shoulder joint angles and other body parts' motion such as torso rotation or heel-strike during walking. Additional models can be derived to be used along with our proposed method for generating robust arm-swing trajectories for patients with various walking impairments.

CHAPTER 8

CONCLUSIONS

This dissertation has presented advancements in robot-assisted gait rehabilitation with self-selected speed. This dissertation was motivated by the shortcomings associated with existing gait rehabilitation procedures and devices. First, they fail to depict realistic walking experiences for patients during rehabilitation. Second, they de-emphasize the role of upper limbs in inducing lower-limb muscle activity. Two major research thrusts have been conducted to address the mentioned shortcomings. The first thrust has focused on enhancing the realism of walking on the Treadport with applications for gait rehabilitation of patients with walking impairment. The second thrust has considered the inclusion of arm swing in gait rehabilitation for more effective rehabilitation of the patients.

As a part of the first major research thrust, Chapter 2 demonstrated the potential of the Treadport for gait rehabilitation of spinal-cord-injury (SCI) patients. The comparison of four SCI patients' gait parameters, while walking on the Treadport and on a traditional treadmill, show that walking on the Treadport can be beneficial for these patients' recovery. The results indicate that walking on the Treadport led to significant improvements in hip and knee ranges of motion, walking speed, and walking symmetry of the patients compared to walking on a traditional treadmill. The results suggest that standard treadmills may impose some constrains on a patient's motion that can be overcome on the Treadport.

The realism of walking on the Treadport was considered in Chapter 3 as another part of the first major research thrust. Two main factors have been identified that significantly influence the walking perception of users on the Treadport: the belt controller and kinesthetic force feedback. Given the mentioned factors, a new belt controller was implemented to realize the self-selected speed capability of the Treadport; when combined with the user's volition, this same controller also enables the user to naturally self-select their walking speed as they would when walking over ground. In addition, a new kinesthetic force-feedback controller was designed for the tether that applies forces to the user's torso based on maintaining the user's sense of balance during belt acceleration. The results of the human-subjects study indicate that both the belt controller and the

kinesthetic force-feedback method significantly contribute to an improved perception of realistic walking on the Treadport. The findings in Chapter 3 should generalize to any locomotion interface that enables walking with self-selected speed.

In the second major research thrust, Chapter 4 presented the design and fabrication of the UWEAR to properly induce arm swing during gait rehabilitation for neurorehabilitative purposes. The proposed design actively provides assistance for the user's arm swing in the sagittal plane, and it has unhindered kinematics in the remaining unactuated degrees of freedom. The biggest design challenges for the UWEAR was to generate sufficient torques for inducing arm swing and to transfer the generated torque thoroughly to the user's arms. The results demonstrate the Underactuated WEarable Arm-swing Rehabilitator's (UWEAR) ability to induce arm-swing in its users under a variety of conditions including different arm-swing frequencies (0.6 Hz or 1.0 Hz, which correspond to a slow and brisk walking pace, respectively), and different user-assistance levels (passive, in which the user relaxes their arms, and assistive, in which the user attempts to swing their arms as being directed by the UWEAR, using only haptic information). Moreover, the UWEAR can diagnose the level of the user's assistance by examining the peak motor torque and shoulder-angle amplitudes.

The effect of several key factors that influence arm-swing patterns during walking was investigated in Chapter 5. Although the effect of slope on human walking has been studied in the literature, to our knowledge, this work is the first to report the effect of slope on arm swing. The results show that walking speed, surface slope, and individuals' height are the most important factors influencing arm swing during walking. These factors most frequently appeared as significant independent variables with a large effect size in statistical analyses. Also, the developed data-driven models can successfully describe arm-swing for normal gait under varying walking conditions. The findings also provide a better insight into how the forearm moves during walking in various conditions.

A method for generating proper arm-swing trajectories in real-time using only measurements of the angular velocity of a person's thighs was described in Chapter 6, to be used during gait rehabilitation with self-selected walking speed. A data-driven linear time-invariant transfer function was developed, using frequency-response methods, which captures the magnitude and phase relationship between the arm angles (measured at the shoulder, in the sagittal plane) and the thighs' angular velocities as a function of stepping frequency, using a large data set of healthy adult subjects. The proposed method generates smooth trajectories that have high correlations with the actual measured arm trajectories of the healthy individuals. The method was verified on gait data sets gathered from patients with Parkinson disease, and even their pathological thigh trajectories resulted in proper arm-swing trajectories. The proposed method can be used in future robotic devices that integrate

arm swing in gait rehabilitation of patients with walking impairments to improve the efficacy of their rehabilitation.

The results of this dissertation contribute to the design and control of robotic devices that facilitate gait rehabilitation at self-selected speeds, which are essential for creating a natural walking experience for the patients. This dissertation deepens the scientific understanding, and has the potential to improve the lives of patients with spinal cord injures, Parkinson disease, and other types of walking impairments. The current trend in gait rehabilitation is toward using more advanced locomotion interfaces. The Treadport creates a unique opportunity for creating such realistic environments with the capability of monitoring and assessing the patients. The developed methods in this dissertation, using the Treadport, are applicable to any similar locomotion interface for simulating realistic walking. The concept design of the UWEAR is a novel approach that capitalizes on whole-body gait rehabilitation. A more effective gait rehabilitation, which requires the inclusion of upper-limb movements in the rehabilitation, can be achieved through the application of the proposed methods in this dissertation.

REFERENCES

[1] *Spinal Cord Injury (SCI) Facts and Figures at a Glance*, National SCI Statistical Center (NSCISC) Std.

[2] B. Dobkin, D. Apple, H. Barbeau, M. Basso, A. Behrman, D. Deforge, J. Ditunno, G. Dudley, and R. Elashoff, "Methods for a randomized trial of weight-supported treadmill training versus conventional training for walking during inpatient rehabilitation after incomplete traumatic spinal cord injury," *J. Neurorehabilitation and Neural Repair*, vol. 17, pp. 153–167, 2003.

[3] A. Koenig, X. Omlin, J. Bergmann, L. Zimmerli, M. Bolliger, F. Muller, and R. Riener, "Controlling patient participation during robot-assisted gait training," *J. NeuroEngineering and Rehabilitation*, vol. 8, pp. 8–14, 2011.

[4] S. J. Lee and J. Hidler, "Biomechanics of overground vs. treadmill walking in healthy individuals," *J. Applied Physiology*, vol. 104, no. 3, pp. 747–755, 2008.

[5] A. L. Hicks, "Treadmill training after spinal cord injury: It is not just about the walking," *J. Rehabilitation Research and Development*, vol. 45, no. 2, pp. 241–248, 2008.

[6] A. Wernig and S. Muller, "Laufband locomotion with body weight support improved walking in persons with sever spinal cord injuries," *Int. Medical Society of Paraplegia*, vol. 30, pp. 229–238, 1992.

[7] V. Dietz and S. Harkeman, "Locomotor activity in spinal cord-injury persons," *J. Applied Physiology*, vol. 96, pp. 1954–1960, 2004.

[8] R. Boian, G. Burdea, and J. Deutsch, "Robotics and virtual reality applications in mobility rehabilitation," in *Rehabilitation Robotics*, S. S. Kommu, Ed. Vienna, Austria: I-Tech Educ. and Publishing, 2007, pp. 27–42.

[9] A. L. Behrman and S. J. Harkema, "Locomotor training after human spinal cord injury: A series of case studies," *Physical Therapy*, vol. 80(7), pp. 688–700, 2000.

[10] Y. Wu, Y. Li, A.-M. Liu, F. Xiao, Y.-Z. Wang, F. Hu, J.-L. Chen, K.-R. Dai, and D.-Y. Gu, "Effect of active arm swing to local dynamic stability during walking," *Human Movement Science*, vol. 45, pp. 102–109, 2016.

[11] M. Punt, S. M. Bruijn, H. Wittink, and J. H. van Dieën, "Effect of arm swing strategy on local dynamic stability of human gait," *Gait & Posture*, vol. 41, pp. 504–509, 2015.

[12] S. H. Collins, P. G. Adamczyk, and A. D. Kuo, "Dynamic arm swinging in human walking." *Proceedings. Biological sciences / The Royal Society*, vol. 276, no. 1673, pp. 3679–3688, October 2009.

[13] D. S. Marigold and J. E. Misiaszek, "Whole body responses: Neural control and implications for rehabilitation and fall prevention," *The Neuroscientist*, vol. 15, no. 1, pp. 36–46, 2009.

[14] N. J. Tester, D. R. Howland, K. V. Day, S. P. Suter, A. Cantrell, and A. L. Behrman, "Device use, locomotor training and the presence of arm swing during treadmill walking after spinal cord injury," *Spinal Cord*, vol. 11(49), pp. 451–6, 2011.

[15] D. P. Ferris, H. J. Huang, and P. C. Kao, "Moving the arms to activate the legs," *Exercise & Sport Science Reviews*, vol. 34(3), pp. 113–120, 2006.

[16] J. Yoon, B. Novandy, C. H. Yoon, and K. J. Park, "A 6-dof gait rehabilitation robot with upper and lower limb connections that allows walking velocity updates on various terrains," *IEEE Trans. Mechatronics*, vol. 15, pp. 201–215, 2010.

[17] O. R. Barnes, B. Hejrati, and J. J. Abbott, "An underactuated wearable arm-swing rehabilitator for gait training," in *IEEE Int. Conf. Robotics and Automation*, 2015. pp. 4998-5003.

[18] H. Elftman, "The function of the arms in walking," *Human Biology*, vol. 11(4), pp. 529–535, 1939.

[19] H. Pontzer, J. H. Holloway, D. A. Raichlen, and D. E. Lieberman, "Control and function of arm swing in human walking and running," *Journal of Experimental Biology*, vol. 212, pp. 523–534, 2009.

[20] R. Hinrichs, "Whole body movement: Coordination of arms and legs in walking and running," in *Multiple Muscle Systems*, J. Winter and S. Woo, Eds. Springer New York, 1990, ch. 45, pp. 694–705.

[21] V. Cimolin, M. Galli, G. Albertini, M. Crivellini, and J. Romkes, "Quantitative analysis of upper limbs during gait: A marker set protocol," *Journal of Applied Biomaterials and Functional Materials*, vol. 10, no. 1, pp. 49–55, 2012.

[22] M. Goudriaan, I. Jonkers, J. H. van Dieen, and S. M. Bruijn, "Arm awing in human walking: What is their drive?" *Gait & Posture*, vol. 40, pp. 321–326, 2014.

[23] J. L. Stephenson, A. Lamontagne, and S. J. De Serres, "The coordination of upper and lower limb movements during gait in healthy and stroke individuals." *Gait & Posture*, vol. 29, no. 1, pp. 11–6, Jan. 2009.

[24] P.-C. Kao and D. P. Ferris, "The effect of movement frequency on interlimb coupling during recumbent stepping," *Motor Control*, vol. 9(2), pp. 144–63, 2005.

[25] H. J. Huang and D. P. Ferris, "Neural coupling between upper and lower limbs during recumbent stepping," *Journal of Applied Physiology*, vol. 97(4), pp. 1299–1308, 2004.

[26] B. Hejrati, D. Hull, J. Black, J. J. Abbott, and J. M. Hollerbach, "Investigation of the Treadport for Gait Rehabilitation of Spinal Cord Injury," in *Int. Conf. IEEE EMBS, pp. 4553-4558*, 2012.

[27] B. Dobkin, D. Apple, H. Barbeau, M. Basso, A. Behrman, D. Deforge, J. Ditunno, G. Dudley, and R. Elashoff, "Methods for a randomized trial of weight-supported treadmill training versus conventional training for walking during inpatient rehabilitation after incomplete traumatic spinal cord injury," *J. Neurorehabilitation and Neural Repair*, vol. 17, pp. 153–167, 2003.

[28] A. Koenig, X. Omlin, J. Bergmann, L. Zimmerli, M. Bolliger, F. Muller, and R. Riener, "Controlling patient participation during robot-assisted gait training," *J. NeuroEngineering and Rehabilitation*, vol. 8, pp. 8–14, 2011.

[29] F. Alton, L. Baldey, S. Caplan, and M. Morrissey, "A kinematic comparison of overground and treadmill walking," *Clinical Biomechanics*, vol. 13, no. 6, pp. 434–440, 1998.

[30] M. P. Murray, G. B. Spurr, S. B. Sepic, G. M. Gardner, and L. A. Mollinger, "Treadmill vs. floor walking: Kinematics, electromyogram, and heart rate," *J. Applied Physiology*, vol. 59, no. 1, pp. 87–91, 1985.

[31] J. R. Nymark, S. J. Balmer, E. H. Melis, E. D. Lemaire, and S. Millar, "Electromyographic and kinematic nondisabled gait differences at extremely slow overground and treadmill walking speeds," *J. Rehabilitation Research and Development*, vol. 42, no. 4, pp. 523–534, 2005.

[32] P. O. Riley, G. Paolini, U. D. Croce, and D. Kerrigan, "A kinematic and kinetic comparison of overground and treadmill walking in healthy subjects," *Gait and Posture*, vol. 26, no. 1, pp. 17–24, 2007.

[33] V. Dietz, G. Colombo, L. Jensen, and L. Baumgartner, "Locomotion capacity of spinal cord in paraplegic patients," *Ann Neurol*, vol. 37, pp. 574–582, 1995.

[34] B. Dobkin, S. Harkema, P. Requejo, and V. Edgerton, "Modulation of locomotor-like emg activity subjects with complete and incomplete spinal cord injury," *J. Neurological Rehabilitation*, vol. 9, pp. 183–190, 1995.

[35] R. Riener, L. Lunenburger, S. Jezernik, M. Anderschitz, G. Colombo, and V. Dietz, "Patient-cooperative strategies for robot-aided treadmill training: First experimental results," *IEEE Transactions on Neural Systems and Rehabilitation Engineering*, vol. 13, no. 3, pp. 380–394, September 2005.

[36] R. Riener, L. Lunenburger, I. C. Maier, G. Colombo, and V. Dietz, "Locomotor training in subjects with sensori-motor deficits: An overview of the robotic gait orthosis lokomat," *J. Healthcare Engineering*, vol. 1, no. 2, pp. 197–216, 2010.

[37] J. F. Veneman, R. Kruidhof, E. E. G. Hekman, R. Ekkelenkamp, E. H. F. van Asseldonk, and H. van der Kooij, "Design and evaluation of the LOPES exoskeleton robot for interactive gait rehabilitation," *IEEE Trans. Neural Systems and Rehabilitation Engineering*, vol. 15, no. 3, pp. 379–386, 2007.

[38] Y. Stauffer, Y. Allemand, M. Bouri, J. Fournier, R. Clavel, P. Metrailler, R. Brodard, and F. Reynard, "The WalkTrainer—a new generation of walking reeducation device combining orthoses and muscle stimulation," *IEEE Trans. Neural Systems and Rehabil Engineering*, vol. 17, no. 1, pp. 38–45, 2009.

[39] A. Hicks, "Treadmill training after spinal cord injury: It is not just about the walking," *J. Rehabilitation Research and Development*, vol. 45, no. 2, pp. 241–248, 2007.

[40] J. M. Hollerbach, R. Mills, D. Tristano, R. R. Christensen, W. B. Thompson, and Y. Xu, "Torso force feedback realistically simulates slope on treadmill-style locomotion interfaces," *Int. J. Robotics Research*, vol. 20, no. 12, pp. 939–952, 2001.

[41] S. D. Kulkarni, M. A. Minor, M. W. Deaver, E. R. Pardyjak, and J. M. Hollerbach, "Steady headwind display with conditional angular rate-switching control," in *IEEE Int. Conf. Robotics and Automation*, 2008.

[42] J. M. Hollerbach, Y. Xu, R. R. Christensen, and S. C. Jacobsen, "Design specifications for the second generation SARCOS Treadport locomotion interface," in *Haptics Symposium, Proc. ASME Dynamic Systems and Control Division*, 2000.

[43] P. Lopez-Meyer, E. Sazonov, and G. Fulk, "Automatic detection of temporal gait parameters in post-stroke individuals," *IEEE Trans. Information Technology in Biomedicine*, vol. 99, pp. 594–601, 2011.

[44] J. Bae, K. Kong, N. Byl, and M. Tomizuka, "A mobile gait monitoring system for gait analysis," in *IEEE Int. Conf. Rehabilitation Robotics*, 2009.

[45] J. S. Bendat and A. G. Piersol, *Engineering Application of Correlation And Spectral Analysis*. John Wiley and Sons, Inc, 1980.

[46] S. M. Ross, *Introductory Statistics*. Burlington, MA: Elsevier academic press, 2005.

[47] J. Perry, *Gait Analysis*. Thorofare, NJ: SLACK Incorporated, 1992.

[48] J. F. Lehmann, B. J. deLateur, and R. Price, "Biomechanics of normal gait," *Phys Med Rahabil Clin North Am*, vol. 3, pp. 125–138, 1992.

[49] M. K. Holden, K. M. Gill, and M. R. Magliozzi, "Clinical gait assessment in the neurologically impaired: Reliability and meaningfulness," *Physical Therapy*, vol. 64, pp. 34–40, 1984.

[50] B. Hejrati, K. L. Crandall, J. M. Hollerbach, and J. J. Abbott, "Kinesthetic force feedback and belt control for the treadport locomotion interface," *IEEE Transactions on Haptics*, vol. 8(2), pp. 1939–1412, 2015.

[51] D. Grow and J. M. Hollerbach, "Harness design and coupling stiffness for two-axis torso haptics," in *Proc. Symp. on Haptic Interfaces for Virtual Environments and Teleoperator Systems*, 2006, pp. 83–88.

[52] C. Cruz-Neira, D. Sandin, T. A. DeFanti, R. V. Kenyon, and J. C. Hart, "The cave audio visual experience automatic virtual environment," *Communications of the ACM*, vol. 35, pp. 67–72, 1992.

[53] A. Vijayakar and J. M. Hollerbach, "Effect of turning strategy on maneuvering ability using the treadport locomotion interface," *Presence: Teleoperators and Virtual Environments*, vol. 11, no. 3, pp. 247–258, 2002.

[54] S. Kulkarni, C. Fisher, E. R. Pardyjak, M. A. Minor, and J. M. Hollerbach, "Wind display device for locomotion interface in a virtual environment," in *World Haptics Conference*, 2009, pp. 184–189.

[55] R. Christensen, J. Hollerbach, Y. Xu, and S. Meek, "Inertial force feedback for the treadport locomotion interface," *Presence: Teleoperators and Virtual Environments*, vol. 9, no. 3, pp. 1–14, 2000.

[56] L. Lichtenstein, J. Barabas, R. L. Woods, and E. Peli, "A feedback-controlled interface for treadmill locomotion in virtual environments," *ACM transactions on applied perception*, vol. 4(1), pp. 1–7, 2007.

[57] J. L. Souman, P. R. Giordano, I. Frissen, A. D. Luca, and M. O. Ernst, "Making virtual walking real: Perceptual evaluation of a new treadmill control algorithm," *ACM Trans. Appl. Percep.*, vol. 7(11), pp. 1–14, 2010.

[58] J. von Zitzewitz, M. Bernhardt, and R. Riener., "A novel method for automatic treadmill speed adaptation," *IEEE Trans. Neural Systems and Rehabilitation Engineering*, vol. 15, pp. 401–9, 2007.

[59] H. Noma and T. Miyasato, "Design for locomotion in- terface in a large scale virtual environment. atlas: Atr locomotion interface for active self motion," *In Proc. ASME Dynamic Systems and Control Division*, vol. 64, pp. 111–118, 1988.

[60] J. Feasel, M. C. Whitton, S. Member, L. Kassler, S. Member, F. P. Brooks, L. Fellow, and M. D. Lewek, "The integrated virtual environment rehabilitation treadmill system," *IEEE Trans. Neural Systems and Rehabilitation Engineering*, vol. 19(3), pp. 290–297, 2011.

[61] A. Koenig, S. Member, C. Binder, J. Zitzewitz, X. Omlin, M. Bolliger, and R. Riener, "Voluntary gait speed adaptation for robot-assisted treadmill training," in *ICORR 2009, Kyoto 22nd, Japan*, 26th of June 2009.

[62] J. Kim, H.-S. Park, and D. L. Damiano, "An interactive treadmill under a novel control scheme for simulating overground walking by reducing anomalous force," *IEEE/ASME Tra*, vol. 99, pp. 1–6, 2014.

[63] B. A. Frishberg, "An analysis of overground and treadmill sprinting," *Medicine and Science in Sports and Exercise*, vol. 15, pp. 478–485, 1983.

[64] A. Crétual and N. Fusco, "Additional energetic cost due to belt speed variations when walking on a treadmill," *J. Electromyography and Kinesiology*, vol. 21, pp. 551–556, 2011.

[65] K. Ogata, *Modern Control Engineering*. Prentice Hall, 2009.

[66] J. H. G. K. S. N. W. D. G. E. Robertson, G. E. Caldwell, *Research Methods in Biomechanics*. Human Kinetics, 2004.

[67] A. V. Hill, *Muscular Movement in Man*. New York: McGraw-Hill, 1927.

[68] M. Meilgaard, G. V. Civille, and B. T. Carr, *Sensory Evaluation Techniques*, L. Franco, Ed. CRC Press, 1999.

[69] J. Kim, C. J. Stanley, L. A. Curatalo, and H. S. Park, "A user-driven treadmill control scheme for simulating overground locomotion," in *Int. Conf. IEEE EMBS*, 2012, pp. 3061-3064.

[70] D. M. F. H. J. Derrac, S. Garcia, "A practical tutorial on the use of nonparametric statistical tests as a methodology for comparing evolutionary and swarm intelligence algorithms," *Swarm and Evolutionary Computation*, vol. 1, pp. 3–18, 2011.

[71] J. M. Ennis and V. Jesionka, "The power of sensory discrimination methods revisited," *J. Sensory Studies*, vol. 26, pp. 371–382, 2011.

[72] L. H. Sloot, M. M. van der Krogt, and J. Harlaar, "Energy exchange between subject and belt during treadmill walking," *J. Biomechanics*, vol. 47, pp. 1510–1513, 2014.

[73] A. L. Behrman, M. G. Bowden, and P. M. Nair, "Neuroplasticity after spinal cord injury and training: an emerging paradigm shift in rehabilitation and walking recovery," *Physical Therapy*, vol. 86, no. 10, pp. 1406–1425, 2006.

[74] F. Sylos-Labini, Y. P. Ivanenko, M. J. MacLellan, G. Cappellini, R. E. Poppele, and F. Lacquanti, "Locomotor-like leg movements evoked by rhythmic arm movements in humans," *PLoS ONE*, vol. 9, no. 3, March 2014.

[75] D. de Kam, J. Duysens, and V. Dietz, "Do we need allowing arm movements for rehabilitation of gait?" in *Converging Clinical and Engineering Research on Neurorehabilitation*, J. L. Pons, D. Torricelli, and M. Pajaro, Eds. Springer-Verlag, 2013, pp. 959–962.

[76] N. J. Tester, D. R. Howland, K. V. Day, S. P. Suter, A. Cantrell, and A. L. Behrman, "Device use, locomotor training, and the presence of arm swing during treadmill walking post-spinal cord injury," *Spinal Cord*, vol. 49, no. 3, pp. 451–456, March 2011.

[77] H. Schmidt, S. Hesse, C. Werner, and A. Bardeleben, "Upper and lower extremity robotic devices to promote motor recovery after stroke– recent developments," in *Proceedings of the 26th annual international conference of the IEEE EMBS*, San Francisco, CA, September 2004, pp. 4825–4828.

[78] A. M. Okamura, C. Richard, and M. R. Cutkosky, "Feeling is believing: Using a force-feedback joystick to teach dynamic systems," *Journal of Engineering Education*, vol. 91, no. 3, pp. 345–349, July 2002.

[79] K. Bowen and M. O'Malley, "Adaptation of haptic interfaces for a LabVIEW-based system dynamics course," in *14th Symposium on Haptic Interfaces for Virtual Environment and Teleoperator Systems*, 2006, pp. 147–152.

[80] H. van Hedel, L. Tomatis, and R. Muller, "Modulation of leg muscle activity and gait kinematics by walking speed and bodyweight unloading," *Gait and Posture*, vol. 24, pp. 35–45, 2006.

[81] J. Perry, *Gait Analysis: Normal and Pathological Function*. SLACK Incorporated, 1992, i was using this to cite the arm flexion/extension plot, BUT that actually comes from Murray1967!

[82] B. Hejrati, S. Chesebrough, K. B. Foreman, J. J. Abbott, and A. S. Merryweather, "Comprehensive quantitative investigation of arm swing during walking at various speed and surface slope conditions," *Human Movement Science*, Under Review, 2016.

[83] S. M. Brujin, O. G. Meijer, P. J. Beek, and J. H. van Dieen, "The effects of arm swing on human gait stability," *Journal of Experimental Biology*, vol. 213, pp. 3945–52, 2010.

[84] M. Pieter, S. M. Brujin, and J. Duysens, "The how and why of arm sing during human walking," *Gait & Posture*, vol. 38(4), pp. 552–562, 2013.

[85] D. S. Marigold and J. E. Misiaszek, "Whole body responses: Neural control and implications for rehabilitation and fall prevention," *The Neuroscientist*, vol. 15, no. 1, pp. 36–46, February 2009.

[86] D. de Kamd, J. Duysens, and V. Dietz, "Do we need allowing arm movements for rehabilitation of gait?" in *Converging Clinical and Engineering Research on Neurorehabilitation*. Springer-Verlag, 2013, pp. 959–962.

[87] S. Nakakubo, T. Doi, R. Sawa, S. Misu, K. Tsutsumimoto, and R. Ono, "Does arm swing emphasized deliberately increase the trunk stability during walking in the elderly adults?" *Gait & Posture*, vol. 40, pp. 516–520, 2014.

[88] M. P. Ford, R. C. Wagenaar, and K. M. Newell, "Phase manipulation and walking in stroke," *Journal of Neurologic Physical Therapy*, vol. 31, pp. 85–91, 2007.

[89] R. C. Wagenaar and R. E. van Emmerik, "Dynamics of pathological gait," *Human Movement Science*, vol. 13, pp. 441–71, 1994.

[90] N. J. Tester, H. Barbeau, D. R. Howand, A. Cantrell, and A. L. Behrman, "Arm and leg coordination during treadmill walking in individuals with motor incomplete spinal cord injury: A preliminary study," *Gait & Posture*, vol. 36, pp. 49–55, 2012.

[91] P. Meyns, L. van Gestel, S. M. Brujin, K. Desloovere, S. P. Swinnen, and J. Duysens, "Is interlimb coordination during walking preserved in children with cerebral palsy?" *Research in Developmental Disabilities*, vol. 33, pp. 1418–28, 2012.

[92] M. P. Ford, R. C. Wagenaar, and K. M. Newell, "Arm constraint and walking in healthy adults," *Gait & Posture*, vol. 26, pp. 135–141, 2007.

[93] F. Sylos-Labini, Y. P. Ivanenko, M. J. MacLellan, G. Cappellini, R. E. Poppele, and F. Lacquanti, "Locomotor-like leg movements evoked by rhythmic arm movements in humans," *PLOS ONE*, vol. 9(3), 2014.

[94] K. Jackson, J. Joseph, and S. Wyard, "A mathematical model of arm swing during human locomotion," *Journal of Biomechanics*, vol. 11, no. 6, pp. 277–289, 1978.

[95] M. Kubo, R. C. Wagenaar, E. Saltzman, and K. G. Holt, "Biomechanical mechanism for transitions in phase and frequency of arm and leg swing during walking," *Biological Cybernetics*, vol. 91, no. 2, pp. 91–98, 2004.

[96] D. Webb, R. Tuttle, and M. Baksh, "Pendular activity of human upper during slow and normal walking," *American Journal of Physical Anthropology*, vol. 93, pp. 477–89, 1994.

[97] R. C. Wagenaar and R. E. van Emmerik, "Resonant frequencies of arms and legs identify different walking patterns." *Journal of biomechanics*, vol. 33, no. 7, pp. 853–61, 2000.

[98] H. Carpinella, C. Paolo, and M. Rabuffetti, "Coordination between upper- and lower-limb movements is different during overground and treadmill walking," *European Journal of Applied Physiology*, vol. 108, pp. 71–82, 2010.

[99] J. Park, "Synthesis of natural arm swing motion in human bipedal walking," *Journal of Biomechanics*, vol. 41, pp. 1417–1426, 2008.

[100] J. P. Kuhtz-Buschbeck and B. Jing, "Activity of upper limb muscles during human walking," *Journal of Electromyography and Kinesiology*, vol. 22, pp. 199–206, 2012.

[101] D. Barthelemy and J. B. Nielsen, "Corticospinal contribution to arm muscle activity during human walking," *Journal of Physiology*, vol. 588, pp. 967–79, 2010.

[102] E. C. Park and G. Hwangbo, "The effects of action observation gait training on the static balance and walking ability of stroke patients," *Journal of Physical Therapy Science*, vol. 27, pp. 341–344, 2015.

[103] É. Desrosiers, S. Nadeau, and C. Duclos, "Balance during walking on an inclined instrumented pathway following incomplete spinal cord injury," *Spinal Cord*, vol. 53, pp. 387–394, 2015.

[104] K. Kawamura, A. Tokuhiro, and H. Takechi, "Gait analysis of slope walking: A study on step length, stride width, time factors and deviation in the center of pressure," *Acta Med Okayama*, vol. 45(3), pp. 179–184, 1991.

[105] S. D. Prentice, E. N. Hasler, J. J. Groves, and J. S. Frank, "Locomotor adaptations for changes in the slope of the walking surface," *Gait & Posture*, vol. 20(3), pp. 255–265, 2004.

[106] P. C. Dixon and D. J. Pearsall, "Gait dynamics on a cross-slope walking surface," *J Appl Biomechanics*, vol. 26(1), pp. 17–25, 2010.

[107] K. Tulchin, M. Orendurff, and L. Karol, "The effects of surface slope on multi-segment foot kinematics in healthy adults," *Gait & Posture*, vol. 32(4), pp. 446–450, 2010.

[108] M. J. Major, M. Twiste, L. P. J. Kenney, and D. Howard, "The effects of prosthetic ankle stiffness on ankle and knee kinematics, prosthetic limb loading, and netmetabolic cost of trans-tibial amputee gait," *Clinical Biomechanics*, vol. 29(1), pp. 98–104, 2014.

[109] A. Fougner, Ø. Stavdahl, P. J. Kyberd, Y. G. Losier, and P. A. Parker, "Control of upper limb prostheses: Terminology and proportional myoelectric control—a review," *IEEE Transactoins on Neural Systems and Rehabilitation Engineering*, vol. 20(5), pp. 663–677, 2012.

[110] D. A. Bennett, J. Mitchell, and M. Goldfarb, "Design and characterization of a powered elbow prosthesis," in *Int. Conf. IEEE EMBS, pp. 2458-2461*, 2015.

[111] K. Petuskey, A. Bagley, E. Abdala, M. A. James, and G. Rab, "Upper extremity kinematics during functional activities: Three-dimensional studies in a normal pediatric population," *Gait & Posture*, vol. 25(4), pp. 573–579, 2007.

[112] G. Rab, K. Petuskey, and A. Bagley, "A method for determination of upper extremity kinematics," *Gait & Posture*, vol. 15(2), pp. 113–119, 2002.

[113] D. A. Winter, *Biomechanics and motor control of human movement*. John Wiley & Sons, Inc., 2005.

[114] J. A. Zeni, J. G. Richards, and J. S. Higginson, "Two simple methods for determining gait events during treadmill and overground walking using kinematic data," *Gait & Posture*, vol. 27(4), pp. 710–714, 2008.

[115] R. M. O'Brien, "A caution regarding rules of thumb for variance inflation factors," *Quality & Quantity*, vol. 41 (5), pp. 673–690, 2007.

[116] R. D. Snee, "Some aspects of nonorthogonal data analysis, part i. developing prediction equations," *J Qual Technol*, vol. 5(1), pp. 67–79, 1973.

[117] C. Lamoth, P. Beek, and O. Meijer, "Pelvis thorax coordination in the transverse plane during gait," *Gait & Posture*, vol. 16, pp. 101–114, 2002.

[118] D. G. E. Robertson, G. E. Caldwell, J. Hamill, G. Kamen, and S. N. Whittlesey, *Research Methods in Biomechanics*. Human Kinetics, 2013.

[119] M. W. Lenhoff, T. J. Santner, J. C. Otis, M. G. E. Peterson, B. J. Williams, and S. I. Backus, "Bootstrap prediction and confidence bands: A superior statistical method for analysis of gait data," *Gait & Posture*, vol. 9, pp. 10–17, 1999.

[120] W. J. Anderst, "Bootstrap prediction bands for cervical spine intervertebral kinematics during in vivo three-dimensional head movements," *Journal of Biomechanics*, vol. 48, pp. 1270–1276, 2015.

[121] X. Huang, J. M. Mahoney, M. M. Lewis, D. Guangwei, S. J. Piazza, and J. P. Cusumano, "Both coordination and symmetry of arm swing are reduced in Parkinson's disease," *Gait & Posture*, vol. 35(3), pp. 373–7, 2011.

[122] A. Gil-Agudo, S. Pérez-Nombela, A. Forner-Cordero, E. Pérez-Rizo, B. Crespo-Ruiz, and A. del Ama-Espinosa, "Gait kinematic analysis in patients with a mild form of central cord syndrome," *Journal of NeuroEngineering and Rehabilitation*, vol. 8(1), pp. 1–10, 2011.

[123] B. Hejrati, A. S. Merryweather, and J. J. Abbott, "Generating arm-swing trajectories in real-time using a data-driven model for gait rehabilitation with self-selected speed," *IEEE Transaction on Neural Systems and Rehabilitation Engineering*, To be submitted, 2016.

[124] J. L. Stephenson, S. J. D. Serres, and A. Lamontagne, "The effect of arm movements on the lower limb during gait after a stroke," *Gait & Posture*, vol. 31, pp. 109–115, 2010.

[125] J. Yoon, J. Park, and J. Ryu, "A planar symmetric walking cancellation algorithm for a foot--platform locomotion interface," *International Journal of Robotic Research*, vol. 29(1), pp. 39–59, 2010.

[126] V. Bonnet, C. Mazzá, and J. McCamley, "Use of weighted Fourier linear combiner filters to estimate lower trunk 3D orientation from gyroscope sensors data," *Journal of Neuroengineering and Rehabilitation*, vol. 10, pp. 10–29, 2013.

[127] E. Grimpampi, V. Bonnet, A. Taviani, and C. Mazzá, "Estimate of lower trunk angles in pathological gaits using gyroscope data," *Gait & Posture*, vol. 38(3), pp. 523–527, 2013.

[128] K. C. Veluvolu and W. T. Ang, "Estimation of physiological tremor from accelerometers for real-time applications," *Sensors*, vol. 11(3), pp. 3020–36, 2011.

[129] J. A. Gallego, E. Rocon, J. O. Roa, J. C. Moreno, and J. L. Pons, "Real-time estimation of pathological tremor parameters from gyroscope data," *Sensors*, vol. 10(3), pp. 2129–49, 2010.

[130] R. Ronsse, N. Vitiello, T. Lenzi, J. van den Kieboom, M. C. Carrozza, and A. J. Ijspeert, "Human-robot synchrony: Flexible assistance using adaptive oscillators," *IEEE Transaction on Biomedical Engineering*, vol. 58(4), pp. 1001–1012, 2011.

[131] R. Ronsse, T. Lenzi, N. Vitiello, B. Koopman, E. van Asseldonk, S. M. M. D. Rossi, J. van den Kieboom, H. van der Kooij, M. C. Carrozza, and A. J. Ijspeert, "Oscillator-based assistance of cyclical movements: Model-based and model-free approaches," *Med Bio Eng Comput*, vol. 49, pp. 1173–1185, 2011.

[132] S. R. Hundza, W. R. Hook, C. R. Harris, S. V. Mahajan, P. A. Leslie, C. A. Spani, L. G. Spalteholz, B. J. Birch, D. T. Commandeur, and N. J. Livingston, "Accurate and reliable gait cycle detection in Parkinsons disease," *IEEE Transaction on Neural Systems and Rehabilitation Engineering*, vol. 22, pp. 127–137, 2014.

[133] A. Ferrari, P. Ginis, M. Hardegger, F. Casamassima, L. Rocchi, and L. Chiari, "A mobile Kalman-filter based solution for the real-time estimation of spatio-temporal gait parameters," *IEEE Transactions on Neural Systems and Rehabilitation Engineering*, vol. DOI. 10.1109/TNSRE.2015.2457511, 2015.

[134] A. Merryweather, M. Hunt, L. Smith, B. Foreman, and M. Minor, "Gait alterations on irregular terrain in older adults with and without Parkinson disease: Fall risk implications," in *Proceedings 19th Triennial Congress of the IEA*, 2015.

[135] K. M. Martinez, M.-L. Mille, Y. Zhang, and M. W. Rogers, "Stepping in persons poststroke: Comparison of voluntary and perturbation-induced responses," *Physical Medicine and Rehabilitation*, vol. 94, pp. 2425–32, 2013.

[136] C. M. Tyrell, E. Helm, and D. S. Reisman, "Locomotor adaptation is influenced by the interaction between perturbation and baseline asymmetry after stroke," *Journal of Biomechanics*, vol. 48, pp. 2849–2857, 2015.